UNIVERSITY OF CAPE COAST

DIODE LASER SPECTROSCOPIC STUDIES OF BIOLOGICAL MATERIALS USING ABSORPTION AND EMISSION TECHNIQUES

BY

BENJAMIN ANDERSON

THESIS SUBMITTED TO THE DEPARTMENT OF PHYSICS OF THE SCHOOL OF PHYSICAL SCIENCES, UNIVERSITY OF CAPE COAST, IN PARTIAL FULFILMENT OF THE REQUIREMNTS FOR AWARD OF DOCTOR OF PHILOSOPHY DEGREE IN PHYSICS
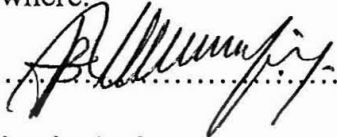
MARCH 2010

DECLARATION

Candidate's Declaration

I hereby declare that this thesis is the result of my own original work and that no part of it has been presented for another degree in this University or elsewhere.
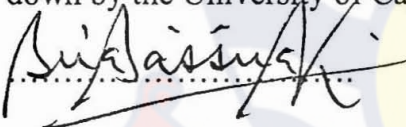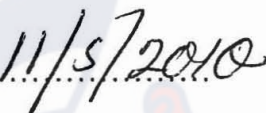
.... Date: ...10/5/2010...

Benjamin Anderson
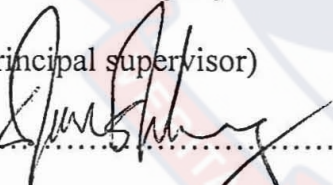
(Candidate)

Supervisors' Declaration

We hereby declare that the preparation and presentation of the thesis were supervised in accordance with the guidelines on supervision of thesis laid down by the University of Cape Coast.

.... Date: ...11/5/2010...
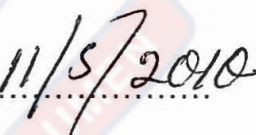
Prof. Paul Kingsley Buah-Bassuah
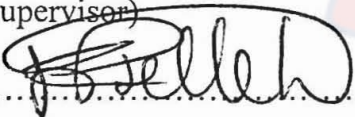
(Principal supervisor)

.... Date: ...11/5/2010...
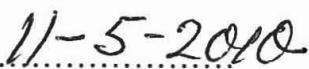
Prof. Sune Svanberg

(Supervisor)

.... Date: ...11-5-2010...

Prof. Jonathan P. Tetteh

(Supervisor)

ii

ABSTRACT

Two diode lasers with optical spectroscopic properties for absorption and emission spectroscopy have been used as sources in the study of economically important biological materials. In the emission spectroscopy a fluorosensor with a diode lasing at 396 nm was used to conduct in-vivo and in-vitro water-stressed study on the leaves of male and female plants by recording their chlorophyll fluorescence induction kinetics at the red and far-red bands as well as their ratios. Using the chlorophyll fluorescence induction kinetics curves in combination with multivariate data analysis method, discrimination and classification models were formulated which made it possible to differentiate and classify the sexes of the nutmeg plant which can be used as a tool for the early sex prediction of the plant. In the absorption spectroscopy molecular oxygen in some fruits and wood species were probed by means of GAs in Scattering Medium Absorption Spectroscopy (GASMAS) technique using a continuous diode laser emitting at 760 nm. The wavelength modulation second derivative absorption signals of the oxygen gas were measured relative to their direct absorption signals and a ratio established. This ratio was found to be directly proportional to the gas concentration in the scattering medium under study. For the wood the equivalent optical path lengths in different directions reflected its anisotropic nature while the differences in equivalent optical path length were found to relate to their densities. The different time constants obtained for the fruits and wood species is a potential technique for identifying and characterizing these species.

ACKNOWLEDGEMENTS

aunts and uncles, especially Mama Victoria Anderson and Uncle George Anderson for their support, understanding and compassion throughout my secondary and tertiary education. Finally, I am thankful to my wife Mavis and children George, Maria and Richard for their support, understanding and tolerance throughout thus project, which took much of my time and attention away from them. I greatly cherish the immense prayerful support given by my family, especially my dear wife.

My sincere thanks and gratitude go ultimately to all other people whose names were not mentioned but are behind my progress throughout my studies, forgive me for that error.
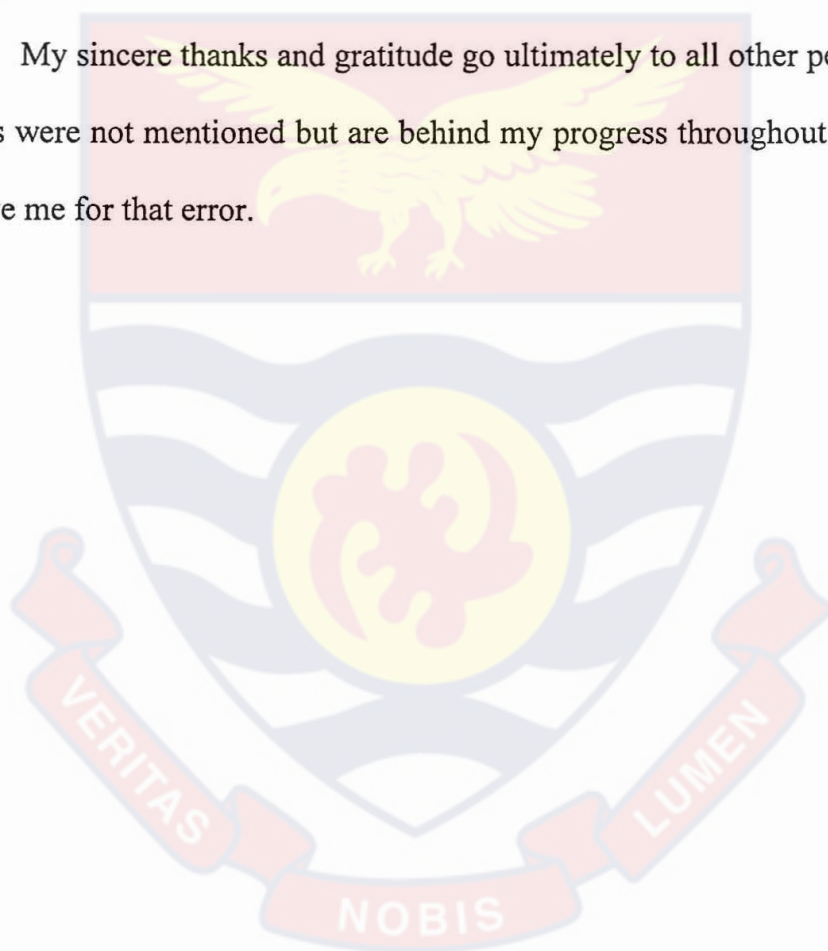
DEDICATION

To My Family
Mavis, George, Maria, Richard, Elijah and Rose.

TABLE OF CONTENTS

Page

x

LIST OF FIGURES

xv

LIST OF TABLES

LIST OF PLATES

CHAPTER ONE

INTRODUCTION

Laser-induced fluorescence of plants and trace-gas assessments has gained considerable interest in several biological, environmental and medical processes and applications. This is because many conventional analytical methods work by separation of species, which is time consuming and expensive. Therefore molecular detection or excitation by laser-based technique has become, particularly, a favourable approach. Combination of laser-based methods with techniques which do not require large quantities of molecular species, but even very few molecules, has opened up many fascinating possibilities to study physical processes of and on such molecules.

In recent times, diode laser as a source has been widely applied on biological materials for assessments and diagnostics. This is because diode lasers enable sensitive detection of photophysical parameters, which are very difficult to assess with conventional techniques using lamps. These diode laser based methods measure the optical parameters of the biological materials in their natural environment reducing or even avoiding the influence of the measurements on the measured parameter.

Several optical-based analytical methods have been developed using diode lasers. The high intensity and spectral quality of diode laser light enable highly

1

sensitive detection of various substances. Some of these methods which were not feasible with low-intensity light sources have become readily applicable.

Great advances that have been made in the development of diode lasers in the operative spectral regions ranges from ultra violet (UV) through the visible (VIS) to the near-infrared (NIR) at room temperatures and have shown promising applications. One of these is the use of diode lasers as light sources for spectroscopic applications. The small size and high operationability of diode lasers are paving way for a new generation of compact, portable and relatively inexpensive sensors. These sensors have been used for chemical species detection, gas sensing and temperature. Other areas of application include velocity, pressure, mass flux, combustion, atmospheric sciences and medicine.

Diode laser-based spectroscopy applies the concept of light interaction with matter on the principle that every atom and molecule may absorb and or scatter or emits. Such phenomena tend to associate specific characteristic spectral features of the material under study to enable the atom or molecule in the material to be identified. Important information on the properties of the atoms or molecules in that medium, thus the material, can be gained for diagnosis, characterization, discrimination and classification of the material for subsequent applications in diverse fields.

There are basically three main types of diode laser-based spectroscopic techniques used for various purposes and they are outstanding for a variety of applications. These are absorption, scattering and emission (fluorescence) techniques. They divide themselves conveniently into groups with respect to the

2

process of interaction. Depending on the type of application, and in turn the type of species to be detected, the different techniques have different applicability. These techniques have been used to obtain information about solids, liquids and gases in various applications in biological, medical and environmental fields (Svanberg, 2004). However, much is left to be done on biological materials using the above techniques.

The reason for the success of the diode laser-based spectroscopic techniques is that laser light has a number of spectacular properties that make it useful for detection of atoms and molecules in solid, liquid and especially gas phase. The most important attribute of diode lasers for spectroscopic applications is that it often has a narrow frequency width. Of special importance is their ability to detect the presence of small or unknown concentrations of species in gas phase under various types of conditions. There are a number of diode laser-based techniques that has been developed during the past two to three decades and the general denominator is their high sensitivity and selectivity.

The narrow frequency width is the basis for the high species selectivity that laser techniques possess. Another is that it has a high directionality with the aid of a lens system. This implies, among other things, that it can be sent over long distances, as is done in techniques for probing the atmosphere, or focused down to micrometer-sized spots. Additionally there are safety advantages in non-invasive sampling and the use of fibre optics light transmission so that the monitoring and control of equipment can be kept at a safe location. In order to be able to run a given instrumentation under optimum or at least suitable conditions, one has to

have a good understanding of the underlying mechanisms of the techniques. This is indeed a matter of crucial importance for the applicability and reliability of the techniques.

The wavelength of all individual diode lasers can be slightly tuned by temperature and current control. The tuning range depends on the laser materials and structure. Due to the linewidth and limited tuneability additional optical techniques are normally required for their application as spectroscopic light sources. Several techniques have been developed in order to operate the diode laser in a single mode with narrow linewidth and to extend the tuning range.

For spectroscopic purposes, especially absorption spectroscopy, in the near infrared (NIR) the detection sensitivity decreases because weaker vibrational transitions are detected. However, this is outweighed in many cases by the tremendous practical advantages of easy to use, robust, reliable devices operating at room temperature with relatively high output emission power and at a single discrete wavelength. In addition, inexpensive spectrometer components can be used. The very narrow wavelength spread of the light emission can ensure that interferences from other transitions are negligible. The ability to directly vary the output emission, that is, by modulation in order to improve detection sensitivities, also remains as a technical advantage.

Diode Laser Absorption and Scattering

Light absorption is a process by which energy of light (or photons) is taken up by an atom or a molecule where the energy difference between two suitable

4

levels matches that of the photon energy. The process results in the reduction of the intensity of the energy radiated into a medium, caused by converting some of or all the energy into another form. For polychromatic irradiation the reduced intensity is detected in a range of radiation frequencies or wavelengths, featuring a spectral finger print known as a spectrum. The study of spectra, especially to determine the chemical composition of substances and the physical properties of atoms and or molecules is termed spectroscopy. For a narrow-band laser only one wavelength is irradiated, and the laser light is attenuated if the wave matches an absorptive transition.

In principle, a laser absorption spectroscopy system consists of a laser light source, a sample to be investigated and a detector. The principle is to illuminate the sample with the laser light source and to detect the attenuated transmitted light. The fundamental method of light absorption spectroscopic detection has been direct absorption spectroscopy, which is based on measuring the intensity of the transmitted light after it has propagated through an absorbing medium and relating it to the initial intensity. When a diode laser is used as the light source, the absorption process is termed diode laser absorption spectroscopy. Since diode lasers are tunable, this technique is generally known as tunable diode laser absorption spectroscopy (TDLAS). TDLAS is a highly selective and versatile technique.

Depending on the molecules making up the sample, some specific frequency or frequencies may be absorbed. The transmitted light intensity for a non-scattering medium depends on the transition probability described by the

absorption coefficient (α), the concentration (c) and the path length (*l*) of the light within the sample. These factors influence the strength and the shape of the absorption spectrum and are specific to the atoms and or molecules.

The absorption coefficient (α) is a basic quantum mechanical property and strongly depends on the frequency or the wavelength of the laser light. For gases α also depends on other physical parameters such as temperature, velocity and pressure of the sample. All these factors influence the strength and the shape of the absorption spectrum. Since absorption of molecules is determined by the number of absorbers encountered, it is obvious that concentration (*c*) and effective pathlength (*l*) of the light through medium influence the absorption in a symmetric way.

Quantitative information of the attenuation due to the absorption of the light beam by the molecules of the sample, in the absence of scattering and emission such as fluorescence, is governed by the Beer-Lambert Law expressed as

$$I(l) = I(0)\exp(-\alpha c\, l), \tag{1}$$

where $I(0) = I_i$ is the irradiance at $l = 0$, that is, the surface of the absorbing material, and $I(l)$ is the irradiance after a path length of *l* units.

When a laser light beam, passing through the sample does not continue in its original straight path but it is deflected to other directions by undergoing multiple reflections in the sample, until the photons are either absorbed or converted to other form of energy, or escape from the medium, the light is considered to be scattered. The scattering process normally maintains the original frequency or the wavelength of the laser light, but it may also change, due to

6

Doppler and Raman effects. Laser light scattering also attenuates the transmitted laser light depending on how dense or thick the medium may be.

The Beer-Lambert absorption equation becomes modified for the case when the sample is found in a highly scattering medium, such as a gas in a porous solid. The attenuation of the light beam due to scattering may often be approximated by the formula

$$I(l) = I(0)\exp(-\beta l), \qquad (2)$$

where the coefficient β being the scattering coefficient, which also depends on wavelength, and the number of scatterers. If both absorption and scattering are causing the attenuation, the total light attenuation coefficient is therefore given as

$$I(l) = I(0)\exp(-\alpha c l - \beta l), \qquad (3)$$

In this case, the path length of the light is affected by the scattering due to the fact that the laser light travels through complex paths inside the medium before detection, due to the multiple scattering. Therefore, the optical path length l becomes longer than the dimensions of the sample.

However, in highly scattering samples, the transmitted laser light intensity is very weak due to the scattering, and weak absorption imprints may be obscured by high noise levels. In this case, using direct diode laser absorption spectroscopic technique would be greatly affected by the high noise levels, though it is basically a highly selective and versatile technique. In many experiments the absorption of the molecules might be very weak, on the per mole level of the sample, for example, are just a few percent. Therefore, for spectroscopic gas investigations modulation techniques may be employed to increase the sensitivity.

An experimental technique that is widely used to monitor weak signals in absorption spectroscopy is harmonic detection (Reid et al., 1978 a, b; Reid & Labrie, 1981; Cassidy & Reid, 1982). Harmonic detection has been used in recent years with tunable diode lasers to measure very weak signals in the ranges of sub-parts-per-billion (ppb) concentrations. In general, the laser is modulated at a high frequency by varying the current of the tunable diode laser while the laser is tuned slowly through the signal feature of interest. The interaction between the sample and the spectrally modulated radiation field leads to the generation of a signal that varies at the modulation frequency. Thus, the signal is detected coherently with frequency-sensitive and phase-sensitive detection electronics such as a lock-in amplifier referenced to the modulation frequency, or some multiple thereof.

This type of detection results in a significant improvement in signal-to-noise ratio. Thus, tunable diode laser absorption spectroscopy based on modulation is a method of choice for gas monitoring in which high sensitivity is required, such as in highly laser light scattering media.

Depending on the choice of modulation frequency relative to the width of the studied absorption feature, the detection frequency, the number of modulation tones, and the method is referred to as wavelength modulation spectroscopy (WMS) (Moses & Tang, 1977; Reid & Labrie, 1981), frequency modulation spectroscopy (FMS) (Bjorklund, 1980; Bjorklund et al., 1983; Lenth, 1984; Lenth et al., 1985) or two-tone frequency modulation spectroscopy (TTFMS) (Cooper & Gallagher, 1985; Janik et al., 1986; Cooper & Watjen, 1986; Cooper & Warren,

1987; Silver & Stanton, 1988; Avetisov & Kauranen, 1996; Avetisov & Kauranen, 1997).

Diode Laser-Induced Fluorescence Spectroscopy

Due to its low demand on systems and samples, fluorescence spectroscopy has been one of the most used optical methods for analysis. After the absorption of photons, the excited molecule emits a characteristic fluorescence spectrum. Like a fingerprint, it allows a differentiated statement about the fluorescing molecule.

Fluorescence has numerous measurement aspects, including intensity and excitation wavelength dependence, and quantities such as fluorescence decay time, anisotropy, polarization conditions, quantum yields and Stokes' shifts, which can be accessible for analysis. These parameters for the detection of substances allow alleviating some difficulties which may occur when applying fluorescence spectroscopy, for example, matrix and quenching effects. There are also cases where one parameter may give little or no information at all; in this case, other parameters may be used. However, there are substances which show an extremely low fluorescence yield or even no fluorescence at all due to other fast decay pathways such as intersystem crossing.

When using diode laser-induced fluorescence (DLIF) spectroscopy, the extraordinary characteristics such as the high spectral intensity and well defined wavelength of diode lasers are specifically utilized. These allow a selective excitation of the sample and the manufacture of compact instruments (Barocsi et al., 2000; Gustafsson et al., 2000; Anderson et al., 2004). By using these lasers, it is

9

possible to record the excitation spectra and thus the excitation wavelength as an additional parameter.

Simplicity, speed, sensitivity, non-destructiveness, and the ability to analyse both organic and inorganic materials using fluorescence spectroscopy are the main strengths of DLIF. Besides outstanding sensitivity and good selectivity, particular advantages of DLIF technique include the capabilities for *in situ* analysis and remote sensing. The major advantage of *in situ* laser-Induced fluorescence (LIF) measurements is absence of sampling and sample preparation procedures preceding the analysis. Such procedures are error-prone, time consuming and expensive.

In the past few years, a variety of laboratory and field instruments based on fluorescence spectroscopy have been introduced. Some instruments use a nitrogen laser (337 nm excitation wavelength) as the excitation source, while others use the 3rd or 4th harmonic of the Nd:YAG laser with excitation wavelength of 355 nm or 266 nm, respectively (Svanberg, 2004). However, these instruments are not as compact as when diode lasers are used (Gustafsson et al., 2000; Anderson et al., 2004). The other advantage of the diode laser is that it can be operated with 9 V battery.

Food crops represent one of the major components of our survival. Since most of the leaves of these plants exhibit distinct native fluorescence it is promising to apply DLIF analysis for detection and characterization of economically important food crops. The employment of fluorescence techniques for analysis of plants has received much attention in recent times (Baker & Rosenqvist, 2004).

A general concept for *in situ* analysis is to increase the dimensionality of the measured data. Since the substances have to be analysed in a complex matrix and in the presence of other interfering compounds, higher information content is crucial for a subsequent analysis since there is no clean-up step and no separation involved. Therefore, the LIF system should be able to record multi-dimensional fluorescence data, for example, fluorescence intensity versus emission wavelength and time.

Biological Samples

Understanding plant processes has become an important scientific topic and an economic factor, which requires effective research. This is because, plants behaviour and characteristics influence wide areas of modern life; many resources may go waste because certain plants have not been classified well in terms of their sexes and thus affect their potential for a good economic yield.

The capacity of a leaf to use and dissipate light energy depends both on genotype and environmental conditions (Griffin et al., 2004). Chlorophyll pigments, the fluorophores from green plants, absorb predominantly in the UV and the visible range, mainly in the blue and red regions. Fluorescence occurs in red (RF) and far-red (FRF) bands (Chapelle et al., 1984; Lichtenhaler, 1988; Govindjee, 1990; Krause & Weis, 1991; Valentini et al., 1994; Agati et al., 1996). Their spectra depend on the concentration of the chlorophyll and/or the photosynthetic efficiency of the leaf as well as on other factors (Krause & Weis,

11

1991; Lichtenhaler, 1992). They also vary with time based on the conditions of the leaf at that specific time (Krause & Weis, 1991; Lichtenhaler, 1992).

The temporal variation of chlorophyll fluorescence, known as induction kinetics (Kautsky effect), has been known for a long time (Kautsky & Hirsch, 1931; Govindjee, 1982; Krause & Weis, 1984; Govindjee, 1990; Lichtenthaler, 1992) and has become an important and useful tool in plant research. This is because the Kautsky effect can provide the necessary information about the apparatus of the molecular energy transduction of the leaves in relation to their properties (Lichtenhaler, 1988; Snel & van Kooten, 1990; Barocsi et al., 2000), from which one can draw useful conclusions about the plants.

Measuring the chlorophyll fluorescence is a widely accepted *in-vivo* method for the investigation of plant conditions, and the method is now applied in larger scale field applications involving issues such as environmental protection or agricultural technologies (Lang et al., 1995; Barocsi et al., 2000; Baker & Rosenqvist, 2004). Research has shown that the excitation wavelength considerably influences the shape of the fluorescence emission spectrum of leaves (Cerovic et al., 1999; Anderson et al., 2004). Laser-induced chlorophyll fluorescence has been used to monitor the growth and quality, and to predict harvest time as well as to screen plant varieties in terms of yield of agricultural products (Cerovic et al., 1999; Nedbal et al., 2000; Takeuchi et al., 2002; Anderson et al., 2004; Baker & Rosenqvist, 2004).

Indirectly, chlorophyll fluorescence phenomenon allows us to study different functional levels as well as the effects of adverse conditions on green

plants. The chlorophyll fluorescence technique is nondestructive, nonintrusive, fast and reliable. Due to these advantages of chlorophyll fluorescence technique, it is an attractive tool for basic and applied research and this makes it easy to use for many purposes in the laboratory and field work. In most laser-induced chlorophyll fluorescence research, ratios of the spectra peaks are used to retrieve the most important information for conclusions to be drawn (Cerovic et al., 1999; Subhash et al., 1999; Saito et al., 2000 (a, b); Anderson et al, 2004).

In practice, it is often necessary to monitor chlorophyll fluorescence spectra as well as induction kinetics from different parts of a leaf. This is because since chlorophyll pigments are not equally distributed in a leaf, chlorophyll fluorescence emission tends to vary. Simply averaging the spectral data does not give a true representation of the conditions. The spectra sets, therefore, become multivariate in nature. Thus, quantitative analysis of these data requires powerful mathematical and/or statistical methods in order to get a sound overview of these multivariate data (Weber, 1961; Berg et al., 2005).

Multivariate data analysis (MDA) provides methods that allow one to extract information and to display multivariate data by reducing the dimensionality to only a few dimensions (Martens & Naes, 1991; Esbensen, 2002; Johnson & Wichern, 2002; Eriksson et al., 2006). An important aspect of multivariate data analysis is that all data points can be used.

Nutmeg (*Myristica fragrans* Houtt) and Pawpaw (*Carica papaya*) are two examples of agriculturally important green plants belonging to a family known as dioecious. Dioecy is a condition where the male and the female flowers are borne

13

on separate plants and both are required for fertilization. It therefore means that, farmers in the nutmeg business have to wait for the trees to flower so that the sex can be determined and the males be thinned out, leaving the optimum situation of one male for every ten female plants. Consequently, a substantial loss of resources and productivity is incurred in its plantation if correct thinning cannot be performed early.

Nutmeg is native in the Moluccas in East Indonesia. It is an evergreen tree that has flowers, and is unisexual. The nutmeg tree yields two spices, namely; nutmeg, which is a seed of the kernel, and mace, which is the net-like crimson-coloured leathery outgrowth covering the kernel. Plate1 shows some branches of mature female nutmeg plant presenting the leaves, mature and immature fruits. Plates 2 and 3 show the abaxial and adaxial side of leaves from male and female nutmeg plant and the fruit and its contents: mace, kernel and nutmeg seed.

The fruits are used as spices and also to flavour milk dishes, cakes, punches, pickles and ketchups. Nutmeg has medicinal and pharmaceutical use. It is used in the perfume and cosmetic industries (Shulgin et al., 1967; Gable, 2006). Nutmeg plants are slow growing and start bearing fruit in the eighth year.

A major problem facing the farmers in the nutmeg industry is how to identify the sex of saplings at an early stage so that they can cultivate in their orchards adequately large number of productive female trees with only a minimal number of male trees. This is because the female plants are commercially valued for production of fruits and seeds. However, quick, accurate and convenient sex diagnostic methods for early sexing of seedling, so that more female plants can be

Plate 1. Branches of mature female nutmeg plant showing the leaves, mature and immature fruits. The burst fruits show the mace, which covers the kernel of the nutmeg seed.

Plate 2. Abaxial and adaxial side of leaves from a) female and b) male nutmeg plants.
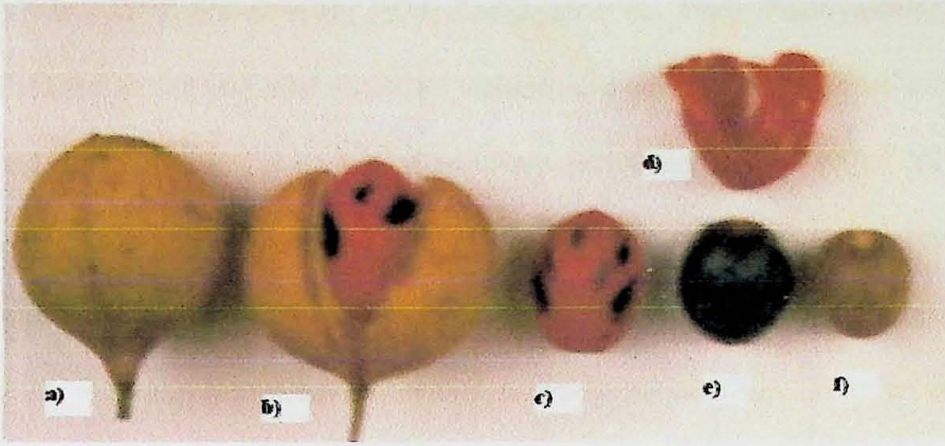
Plate 3. a) Nutmeg fruit from a mature female nutmeg plant, b) is a burst fruit showing the kernel covered by the mace, c) is the mace covering kernel of the nutmeg seed, d) is the mace without the kernel e) is kernel covering the nutmeg seed and f) is the nutmeg seed.

grown to make cultivation profitable, have not been achieved so far. The selection between female and male has remained frustratingly unsuccessful (Shibu et al., 2000). Therefore, farmers have little or virtually no control whatsoever in manipulating the sex ratio of saplings at planting. Thus, early sex diagnosis of nutmeg seedlings would be of immense importance to nutmeg industry. The issue of sex determination in nutmeg is a conceptually interesting area of research apart from its commercial importance.

Attempts to develop methods capable of identifying sexes at early stages have been initiated in various fields of study in recent years. Some techniques utilize molecular marker tools (Mulcahy et al., 1992; Hormaza et al., 1994; Biffi et al., 1995) and sex-specific DNA markers (Shibu et al., 2000) while others are based on morphological, physiological and biochemical parameters (Flach, 1966; Phadnis

& Choudhary, 1971; Nayar et al., 1977; Zachariah et al., 1986; Packiyasothy et al., 1991). Polymerase chain reaction (PCR) techniques have also been introduced as a diagnostic method for early sexing of seedlings (Parasnis et al., 2000). All these techniques, however, are intrusive and destructive. It is therefore important to develop simple, quick and non-intrusive methods that can be used to identify and discriminate between the sexes of plants as early as possible in order for the farmers to make informed decisions.

Since, the capacity of a leaf to use and dissipate light energy is a function of genotype of the leaves (Griffin et al., 2004), laser-induced chlorophyll fluorescence looks as a promising technique to be attempted in discriminating the sexes of nutmeg.

A further interesting aspect of agriculture is the optimum handling of post-harvested fruits to avoid losses in the ripening process. In food processing, fruits are considered nearly acidic and the acidity naturally controls the type of organism that can grow in them, with yeasts and moulds being the only spoilage organisms likely to be found on fruit products. Moisture content, oxygen concentration, temperature, nutrients, pH and inhibitors are the major factors that influence the growth and activity of micro-organisms in foods (Mountney & Gould, 1988). Obviously, by manipulating any of these factors, the activity of micro-organisms within foods can be controlled. These micro-organisms are broadly classified into aerobic and anaerobic.

The quantity of molecular oxygen concentration in fruits is an important factor that determines the quality and shelf-life of the fruit. This is because

molecular oxygen is a biological active molecule that determines the type of respiration process, aerobic or anaerobic, that should take place in the fruit. Aerobes grow in the presence of atmospheric oxygen while anaerobes grow in the absence of atmospheric oxygen. Between these two extremes are the facultative anaerobes which can adapt to the prevailing conditions and grow in either the absence or presence of atmospheric oxygen. Thus, controlling the availability of free oxygen is a means of controlling microbial activity within a fruit.

Respiration rate in normal aerobic respiration, where carbon dioxide is produced after taking in oxygen, decreases with decreasing oxygen concentration and increasing carbon dioxide concentration. On the other hand, fermentation, which is an anaerobic respiration process, is initiated when there is a continual decrease in oxygen concentration to critical levels and this causes a rapid decay of the fruit. This produces off-flavours and thus loss of quality as well as shorter shelf-life (Barmore, 1987; Gillies et al., 1997; Toivonen & DeEll, 2001). All this is because the organic compounds' assess to oxygen affects the metabolic process of respiration that releases energy necessary to maintain the life processes of the fruit. Ambient temperature is also a very important factor here because respiration is highly dependent on the temperature (Fidler & North, 1967; Yearsley et al., 1997).

However, the oxygen requirements vary from fruits to fruit and very high carbon dioxide concentrations can also cause damage to the fruit (Karel & Jurin, 1963; Hertog et al., 1998). An ideal situation would be the one resulting in an oxygen concentration low enough to slow down respiration and maturation but

18

higher than the critical concentration for initiation of anaerobic respiration (Karel & Jurin,1963; Mannapperuma & Singh, 1994).

These discussions show that there is great interest in optimizing both oxygen and carbon dioxide concentrations during the post-harvest period of fruits. This has brought about the development of conventional methods, such as controlled atmosphere (CA) storage and modified packaging (MAP), to prolong the post-harvest lifetime and inhibit physiological deterioration in fruit. The physiological tolerance to oxygen and carbon dioxide of a particular fruit determines CA storage and MAP (Cameron et al., 1995; Beaudry, 1999).

Thus, for optimal gas concentrations, there is the need for a technique to measure and model the internal gas content and gas exchange in fruits and package systems. A common technique for assessing the gas content has been the use of a flush-through system, in which the gas exchange can be estimated from the concentration difference between the inlet and outlet gas flow (Andrich et al., 1994; Varoquaux et al., 1995). In this technique, the flow of the gas has to be relatively high in order not to make systematic errors. In order to monitor small concentration differences the technique normally requires sensitive detection, which is often accomplished by a gas chromatographic system combined with unselective detectors, or more selective spectroscopic devices such as laser-based photoacoustic trace gas detectors (Oomens et al., 1996).

The other technique normally used, for measuring especially the internal gas contents and its dynamics, is the intrusive electrode-based probes or extraction of gas from the fruit interior by syringes (Oomens et al., 1996; Dadzie et al., 1996;

Konopacka & Plochatski, 2004). These intrusive techniques destroy the tissue, which affect the ongoing physiological processes. A non-intrusive compact and easily implemented technique for measuring gas exchange inside fruits would thus be of interest for assessments of internal gas dynamics relevant to, for instance, the optimization of CA storage and MAP of fruits. This can be helpful to sort fruit correctly and thereby improve the quality of fruit delivered to the consumer (Song et al., 1997) by optimizing the concentration of oxygen during the post-harvest time of the fruit. Thus, biologically active molecular oxygen, whose concentration is of crucial importance for ripening processes and the quality of fruit, is an important topic of study.

Diode laser sources can be used to probe any gas provided the absorption lines of the gas is in reach of diode laser, but its limitation could be the bulk material containing the gas. Further, fruits are porous materials that contain water and strongly absorbs beyond 1.4 μm, and so the radiation is heavily scattered. However, by using single-mode continuous-wave diode laser radiation in-combination with modulation techniques the gas can be detected sensitively, without disturbance from the broad absorption features of the bulk material. Diode lasers are used because they are highly suitable for sensitive absorption spectroscopy with high spectral resolution and they are available in different wavelength ranges. Diode lasers have uncomplicated wavelength tunability, and relatively low cost compared to other lasers.

Molecular oxygen gas is detectable in fruits when employing their A-band, which is situated around 760 nm (Sjöholm et al., 2001; Somesfalean et al., 2002).

20

Technique of studying free gas embedded in scattering materials, denoted GASMAS an acronym for gas in scattering media absorption spectroscopy (Sjöholm, 2001) has been demonstrated. The gas contents in the scattering medium give rise to signals of certain strength, which is determined by the gas concentration as well as the average path length travelled by the light in the scattering medium. In particular, gas and transport of gas through the porous material can be studied either in transillumination or backscattering geometry (Sjöholm et al., 2001; Somesfalean et al., 2002; Persson et al, 2005).

The GASMAS technique relies on the fact that the absorption features for free gas are about 10^3 times narrower than the spectral features of the surrounding liquid and solid. This makes it possible to discern the gas. A proper diode laser with single mode output can be tuned on a particular molecular transition by just changing the injection current and/or the temperature. Schemes based on wavelength modulation of the source through application of an oscillatory component to a driving current allow for effective noise reduction detection techniques. Other advantages are that diode lasers are compact and are easy to operate frequently at room temperature.

Leaving plants and fruits, we now turn to different field of the biosphere, the properties of wood derived from trees. Wood is an extremely versatile material with a wide range of physical and mechanical properties among the many species of trees. It is a renewable resource with an exceptional strength-to-weight ratio (Simpson et al., 1980; Hoadley, 1990; Miller et al., 1994), and a valuable engineering material. A chief attribute is its availability in large variability

regarding properties to fit almost every demand. Throughout history, the unique characteristics and comparative abundance of wood have made it a natural material for houses and other structures, furniture, tools, vehicles, and decorative objects. Today, for the same reasons, wood is appreciated for a multitude of uses.

All wood is composed of cellulose, lignin, hemicelluloses, and minor amounts (5% to 10%) of extraneous materials contained in a cellular structure. Variations in the characteristics and volume of these components and differences in cellular structure make woods heavy or light, stiff or flexible, and hard or soft. The properties of a single species are relatively constant within limits; therefore, selection of wood by species alone may sometimes be adequate. However, to use wood to its best advantage and most effectively in engineering applications, specific characteristics or physical properties must be considered.

Generally, wood identification can often be made quickly on the basis of readily visible characteristics such as colour, odour, density, presence of pitch, or grain pattern. The grain patterns and colours of wood make it an esthetically pleasing material, and its appearance may be easily enhanced by varnishes, lacquers, and other finishes (Panshin & De Zeeuw, 1980; Hoadley, 1980).

Physical properties such as directional properties, moisture content, dimensional stability, thermal and pyrolytic (fire) properties, density, and electrical, chemical, and decay resistance (Winandy, 1994; Simpson & TenWolde, 1999) are the quantitative characteristics of wood. These properties vary along three mutually perpendicular axes: longitudinal, radial, and tangential as shown in figure 1, because of the grain or fibre direction and the manner in which a tree increases in

diameter as it grows. The longitudinal axis is parallel to the fiber (grain) direction, the radial axis is perpendicular to the grain direction and normal to the growth rings, and the tangential axis is perpendicular to the grain direction and tangential to the growth rings.
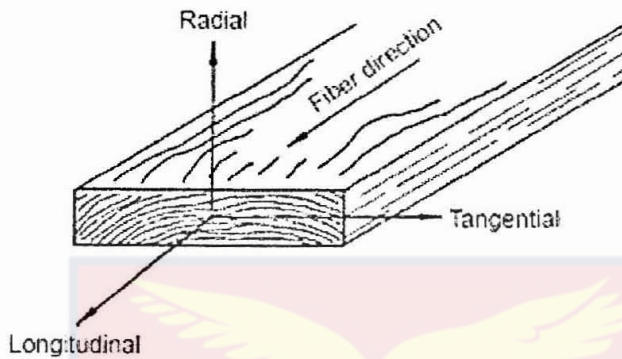
Figure 1. Three principal axes of wood with respect to grain direction [After modification: (Winandy, 1994)].

Wood finishers refer to wood as open grained and close grained, which are terms reflecting the relative size of the pores, and this determines whether the surface needs a filler or not (Hoadley, 1980, 1990). The pores can be filled with air or other gases which may be an undesirable situation. Therefore, the studying of the gas and the influence of the density and the anisotropy of the wood on the gas will give much information on the wood.

Absorption spectroscopy is the same common method that can be used to monitor the gas contents. However, because wood is inhomogeneous and porous means that it is highly scattering, making the optical path length through the sample undefined like in fruits. The GASMAS technique can be applied to monitor free

molecular oxygen and its transport in wood in order to probe the influence of density and anisotropy of the wood on this gas.

Scope of work

The research work presented in this thesis focuses on the use of diode laser spectroscopy on biological samples for agricultural applications. Special emphases are placed on the applied nature of diode laser spectroscopy, more than on the fundamental aspects of the laser-matter interaction. The research work is in two parts; one part of the work makes use of the gas in scattering media absorption spectroscopy (GASMAS) technique, using oxygen as the sample gas, in extracting physical information from different types of woods and fruits for forestry and agricultural applications.

The other part exploits diode laser-induced chlorophyll fluorescence, an emission technique, as applied to biological samples for plant selection processes and rapid classification in agricultural crop improvement programmes. That is, to identify ways in which laser-induced chlorophyll fluorescence induction kinetics and multivariate data can be used effectively to improve plant selection processes and rapidly classify plants, especially male and female plants, in agricultural programmes.

Organization of Thesis

The thesis consists of five main chapters; chapters one to five. The present one, Chapter one, gives an introduction to spectroscopy and diode lasers, in

particular the concept of diode laser absorption as well as diode laser-induced fluorescence. It also provides a discussion of the biological samples used in this research. The background to the work, the scope of this work and the organization of the thesis are also included in this first chapter. The literature on weak optical absorption in combination with modulation techniques for highly scattering media as well as laser-induced chlorophyll fluorescence is reviewed in chapter two. Various analyses techniques are also reviewed in chapter 2.

Chapter 3 seeks to offer the experimental methods for studying absorption and fluorescence phenomena involved in this research work. The results and analyses of the various experiments and their discussion are then presented in Chapter four. In the fifth and final chapter, conclusions are drawn and pertinent recommendations given to aid further research in this area.
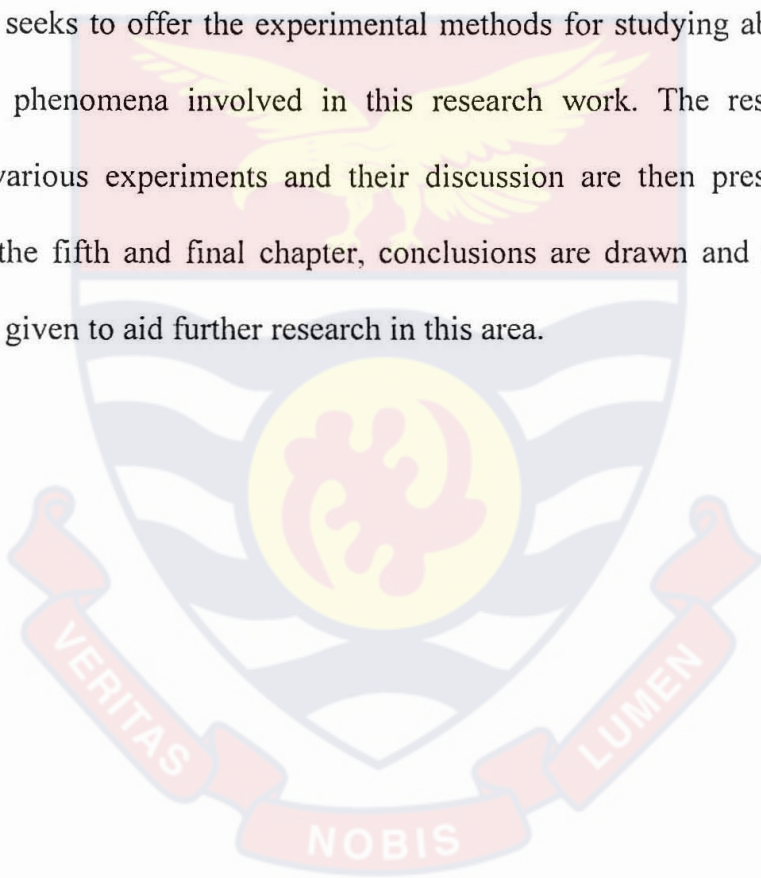
CHAPTER TWO

LITERATURE REVIEW

Diode Lasers

A typical diode laser of today is based on the double heterostructure, architecture where the active (laser) medium is sandwiched between two other semiconductor materials with higher band gap energies. Homostructure devices, due to their inefficiency, are no longer used.

For any practical application the diode laser forms part of a package. A single unpackaged double heterostructure diode laser looks like tiny squares of metallic "confetti". An example of a single double heterostructure diode laser in an electronic can with its electrical components and leads is shown in Plate 4.
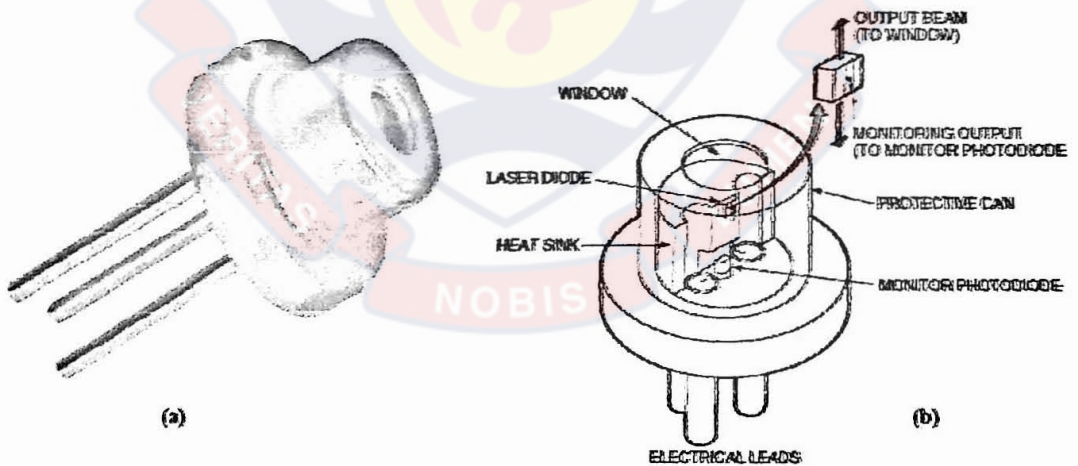
Plate 4. **(a) An example of single double heterostructure diode laser in an electronic can with metal case (b) its electrical components and leads (With permission from Spectra physics, a division of Newport Corporation)**

26

Diode lasers generate light from recombination of electron-hole pairs at a forward-biased junction. Below a threshold, the laser does generate spontaneous emission with an intensity that depends on the drive current. They have reflective surfaces that create optical feedback and this has little impact when the drive current is below the point needed to produce a population inversion, but it is critical in the laser action.

At low drive current, energy release by the electron-hole pairs in the form of photons is by spontaneous emission. As the drive current increases, it produces more excitons that emit light spontaneously, increasing the likelihood that a spontaneously emitted photon will encounter and stimulate emission from an exciton that has yet to release its extra energy. Once the drive current reaches a high enough level, it produces a population inversion between the exciton state and the atoms with the extra electron bound in the valence band. That leads to a cascade of stimulated emission as the laser crosses the threshold.

Diode lasers have a well-defined current threshold at which their output shifts from low-power spontaneous emission to higher-power stimulated emission, for laser operation. Below the threshold, the diode laser operates as a relatively inefficient light emitting diode (LED). Above the current threshold, the diode operates as a laser, converting a much higher portion of the input electrical power into light energy. Therefore the threshold current is an important factor in diode laser performance (Hecht, 2008).

Electrical power needed to reach the threshold current and fraction of the above-threshold current that is not converted into light winds up as heat dissipated

in the laser. This extra heat is not just wasted power but degrades the performance of the laser and tends to shorten its lifetime, so lower threshold laser tend to have longer lifetimes (Siegman, 1986; Silfvast 2004). High currents also stress the laser by putting highly concentrated power through the junction.

Diode laser resonators are constructed by their orientation relative to their active layer where the stimulated emission is generated. Edge-emitters are diode lasers resonated in the plane of their junction layer because their output comes from the active layer at the edge of the laser chip and they take a few different forms. Their advantage is that they can extract laser gain from the length of the laser chip to produce relatively high power. Examples of these types are Fabry-Pérot lasers (FP) and distributed feedback lasers (DFB) (Siegman, 1986; Silfvast, 2004).

Fabry-Pérot lasers (FP) have the simplest type of diode laser resonator, a linear cavity with flat mirrors on the two ends. However, such lasers are possible to have high gain and high powers (Siegman, 1986; Silfvast, 2004). They emit light from both facets; however, in practice one facet is coated to reflect all or most of the incident light, and the beam emerges from the other facet. The weak residual light emerging from the rear facet can be monitored to provide control of the laser operation.

Cavity modes of FP diode lasers are spaced widely in the diode lasers because the resonator consisting of the tiny laser structure is short. Thus, FP lasers typically emit most of their light on one main wavelength mode at any one time, but may have side bands. However, the gain curve of diode lasers is broad and the refractive index varies with temperature, which itself is a function of drive current.

28

The FP laser wavelength might easily shift to another wavelength when the driving current of its intensity is changed, a process known as mode-hopping. Because of this behaviour FP laser are widely used. FP can be used also where low cost is important and precise wavelength control is not critical.

For distributed feedback (DFB) lasers, a diffraction grating is fabricated in the active layer. Regularly spaced gain region reflects light back into the active layer at a narrow range of wavelengths, so only a specific wavelength receives the feedback needed for laser oscillation. The grating is positioned where there is no laser gain resulting in what is called a distributed Bragg reflection (DBR) laser.

The spacing D of the grating selects the oscillating wavelength according to a formula that also depends on refractive index n and an integer m that denotes how light is being diffracted by the grating:

$$D = \frac{m\lambda}{2n} \qquad (4)$$

In practice m = 1 or 2 is used. DFB resonators maintain the laser in a stable single longitudinal mode, limiting the range of emitting wavelength and preventing mode-hopping, which is critical for gas absorption spectroscopy (Somesfalean 2004). However, since the refractive index of the laser depends on operating temperature, the oscillation wavelength of the laser may shift slightly with temperature. The maximum wavelength tuning is typically of the order of a few nanometers

Again, the diode laser emission can be limited to a narrow linewidth by an external cavity with appropriate tuning optics such as a diffraction grating (Somesfalean, 2004). With one facet coated to transmit nearly all light emerging from the active layer into external optics, a unique wavelength can be selected. The

selected wavelength is tuned by adjusting the optics to feed the light at a specific wavelength back into the active layer of the laser, with the output of the laser at the other end corresponding to that of the wavelength selected by the grating. This wavelength selection technique provides a good optical spectroscopy source for gas absorption spectroscopy.

The emitting area of edge emitters are thin and wide, producing rapidly diverging beams that are hard to focus. They are also hard and expensive to package.

Fortunately, external optics can correct for this broad beam divergence. A cylindrical lens, which focuses light in one direction but not in the perpendicular direction, can make the beam circular in shape. Collimating lenses can focus the rapidly diverging beam from an edge emitter so it has similar properties as the beam from a helium-neon laser. The addition of collimating optics reduces the beam divergence.

Generally, optical feedback induced by large bandwidth optical components, such as glass plates, lenses, mirrors in the optical path, etc. as opposed to a wavelength selective grating with a narrow bandwidth, constitutes an unwanted effect that disturbs the longitudinal mode structure of the diode laser. It can induce mode jumps, broaden the linewidth and cause unstable output power. So the common practice in all experiments involving free-running diode lasers is to slightly angle all transmissive optics and detector surfaces, to reduce the back reflections to a minimum.

An important alternative to the edge emitting diode lasers is the surface-emitting laser, in which the beam emerges from the surface of the chip. They produce beams with much lower divergence that is easier to focus. Surface emitters have other advantages regarding the beam quality and come in two basic varieties: vertical-cavity surface emitting lasers (VCSELs) that oscillate perpendicular to the junction layer, and hybrid lasers that oscillate in the junction plane but output directly through the surface.

The overall gain within a VCSEL cavity is low because light oscillate between a top and bottom mirrors that passes through only a thin slice of active layer. Though the gain per unit length may be high in the active layer, the active layer itself is so thin from top to bottom that the total gain in a round-trip of the VCSEL cavity is small. To sustain oscillation, resonator mirrors on top and bottom of the VCSEL are made to reflect virtually all the stimulated emission back into the laser cavity.

The structure of the VCSEL is limited to generate powers in a range well below the maximum available from edge emitters. However, (VCSELs) have extremely low thresholds currents, making them significantly more efficient. Their high efficiency and low drive current also give them a long lifetime.

The optical properties of diode lasers depend on their structures, and they differ from those of other lasers. All diode lasers are physically small and emit from a small aperture and this affects beam properties including divergence, coherence, and mode structure. This is due to the fact that a beam emitted through a

small aperture, d, has a divergence angle θ, which is proportional to the wavelength divided by the aperture.

Diode Laser as a Spectroscopic Source

For spectroscopic use, added benefits of the diode laser include, for example, high spectral purity, high wavelength stability, uncomplicated wavelength tuning, and excellent modulation capabilities. Diode lasers have many spectroscopic applications owing to their increased wavelength coverage, high output power, high reliability, and low price.

FP lasers can oscillate in more than one longitudinal mode, and hop between modes when operating conditions change. DFB, DBR and external-cavity lasers limit laser oscillation in a single stable longitudinal mode, giving them the extremely narrow bandwidth required for absorption spectroscopy. The short cavity of VCSELs limits them to oscillating in a single longitudinal mode, but their bandwidth is not as narrow as DFB or DBR lasers, which internally stabilize the output wave length. Large-aperture VCSELs oscillate in multiple transverse modes.

Wavelength emitted by diode lasers depend on the composition of the semiconductor (Nakamura et al., 2000). The two parameters that most directly affect the structure of diode lasers are the band gap of the material and the lattice constant, or spacing between atoms. The band gap depends on the atomic composition of the semiconductor; in general, changing the composition changes the band gap with some exceptions. Table 1 lists important types of semiconductor lasers and their usual wavelengths.

Table 1. Major diode laser materials and wavelengths (Hecht, 2008).

Material	Wavelength Range (μ m)	Absorbing Species
AlGaN	0.350 –0. 400	NO_2, Chlorophyll
GaInN	0.375 –0. 440	NO_2, Chlorophyll
ZnSSe	0.447 – 0.480	NO_2
ZnCdSe	0.490 – 0.525	
AlGaInP/GaAs	0.620 – 0.680	NO_2, Chlorophyll
$Ga_{0.5}In_{0.5}P$/GaAs	0.670 – 0.680	
GaAlAs/GaAs	0.750 – 0.900	O_2, H_2O, NH_3
GaAs/GaAs	0.904	
InGaAs/GaAs	0.915 – 1.050	H_2O
InGaAsP/InP	1.100 – 1.650	CO, CO_2, C_2H_2, CH_4, NH_3
InGaAsSb	2.0 – 5.0	Hydrocarbons, CO, CO_2, N_2O,
PbCdS	2.7 – 4.2	Hydrocarbons, NO, SO_2, NO_2,
PbSSe	4.2 – 8.0	Hydrocarbons, NO, SO_2, NO_2,
PbSnTe	6.5 – 30.0	Hydrocarbons, NO_2, SO_2, ...
PbSnSe	8.0 -30.0	Hydrocarbons, NO_2, SO_2, ...

Most of these diode lasers can be operated at room temperature except for the infrared diode lasers with wavelength from 2.7 – 30 μm, which require some form of cooling in their operations. This is due to their high heat generation, which reduces their efficiency.

The development of the blue diode lasers based on gallium indium nitride (GaInN) was one of the top laser breakthroughs of the 1990s. This compound can be used for blue and violet lasers. By adding aluminum to the compound the band gap can be extended well into the ultraviolet. Longer wavelength visible diode lasers are made by adding indium and reducing gallium concentration. Blue diodes emitting at 440 nm are standard products and ultraviolet diodes emitting at 375 nm are also available.

Diode lasers with active layers of GaAlAs or GaAs are fabricated on GaAs, and are usually called "gallium arsenide" lasers. They are among the oldest and best-developed family of lasers. Pure GaAs active layers nominally emit at 904 nm, but replacing some of the gallium with aluminum increases the band gap to generate shorter wavelengths. The shortest wavelengths from GaAlAs lasers typically are around 750 nm.

The strong molecular fundamental rotational-vibrational absorption bands in the middle infrared region (2 – 15 μm) of several atmospheric species make the lead salt diode lasers especially attractive for spectroscopic applications and, in fact, many scientific trace gas spectrometers incorporate a diode laser of this type.

However, these lasers operate only at cryogenic temperatures which increases device cost and makes operation and handling more complex. In addition, the reliability of these lasers for practical spectroscopic implementations has for a long time been regarded as unacceptable among optical spectroscopist.

The infrared diode lasers are only produced in small batches and at a much lower level of manufacturing sophistication, and cannot benefit from the high

manufacturing capabilities as the visible and near-infrared diode lasers. Infrared lasers have not been used in the work presented in this thesis - instead visible and near-infrared diode lasers were employed.

Wavelength Tuning of Diode Lasers

One of the most important characteristics of a diode laser for atomic and/or molecular spectroscopy is its tunability. The wavelength of a diode laser can be tuned by altering the temperature or by varying the drive current. A change in the drive current changes the junction temperature (Joule heating). The wavelength changes because of the temperature dependence of the bandage, which shifts the gain curve. A further influence is the temperature dependence of the refractive index, which alters the optical path length in the cavity. These two temperature dependencies are quite different; for example, in an AlGaAs diode laser, the gain curve tunes about 0.25 nm/^{0}C and the change in the optical length of the cavity tunes about 0.06 nm/^{0}C. These results in a temperature-wavelength tuning curve that consists of several continuous tuning ranges, which are interrupted in the FP lasers by mode jumps making a large portion of the total wavelength range covered by a particular FP diode laser inaccessible.

In practice a continuous tuning range of 20-80 GHz before the diode laser jumps to a different longitudinal mode is typical for most lasers operating in the visible and near-infrared region [Siegman, 1986; Silfvast, 2004]. The laser temperature can be tuned between 0 – 60 ^{0}C and in some diode lasers up to 85 ^{0}C, when using a Peltier element in close connection to the diode laser capsule. In

practice though, one usually does not go below 5 – 10 ^{0}C or above 50 ^{0}C, to avoid water condensation and thermal degradation which significantly shortens the diode laser lifetime.

Typically, coarse wavelength tuning of a diode laser is accomplished by changing the temperature while fine tuning is realized by changing the drive current. One of the important advantages of the diode lasers over other optical sources is that their amplitude and frequency can be modulated very easily and rapidly by changing the injection current. The fundamental concept of all modulation techniques in spectroscopy is to shift the detection band to a higher-frequency region, where the noise level is small. This also enables effective attenuation of low-frequency components by conventional filtering. The shift to a high-frequency region can be accomplished by either amplitude modulation (AM), frequency modulation (FM) or fast scan integration.

Diode Laser Light-Matter Interaction

The interaction of light with matter is the combined effect of the properties of the light source and the characteristics of the matter. In general, when the light source is monochromatic in nature, for example a diode laser, the variables involved in the light –matter interaction process is limited.

There are several factors that influence the light-matter interaction. The power density provided by the source is considered one of the main factors. The amount of source power coupled into the medium under irradiation is a function of the laser power output. At a constant power density, that is, the power per unit area,

36

the radiant fluence rate in the sample at the core of the spot size increases with the spot size.

When laser irradiation reaches the matter surface under an angle, a progressively higher percentage of photons will be reflected off the surface at an increasing angle of oblique incidence. For example, collimated irradiation presents a greater challenge than diffuse irradiation in deriving an expression for the light distribution inside a turbid medium that is irradiated by a laser beam.

The fundamental interaction of laser radiation with matter depends in part on the wavelength of the light and the dimensions of the particles involved in the interaction. These particles can be of atomic size to complex molecule in the case of biological materials. For biological materials, the tissue type and the state as well as the medium of the biological sample primarily influence the optical properties of the sample. Therefore, these optical properties are used to characterize light propagation through these materials.

When light enters medium, the photons may be annihilated, redirected, or converted into lower energy photons. This translates into absorption or scattering events or both in the material. Optical properties are different for distinctive biological tissue, and these differences are not always distinguishable by visual examination. The optical parameters are in fact a function of delivery protocol of the light source, tissue composition, and temperature and water content of the tissue. Different tissue and tissue constituents will interact with light according to their specific optical parameters, and require individual attention in the classification of their optical properties.

Laser Absorption Spectroscopy

Annihilation of photonic energy from the laser source while interacting with electrons, atoms or molecules is termed absorption. This interaction brings about the conversion of the original photons into new photons with lower energy, e.g., fluorescence or phosphorescence or into heat.

When a photon, which is the particle characterization of the light wave, interacts with an atom or molecule, light resonance absorption may occur. An electron is excited to one of the higher available discrete energy levels by absorbing all of the photon energy. This occurs only if the photon energy precisely matches the atomic or the molecular energy difference corresponding to the electron jump. If it does not, the absorption does not take place and another type of photon-to-electron interaction may occur.

Once the electron reaches the new energy level, it will remain there for a discrete amount of time before spontaneously falling back, e.g., to the original energy level. During this transition, the total energy of the process must be maintained to satisfy the law of conservation of energy. Consequently, a new photon is emitted from the atom or molecule with the same energy as the original photon. The ability of matter to absorb photons is represented by the parameter μ_a with units per length (per mm or per cm), which is defined as the probability per unit path length that a photon will encounter an absorption event.

As already noted, the transmitted intensity $I(v)$ through a medium at frequency v is attenuated exponentially according to Beer-Lambert law:

$$I(v) = I_0(v)\exp(-\sigma(v)cl) \qquad (5)$$

where $I_0(v)$ is the original intensity, $\sigma(v)$ is the absorption cross-section, c is the concentration of the absorbing species and l is the length of the path through the medium. Figure 2 illustrates a gas absorption line showing original light intensity I_0 and the transmitted light intensity I.
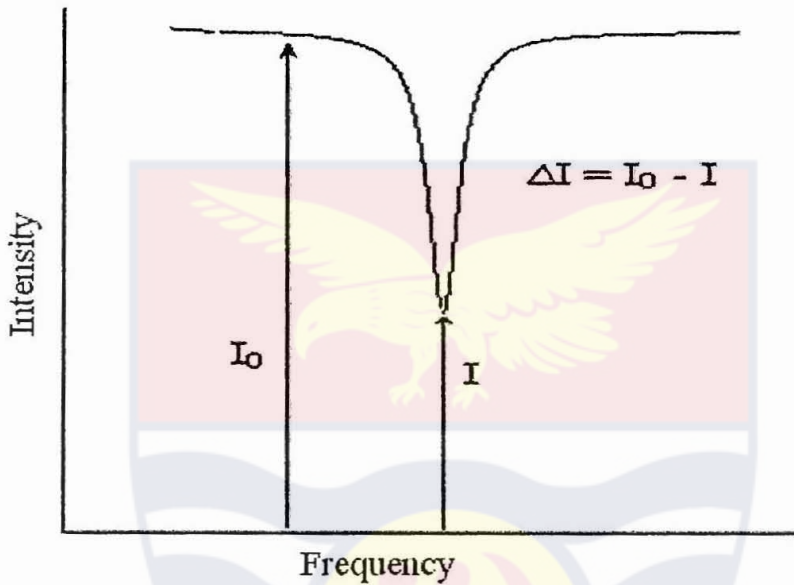
Figure 2. Gas absorption line showing original light intensity I_0 and the transmitted light intensity I.

The absorption cross-section can in turn be expressed as a function of a line-strength S and line-shape function Φ $(v-v_0)$ according to

$$\sigma(v) = S\Phi(v - v_0) \qquad (6)$$

where v_0 is the frequency at the line centre. The absorption cross-section is commonly expressed as absorption coefficient α (v) given as

$$\alpha(v) = \sigma(v)N \qquad (7)$$

where N represents the number density of the species present.

Different mechanisms exist that tend to contribute to broaden the linewidth of the absorption line (Demtröder, 2003). These mechanisms are classified into homogeneous ones, which are the same for all molecules, and nonhomogeneous ones, which act differently for different molecules. A basic broadening is always present and is a direct result of the Heisenberg uncertainty relation.

According to this relation, the limited lifetime of any state gives rise to a natural line width such that a state with an uncertainty in time, Δt will have a corresponding uncertainty in energy ΔE, and thus in frequency, Δv, expressed as

$$\Delta E \, \Delta t \geq h/4\pi \tag{8}$$

with the minimum energy, ΔE_{min} given in terms of Δv as

$$\Delta E_{min} = h \, \Delta v \tag{9}$$

In frequency units the natural line width, which is a homogeneous broadening, is given by

$$\Delta v_N = 2\Delta v = (2\pi\tau)^{-1}. \tag{10}$$

where τ is the mean lifetime of atom or molecule. This equation is true, since it can be shown that $\Delta t = \tau$. Under standard conditions this natural linewidth is in the order of 0.1 to 100 MHz.

The effective natural linewidth is dominated by thermal motion and collisions of the atoms and the molecules and is influenced by temperature, T, and the pressure, P, of the atoms or molecules. This is typical for gases. At low pressures, the varying velocities and flight directions of the particles under study cause different absorption frequencies within a certain interval. The line broadening resulting from different atoms or molecules, contributing to different parts of the

40

line profile, is called the Doppler broadening. The Doppler width Δv_D, with a full-width at half-maximum (FWHM) or half width of Δv, which is described by a Gaussian line shape, is

$$g_D(v - v_0) = \frac{2}{\Delta v_D} \left(\frac{In2}{\pi} \right)^{\frac{1}{2}} \exp\left\{ -\left[\frac{4(v - v_0)^2}{\Delta v_D^2} In2 \right] \right\}$$ (11)

with

$$\Delta v_D = 2v_0 \left(\frac{2kT \, In2}{Mc^2} \right)^{\frac{1}{2}},$$ (12)

v_0 is the central frequency of the source of radiation, R is the general gas constant with Boltzmann's constant k. M is the atomic weight and c the speed of light. The typical Doppler width in the visible range for a typical light source with T and M is about 10^3 MHz (or 10^{-3} nm) and in the infra-red (10 µm) the width is about 50 MHz (Svanberg, 2004).

With increasing pressure, collisions between different kinds of atoms results in pressure broadening, the Lorentzian broadening. The intensity distribution of such line broadening, with FWHM or half width of $\Delta v = (2\pi\tau)^{-1}$, is given by

$$I(v) = \frac{S}{\pi} \left(\frac{\Delta v}{\Delta v^2 + (v - v_0)^2} \right),$$ (13)

where τ is the effective lifetime of the excited state; generally much shorter than the actual lifetime, and S is the line strength.

The collisional width Δv_p (P, T) is calculated for any temperature and pressure using the relation

$$\Delta v_p(P,T) = \Delta v_p(P_0,T_0)\left[\left(\frac{P}{P_0}\right)\left(\frac{T_0}{T}\right)^{\frac{1}{2}}\right] \qquad (14)$$

The collisional width, Δv_p (P, T) of the resulting Lorentzian curve is about 0.5 to 5 GHz at atmospheric pressure and room temperature. At intermediate pressures, normally between 10 to 100 Torr, the spectral line will be described by the Voigt profile, which is a convolution of a Gaussian and a Lorentzian profile.

Scattering Spectroscopy

Interaction between optical radiation and small particles, such as atoms or molecules in which no energy is lost, results in a more complex mechanism. Scattering is said to have occurred when the photons from the laser do not match any energy level difference of the interacting matter. The scattered photons are redirected by the interacting matter into new directions. There are three kinds of scattering processes, namely, Rayleigh, Raman and Mie scattering. They are grouped based on the wavelength and the size of the scattering particles.

In cases where non-resonant laser radiation interacts with particles' sizes that are smaller than the wavelength of the laser radiation, Rayleigh scattering occurs. It is an elastic process meaning that the scattered photons have the same energy as the incoming ones. The condition for this type of scattering is expressed as

$$\lambda >> r \qquad (15)$$

where r is the radius of the atomic dimension, λ the wavelength.

42

Both Raman and Rayleigh scattering regain non-resonant radiation. However, in Raman scattering vibrational or rotational energy can be subtracted or added to the primary photon energy leading to an inelastic scattering process. In the case of Rayleigh scattering the molecule returns to the original energy level via a virtual excited state and a photon is produced with the same energy as the original one just like in the case of resonance absorption. The difference is that there is no time delay between the energy transitions and the emission of the photon.

If the incident photon supplies energy to the molecule that is not returned, then the molecule will have a net gain in energy and the emitted photon will have a lower energy, and we talk about Stokes Raman scattering. If, on the other hand, the molecule transfers energy to the photon we deal with anti-Stokes Raman scattering.

The average scattering cross-section, σ as a function of wavelength, λ is given by

$$\sigma(\lambda) = \frac{128\pi^5 \alpha^2}{3\lambda^4} \frac{6+3\delta}{6-7\delta} \tag{16}$$

with

$$\alpha = \frac{(n-1)}{2\pi N_0} \approx \frac{(n^2-1)}{4\pi N_0} \tag{17}$$

The N_0 is the density of molecules per unit volume at standard pressure and temperature, and δ is the depolarization factor. For n near unity, the Rayleigh scattering cross-section can be written as

$$\sigma_R = \frac{8\pi^3}{3} \frac{(n^2-1)^2}{\lambda^4 N^2} \tag{18}$$

showing a characteristic $1/\lambda^4$ dependence on the wavelength.

43

When the dimension of the particle is of the order of magnitude or greater than the wavelength of the radiation with which the light radiation interacts, the interaction is described by Mie scattering.

The average scattering angle distribution weighted over the probability of each scattering angle, is called the scattering phase function. It is expressed by

$$g = \int P(\theta)\cos\theta d\omega = \int_{4\pi} P(s,s')(s,s')d\omega. \qquad (19)$$

where $P(\theta)$ equals the probability of a photon being scattered in the direction θ, and $P(s,s')$ equals the probability of a photon coming in from direction s is redirected into direction s' (and the integration in equation (19) takes place over the full 4π steradian spherical geometry). When a sample material is illuminated by a light source, several of these scattering effects may occur simultaneously.

Most biological surfaces have a rough texture and therefore angles of incidence affect the light distribution within the media. This is as a result of gradual loss of photons of light across the surface due to increased reflection at larger angles of incidence, following Snell's law of reflection. In addition the interface between the two media will be subject to Snell's law of refraction, which determines the direction of the rays of light at the boundary of the various media. The initial encounter with a different index of refraction will be when entering the biological medium itself, and subsequently the inhomogeneities within the medium.

Absorption within Scattering Medium

In the presence of strong scattering due to particles the Beer-Lambert law is no longer valid, since it neglects the presence of other causes of light extinction

44

from absorption. Light scattered out of the probing light beam will normally not reach the detector. Extinction due to scattering by solids and liquids can be assumed to be varying slowly with wavelength, λ. In contrast, gases have sharp absorption lines.

Applying the principles of differential absorption – defined as part of the total absorption of any molecule "rapidly" varying with wavelength, then the gas absorption coefficient, $\alpha_a(\lambda)$ shows rapid variation with wavelength, λ. Thus, a more comprehensive description of the gas absorption in a scattering medium can be expressed as

$$I(\lambda) = I_i(\lambda)\exp\{-[\alpha_a(\lambda)c + \alpha_s(\lambda)]l\} \tag{20}$$

where $\alpha_a(\lambda)$ is the absorption coefficient due to the gas within the medium, $\alpha_s(\lambda)$ is the scattering coefficient due to the scattering of the medium, c is the concentration of the gas present in the medium and I_i is the intensity of the light before entering the scattering medium. Expressing intensity, $I_0(\lambda)$ of the light in the scattering medium in terms of the scattering properties of the medium as

$$I_0(\lambda) = I_i(\lambda)\{\exp[-\alpha_s(\lambda)l]\} \tag{21}$$

equation (20) can be written as

$$I(\lambda) = I_0(\lambda)\exp[-\alpha_a(\lambda)cl] \tag{22}$$

The technique of observing differential absorption is insensitive to extinction processes, which vary only slowly with wavelength, since such processes attenuate the total available light intensity; however, they have influence on the detection limit. Likewise slow variations in the spectral intensity of the light source or in the transmission of the optical system are also eliminated.

45

This procedure is only applied to species that contain reasonably narrow absorption features. This, thus, limits the number of molecules detectable by this technique. Care is also taken to ensure that the transmission of the instrument and the spectral response curve of the detector are only slowly varying functions of the wavelength. At short wavelengths, the usable spectral range of differential optical absorption is limited by rapidly increasing Rayleigh and Mie scattering.

For small concentrations, the measurement is between two large values of light intensities I and I_0. And in such cases, absorbance, A is small and therefore difficult to use direct absorption measurements in a finite path length, l. This is because near the absorption signals are noisy as a result of the inherent radiation source noise.

According to Beer-Lambert's law for small concentrations, the transmitted intensity can be approximated as

$$I(\lambda) = I_0(\lambda)[1 - \alpha_a(\lambda)cl] \tag{23a}$$

Therefore, the absorbance, A is given as

$$A = \frac{\Delta I}{I_0} = \alpha_a(\lambda)cl \tag{23b}$$

The limit of concentration detectability is determined by the path length and signal-to-noise ratio in the spectrum. Detectability is increased in direct response to reduction of the noise. The noise level is a function of the source intensity, the number of scans, the spectral resolution, the stability of the optical components, and especially the quality of the detector. Lowering the noise level in the spectrum

and increasing the size of the absorption features are the two ways to lower the detection limit for a given gas sample.

The detection limit for a particular substance depends on the differential absorption cross section, the minimum detectable absorbance, A and the length of the light path. In general A is determined by photoelectron statistics (short noise), which is a function of light intensity, and noise, B. Photoelectron shot noise is proportional to $N^{-1/2}$, where N is the total number of photons recorded around the center of the absorption line during the time interval t of the measurement (Sigrist, 1994).

The main approach used to increase the size of the spectral features is to lengthen the optical path. The principal limitation on the path lengthening is that it should not waste the available photons. So, while for a given minimum detectable absorbance the detection limit improves proportionally to the length of the light path, the actual detection limit will not always improve with a longer light path. This is because with a longer light path the received light intensity $I(\lambda)$ tends to become lower, increasing the noise associated with the measurements of $I(\lambda)$ and thus increasing the minimum detectable absorbance. A sensitive technique is employed to get the absorption signal out from the noise. The wavelength modulation technique has been considered to be one of the best ways for improving absorption sensitivity (Silver, 1992; Reid & Labrie, 1981).

Modulation Techniques in Laser Absorption Spectroscopy

Application of modulation in absorption spectroscopy is to increase the sensitivity in the optical measurement (Kluczynski & Axner, 1999). Different modulation techniques using diode lasers are amplitude and frequency modulations.

Amplitude modulation (AM) is accomplished by mechanically chopping the laser beam at frequencies not higher than a few kHz, which represent the highest modulation frequency of commercially available choppers. AM is combined with phase-sensitive detection. The AM signal is detected by a lock-in amplifier operating at the chopper frequency while the laser wavelength is slowly scanned across the absorbing feature. The minimal detectable change in absorbance with this method is low, generally not better than 10^{-3}. The slow wavelength scan makes this method susceptible to environmental fluctuations, such as temperature changes and atmospheric turbulence along the laser beam path. However, advantages with this method are the very simple set-up and that the measured spectrum provides absolute calibration, since the absorption feature is recorded together with the off-absorption light intensity.

Modulation of the diode laser drive current leads to the generation of sidebands in the laser field. If no molecular absorption is present there is a cancellation of the beat notes prodded between the sidebands and the carrier. If the laser field is scanned across an absorbing feature, the balance is lost and a beat signal appears which is detected by frequency and phase-sensitive electronics, either by lock-in amplifier or by a mixer.

Different frequency modulation (FM) techniques are very attractive in conjunction with diode lasers because of the ease with which such lasers can be modulated by applying an ac (modulation) current directly on the drive current. A strong reason for frequency modulation is to move the detection band into a higher frequency region, where the noise of different origins is strongly reduced.

Depending on the modulation frequency, the FM techniques are divided into three different subgroups, namely, wavelength-modulation spectroscopy (WMS), frequency-modulation spectroscopy (FMS), and two-tone frequency-modulation modulation spectroscopy (TTFMS). WMS makes use of modulation frequencies much lower than the halfwidth of the absorption line, FMS uses a modulation frequency comparable to or higher than the halfwidth, while TTFMS for technical convenience uses two modulation frequencies also comparable to or higher than the halfwidth, usually separated by a few MHz. For all FM techniques, WMS, FMS as well as TTFMS, the absence of a large and sometimes sloping intensity background in the FM is a great advantage. However, the recorded spectrum does not provide any absolute calibration which constitutes a drawback. Owing to this, a separate signal calibration has to be made.

FMS and TTFMS use much higher modulation frequencies than normally employed in WMS, typically in the radio-frequency region (0.1 – 3 GHz). In FMS and TTFMS only discrete components in the detection electronics are used (essentially a phase-shifter and a mixer), and a properly designed bias-T is essential to impedance match the sine-wave generator and the diode laser. The reason for applying FMS is two-fold: large modulation frequencies maximize the differential

49

absorption experienced by the sidebands and the laser excess noise is negligible at these frequencies. In TTFMS large modulation frequencies can be applied to maximize the differential absorption experienced by the sidebands. However, detection is performed at a lower beat frequency, typically in the MHz range, allowing the use of relatively inexpensive and low-bandwidth detectors and demodulation circuitry, which constitutes a technical convenience. A further advantage of TTFMS is that the phase-sensitive detection recovers the signal at a frequency that is different from those of the two signal generators. Thus, cross talk into the signal channel can be avoided, eliminating a potential noise source.

WMS usually employs modulation frequencies in the range $1 - 100$ kHz (low-frequency WMS) and sometimes also in the $1 - 10$ MHz (high-frequency WMS) region. Frequency and phase-sensitive detection can be made either at the fundamental frequency (1ν) or at some higher harmonics, second (2ν), third (3ν), etc. which produce lineshapes similar to the derivatives of the original absorption lineshape. This has given rise to the often used name derivative spectroscopy. Most frequent detection is at twice the modulation frequency (2ν). The implementation of low-frequency WMS is relatively simple: the modulation current is superimposed on the laser drive current directly via the diode laser driver and a commercially available lock-in amplifier is used for detection. This is the reason for the extensive use of this technique.

The wavelength modulation technique is one of the derivative spectroscopy methods for achieving a high signal-to-noise ratio and resolving problem of scattered light or stray effects in absorption spectroscopy. Although derivative

50

spectroscopy methods are basically identical, the trace-gas detection methods that use current-modulated diode lasers are generally separated into two categories, the wavelength modulation (WM) and frequency modulation (FM) techniques, depending on the order of magnitude of modulation in comparison with the width of the absorption feature (Reid et al., 1978; Reid & Labrie, 1981; Bomse et al., 1992; Supplee et al., 1994; Gustafsson et, al., 2000).

Derivative spectroscopy is a very widespread technique within the near-infra-red region for gas absorption. This is therefore important in near-infra-red spectroscopy, because the bands in the near-IR spectral range, as a rule, overtones or combination modes of fundamental modes in the mid-infra-red, and such overtones always have broader bands within which there are sharp absorption lines. In order to draw fine absorption bands out against a background of broad and mutually-overlapping bands, derivatives are used.

Wavelength modulation (WM) techniques are characterized by a modulation frequency υ that is much smaller than the line width of the absorption feature $\Delta\upsilon_{Line}$ ($\upsilon \ll \Delta\upsilon_{Line}$). Near atmospheric pressure, the absorption lines usually extend over several GHz (Rothman et al., 1992; Rothman et al., 1998) making WM techniques easier to implement than FM techniques in their single and two-tone varieties, where the modulation frequency υ is comparable or higher than the line width of the absorption feature $\Delta\upsilon_{Line}$ ($\upsilon \gg \Delta\upsilon_{Line}$).

The modulation frequencies generally used in WMS are generally between some kilohertz or some tens of kilohertz; whereas the FM amplitude $\Delta\upsilon$ is of the

same order of magnitude as the width of the analyzed absorption feature, that is, several gigahertzes at atmospheric pressure.

Harmonic signals are produced using tunable diode lasers (TDL) when a sinusoidal modulation of angular frequency ω_m is superimposed upon the diode current, resulting in a time variation of the diode frequency given by the expression

$$v(t) = \overline{v} + M \cos \omega_m t \qquad (24)$$

where $\overline{v}$ is the mean frequency of the time, t varying diode frequency and M, the sinusoidal modulation amplitude. The mean frequency $\overline{v}$ is slowly tuned by low frequency, ω_m ramping of the diode current. For modulate amplitudes of modulation, it can be assumed that the incident laser intensity is independent of frequency v over the narrow range of frequency required to modulate and tune over an isolated line in TDL experiments (Olson et al., 1980; Reid & Labrie, 1981; Iguchi, 1986). In harmonic detection, the concern is with weak absorption lines, and analysis is confined to values $\alpha'(v)l$, such that $\alpha'(v)l \leq 0.05$ (Reid & Labrie, 1981).

The time dependent term of $I(v(t))$, $\alpha'(\overline{v} + M \cos \omega_m t)$, is an even function of time and can be expanded in a cosine Fourier series as

$$\alpha'(\overline{v} + M \cos \omega_m t) = \sum_{n=0}^{\infty} A_n(\overline{v}) \cos n\omega_m t \qquad (25)$$

where $A_n(\overline{v})$ is the nth Fourier component of the modulated absorption coefficient and $\overline{v}$ is considered to be constant over a modulation period.

If the modulation amplitude M is sufficiently small the Fourier components can be expressed as (Reid & Labrie, 1981)

$$A_n(\bar{v}) = \frac{2^{1-n}}{n!} M^n \frac{d^n \alpha(v)}{dv^n}\Bigg|_{v=\bar{v}}, \qquad n \geq 1 \qquad (26)$$

This small amplitude limit is often referred to as derivative spectroscopy as the output signals are proportional to the derivatives of the absorption line.

Individual Fourier components of the detected laser beam, after passing through the sample, can be selected using a lock-in amplifier set to detect at the nth harmonic of the modulation frequency, ω_m provided the time constant of the low-pass filter of the lock-in amplifier is substantially longer than the period of the modulation (Iguchi, 1986). In this case the processed signal S(nv) is proportional to

$$S(nv) = \Delta I = I_0 A_n(\bar{v})l, \qquad n \geq 1 \qquad (27)$$

Wavelength modulation spectra are normalized by I_0 to directly match the Beer-Lambert law.

Equation (26) can be rewritten as

$$\frac{v(t) - v_0}{\Delta v} = \frac{\bar{v} - v_0}{\Delta v} + \frac{M}{\Delta v} \cos \omega_m t = k + m \cos \omega_m t, \qquad (28)$$

where v_0 is the central frequency and Δv the half width at half maximum (HWHM) of the absorption line. The k and m are defined as

$$k = \frac{\bar{v} - v_0}{\Delta v} \qquad (29)$$

and

$$m = \frac{M}{\Delta v} \qquad (30)$$

This normalized modulation amplitude, m is called the modulation index.

The case where the gas pressure broadening dominates the absorption line, $\alpha'(v)$, described by a Lorentzian function and absorption coefficient at line centre normalized to unity, is given by

$$\alpha'(k,m)_L = \frac{1}{1+\left(k+m\cos\omega_m t\right)^2} \tag{31}$$

Examples of a direct absorption signal, the first derivative signal, $S(1v)$ and the second derivative signal, $S(2v)$ of α (v) described by a Lorentzian function are shown in Figure 3.
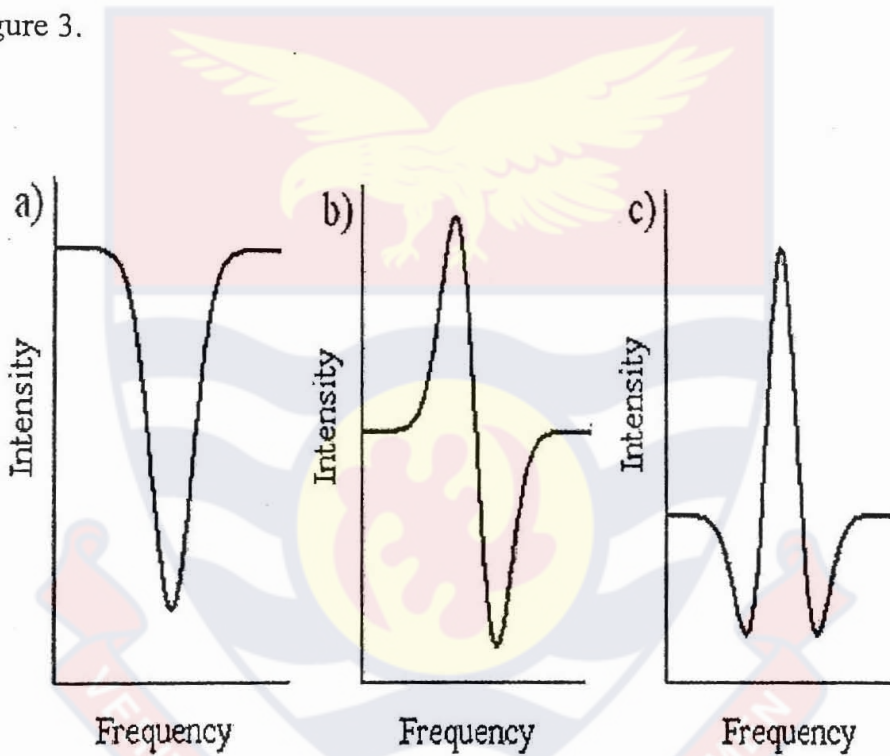
Figure 3. Plots of intensity verses frequency for various absorption signals. a) direct absorption signal without derivative, b) first derivative signal, $S(1v)$ and c) the second derivative signal, $S(2v)$ of α (v) described by a Lorentzian function.

When Doppler broadening is dominant, the absorption line, $\alpha'(v)$, described by a Gaussian function, is given by

$$\alpha'(k,m)_{G} = \exp\left[-\ln2(k + m\cos w_m t)^2\right] \qquad (32)$$

The differences between Gaussian and Lorentzian line shapes are seen at small and large values of m but the general behaviour is similar, in particular at a specific value of m, the two line shapes have common maximum second derivative signal, $S(2v)$ (Reid & Labrie, 1981).

WMS shifts the detection bandwidth from dc, where measurements are limited by the excess $(1/v)$ noise, to frequencies where radiation-induced detector shot-noise is instead the limiting factor (Cooper & Gallagher 1985). This method involves the superposition of a small modulation at frequency v on the radiation injection current (Jacobsen et al., 1982).

Typically, the amplitude of the current modulation is comparable to the width of the spectral feature under study. As the laser beam traverses the sample, optical absorption by the target gas convert some of the wavelength modulation into amplitude modulation of the laser intensity.

This induced amplitude modulation occurs at the modulation frequency v and its integral harmonics, nv ($n = 1, 2 \ldots$). Phase-sensitive electronics, such as lock-in amplifier, are used to demodulate the detector photocurrent at a selected harmonic of the modulation frequency (typically $n = 2$).

By implementing this technique at sufficiently high frequencies, excess laser noise is minimal and detector-limited sensitivity is achieved. Although the optimum frequencies are laser dependent, studies have shown that detection frequencies as low as 50 kHz are often sufficient to achieve these objectives (Silver & Kane, 1999; Sjöholm et al., 2001; Somesfalean et al., 2002).

The second harmonic signals, $S(2v)$ produced by *WMS* are directly proportional to absorbance, but the factor relating the $2v$ signal to absorbance at line centre is best determined by direct experimental calibration. Ideally, such calibration is done by comparing a direct transmission measurement of absorption with a $2v$ measurement for the specific absorption feature under study or by calibrating the $2v$ signal directly to a known gas concentration (Silver & Kane, 1999; Somesfalean et al., 2002).

Studies have shown that signal-to-noise ratios (SNRs) of WMS can be more easily accounted for; generally they vary inversely with the square root of the bandwidth approaching megahertz rates, so that high bandwidth detection can be obtained with moderate degradation of the signal. Due to the high frequency modulation capacities of diode lasers, detection bandwidths approaching megahertz rates are feasible for major species such as water and methane that have large line strengths (Silver & Kane, 1999; Andersson et al., 2006).

Gas in Scattering Medium Absorption Spectroscopy (GASMAS) Technique

In contrast to solids and liquids, free gases exhibit exceptionally sharp absorptive features. Solids and liquids have slow wavelength dependence due to their absorption and scattering properties. Therefore, detected radiations in bulk materials are not influenced when the wavelength of a single-mode probing laser is slightly changed. However, detecting these gas species in highly scattering media of relatively small geometric dimensions is one of the difficult tasks since the concentration and especially the optical path lengths are relatively very short.

Using modulation techniques, even in the presence of a large background, the implanted gas gives rise to tiny but narrow signal that can be picked and this gave birth to a measuring technique known as gas in scattering medium absorption spectroscopy (GASMAS) (Sjöholm et al., 2001).

The GASMAS technique provides new opportunities for studying gas enclosures in natural and synthetic materials. This new technique can be used for characterization and diagnostics of free gas in scattering solids and turbid liquids. Initial demonstrations included proof of-principle measurements of the embedded oxygen concentration relative to an equivalent column of air and of the internal gas pressure as well as assessment of the gas exchange.

For any ambient gas absorption measurement technique to be useful, there are some basic but very important requirements that the technique must fulfill. It must be sufficiently sensitive to detect the gas under consideration and be specific, which means that the result of the measurement of a particular gas must be neither positively nor negatively influenced by any other trace gas species simultaneously present in the probed volume of air. Given the large number of different molecules present in air, this is not a trivial condition.

Simplicity of design and use of the instruments based on it; capability of real-time operation and the possibility of unattended operation and dependence of the measurement on ambient conditions are further considerations. In fact, these are the conditions characterizing the new gas in scattering medium absorption spectroscopy (GASMAS) method.

The absorption and scattering cross sections of the bulk materials display slow wavelength dependence; thus these properties are assumed to be constant over the wavelength range tuned, making the technique similar to differential absorption spectroscopy. Wavelength modulation techniques are used to increase the detection sensitivity and to discriminate effectively against background signals, allowing for detection of around absorption fractions of the light received.

The laser source for this technique fulfills two different groups of requirements: from the physical point of view it is tunable, single mode and it is possible to modulate its emission frequency; from the practical point of view the laser is small, simple to handle, reliable and, relative cheap. Thus diode lasers are very suitable.

Further consideration as far as the single mode operation is concerned is that, usually the investigation is done on light gas molecules at room temperature and pressure, so that linewidths are of the orders of GHz. The technique does not accept multimode emission from diode laser, as the different modes have spacing of hundreds of GHz and there is a power competition among them.

It is always advantageous to remove any baseline, especially during a calibration, that is, any constant level in the independent data, so that the variations in the data are favoured over the absolute levels. This is reason why the $2v$ signal becomes very important in this technique.

In a scattering medium, the mean path length, l_{spl} of the light is much longer than the straight injection-detection distance of the light, or the geometrical dimensions of the scattering material as a result of the scattering. There will be a

58

larger probability to find more gaseous molecules in a highly scattering material, since the light will travel a longer distance along more complicated pathways. Therefore, the effective gas absorption in the scattering medium can be related to the concentrations in a column of free air.

As consequences of the scattering, the absorption cross section is considered to be the sum of two cross sections, one that varies slowly with the wavelength, for instance, describing a general slope. The other one varies rapidly with wavelength due to an absorption line. The extinction due to the scattering is slowly varying with wavelength, which is the characteristic of solids and liquids. Thus, this technique describes the part of the total absorption where any molecular absorption "rapidly" varying with wavelength – differential absorption.

As the diode laser wavelength is selected, basically by generally scanning across the gas absorption feature, the full absorption profile is acquired and fitted to calibrate or as a reference spectra for the determination of the absorbance. From the Beer-Lambert law for small gas concentrations, absorbance in this case is given by

$$A_s = \Phi_a(\lambda)cl \qquad (33)$$

which is proportional to the strength of the $2v$ wavelength modulation spectroscopy signal, S_{WMS}, as shown in Figure 4, as long as the absorption is small. The amplitude of the $2v$ signal is dependent both on the relative differential absorption due to the gas of interest and the amount of light reaching the detector, i.e. the absolute size of the absorption dip. Thus, for standardization, the $2v$ signal is normalized using the direct signal, S_{Dir}. This normalized signal is referred to as the GASMAS signal and is denoted GMS, i.e.
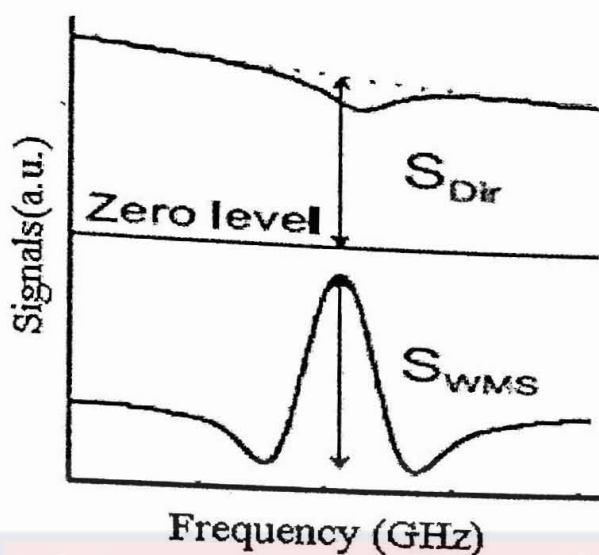
Figure 4. Second harmonic component (*2v*) of WMS signal and its corresponding pure absorptive imprint (Alnis et al., 2003).

$$GMS = \frac{S_{WMS}}{S_{Dir}} \qquad (34)$$

Thus, the GMS is also proportional to the absorbance as long as the absorbance is small. The S_{WMS} is calculated from the peak-to-peak value of the *2v* signal.

One simple way of calibrating the arbitrary GMS and transform it into a more meaningful quantity is by using the method of standard addition or by performing a long-path measurement, where the direct absorption signal would be strong enough for observation.

If an equivalent absorbance of the gas in the scattering medium is equated to that in air, then

$$c_{air}L_{eq} = c_{sm}l, \qquad (35)$$

where c_{air} and c_{sm} are the gas concentrations in air and in the scattering medium respectively, which in this case are the same. Therefore, L_{eq} represents the

equivalent distance in air that results in the same absorbance as that detected in the scattering medium, referred to as the equivalent mean path.

The equivalent mean path length, L_{eq} is determined by the standard addition technique commonly used in physical chemistry. In this technique, known amounts of the species of interest are added to the sample species of unknown concentration which can then be evaluated. The L_{eq} depends on both the concentration of the gas and the scattering coefficient of the scattering material.

The gas concentration c_{sm} in the scattering medium can be extracted if l is separately determined by using temporally resolved measurement, where the time history of the photons traversing the sample is monitored (Somesfalean et al., 2002). With the known absorption coefficient of the trace gas and the GMS value, the c_{sm} is calculated. High gas content and strong scattering properties in not too small samples are the major factors leading to high GMS values.

In performing measurements with the proposed technique, two basic geometric configurations can be considered; one is a trans-illumination arrangement and the other one a reflection scheme as shown in Figure 5.
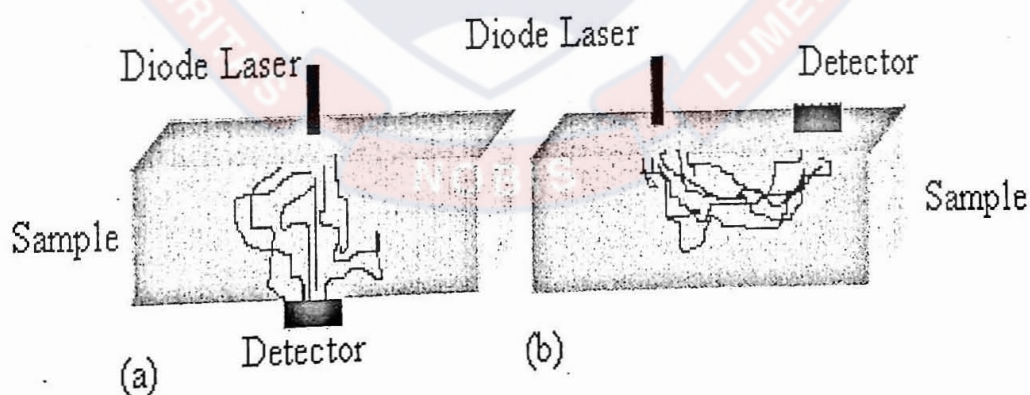
Figure 5. Two basic geometric configurations for gas in scattering media absorption spectroscopy; (a) trans-illumination and (b) reflection scheme.

This procedure can only be applied to species the spectrum of which contains reasonably narrow absorption features. This technique is insensitive to extinction processes, which vary only slowly with wavelength, like those due to solid and liquid particles. Since such processes attenuate the total available light intensity, however, they have a strong influence on the detection limit. Likewise, slow variations in the spectral intensity of the light source or in transmission of the optical systems are eliminated.

Measurements of the GASMAS type are useful for analyzing the gas diffusion properties of porous materials. By monitoring the rate at which gaseous molecules re-invade a sample previously exposed to a different gas, diffusion coefficients can be evaluated. Such gas transport studies using the GASMAS technique have also been demonstrated (Somesfalean et al., 2002).

A limitation associated to this technique is that, the scattering material and other compounds in the medium should not be in the absorption range of the light source. Water is widely distributed in all types of biological tissues and strongly absorbs light for wavelength larger than 1400 nm (Svanberg. 2004). Thus, this technique works very well in wavelength well below this limit. Likewise, in human tissue, hemoglobin absorbs strongly below 600 nm. and longer wavelength must be employed.

Fluorescence Phenomenon

Excitation of a molecule by a photon, which occurs as a result of the interaction of the light wave with electrons in the molecule, can only occur with

62

incident light of specific wavelengths falling on absorption bands of the molecule. In the decay of the excited state several processes may be involved.

When molecules emit light from electronically excited states after the excitation of the molecule by ultraviolet or visible light photon it results in Photoluminescence. The electronic configuration of the excited state and the pathway of emission from the molecule determine the type of photoluminescence, which is made up of fluorescence and phosphorescence.

Fluorescence is an emission process from a singlet excited state and emitted photons due to radiationless relaxation in the excited state have longer wavelength than the excitation wavelength. Molecules that emit fluorescence light are usually called fluorophores (or fluorescent molecules) and the characteristic time that a molecule remains in an excited state prior to returning to the ground state is called fluorescence lifetime and is an indicator of the time available for information to be gathered from the emission profile. Fluorophores may undergo conformational changes and/or interact with the surrounding molecules for the duration of the excited state lifetime.

The electronic states of a fluorescent molecule (fluorophore), especially for biological molecules, can be described by a Jablonski energy diagram (Lakowicz, 1999), as shown in figure 6. This illustrates an excitation from the ground singlet state S_0 to the excited singlet states S_1 and S_2. A molecule rapidly relaxes down to the lower level of S_1 or S_2 by internal conversion (IC), which is a non-radiative process. De-excitation to the ground singlet state S_0 can result in the emission of a fluorescence photon or can occur through internal non-radiative conversion.

63
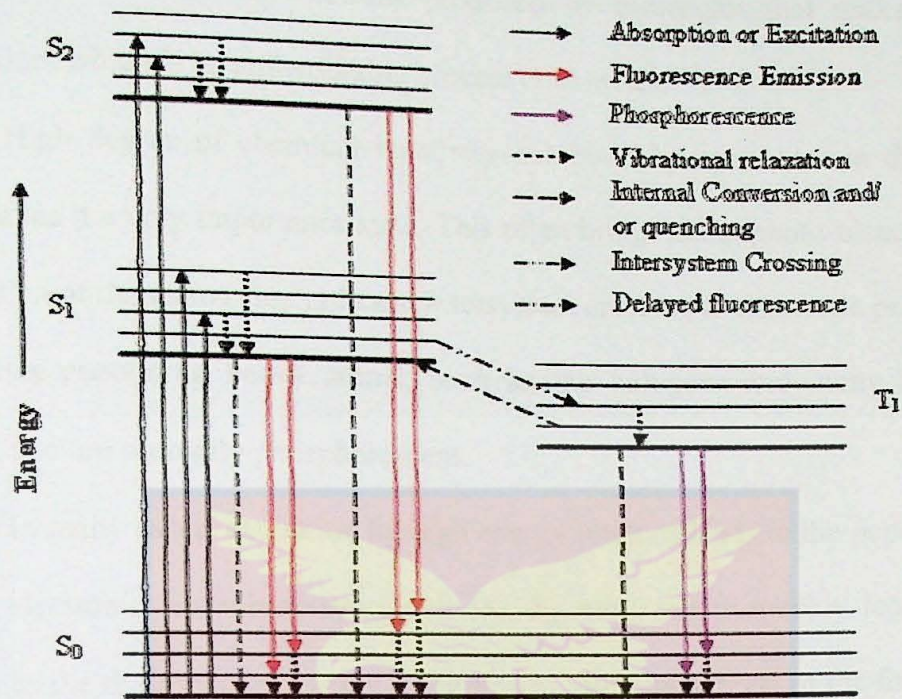
Figure 6. A typical Jablonski diagram illustrating the ground singlet state S_0, first excited singlet state S_1 and the second excited singlet state S_2, and the excited triplet state T_1 [Modified after (Lakowicz, 1999)].

The relaxation can take place to any vibrational level in S_0 and hence the total fluorescence from the molecule will not be a sharp peak at one distinct wavelength, but a broader distribution.

From the excited state S_1, a transition can also take place to a triplet state T_1, even though this is spin-forbidden and the transitions from the triplet state T_1 back to S_0 are also spin-forbidden. Thus, it will take a relatively long time before the molecules relax, through internal conversion and or by emission of a photon, a process called phosphorescence, which is similar to fluorescence, but with a much longer time constant (Lakowicz, 1999). The probability for intersystem crossing is

low due to the unpaired electrons produced by molecules that undergo spin conversion, which is an unfavourable process (Lakowicz, 1999).

High degree of chemical reactivity exhibited by molecules in the triplet state makes it a very importance state. This often brings about photo-bleaching and production of damaging free radicals. Intersystem crossing is also made possible by molecules containing heavy atoms, such as the halogens and many transition metals, and are normally phosphorescent.

In many cases, excitation by high energy photons leads to the population of higher electronic and vibrational levels (S_2, S_3, etc.), which quickly loose excess energy as the fluorophores relaxes to the lowest vibrational level of the first excited state. Some fluorophores emit from higher energy states.

As noted, since some energy is lost in the non-radiative relaxations, fluorescence has a lower energy and thus a longer wavelength than the exciting photon. The maximum wavelengths difference between the excitation and emission spectra of a particular fluorophore is well-known as the Stokes shift. The molecular structure of the molecule determines the size of the Stokes shift. The value of the shift can range from few to over several hundred nanometers. Fluorescein for example has a Stokes shift of approximately 20 nm, while quinine has a shift of 110 nm and that for the porphyrins is over 200 nm (Lakowicz, 1999).

Fluorescence quantum yield, defined as the probability that an excited fluorophore will produce fluorescence, of a given fluorophore varies with its environmental factors. These factors include interactions between the fluorophore and surrounding molecules and the localized concentration of the fluorescent

species. The effects of these factors vary widely from one fluorophore to another (Lakowicz, 1999). The fluorophore in the excited state can be considered as completely different as in the ground state, and thus can display an alternate set of properties in regard to interactions with its environment in the excited state relative to the ground state.

Most natural and artificial samples exhibit auto-fluorescence or endogenous fluorescence, that is, fluorescence from natural fluorophores (Svanberg, 2004). Fluorescence distributions, under UV light irradiation, from several fluorophores yield a broad UV and visible wavelength distribution. With visible light irradiation, fluorophores yield a broad fluorescence in the visible and sometimes in the near infrared region. The signal-to-noise ratio for fluorescence signals is frequently high, providing a good sensitivity to the process. In complex biological systems, due to energy transfer or the presence of a quenching agent, fluorescence may vary locally over a wide range, resulting in intensity fluctuations or spectral shifts. Different fluorophores have different decay times and the same fluorophore may have different spectra and decay times under different conditions which can be of diagnostic value. Thus, fluorescence is specific and selective in nature, which makes the phenomenon an important tool for discrimination.

A conventional fluorescence spectrum is fluorescence intensity against emission wavelength at a fixed wavelength or fluorescence intensity received within a fixed spectral band as a function of the excitation wavelengths. More generally, a fluorescence emission and excitation spectrum is a three-dimensional representation, fluorescence intensity as a function of both the excitation and the

emission wavelengths. The method offers a fundamental improvement in the sensitivity and reliability of detection, especially when multiple fluorophore are present in the same location.

Fluorescence spectra from natural molecules are very complex and the contributions from the different fluorophore can usually not be separated. Different excitation light sources may decrease the overall intensity of the fluorescence spectrum without changing its shape. Naturally, the shape of the spectrum depends on the excitation wavelength, since this determines what energy transitions in the fluorescence are possible.

Several other relaxation pathways that have varying degrees of probability compete with the fluorescence emission process. The excited state energy can be dissipated non-radiatively as heat. The excited fluorophore can also transfer energy to another molecule in different types of non-radiative process, such as quenching and photo-bleaching. The two phenomena are distinct in that quenching is often reversible whereas photo-bleaching is not.

Quenching arises from a variety of competing processes that induce non-radiative relaxation of excited state electrons to the ground state, which may be either intra-molecular or inter-molecular in nature. Most quenching processes act to reduce the excited state lifetime and the quantum yield of the affected fluorophore and thus lower fluorescence emission dramatically or, in some cases, completely eliminate it. A common example of quenching is observed with the collision of an excited state fluorophore and another (non-fluorescent) molecule in its environment, resulting in radiationless deactivation of the fluorophore and its return

to the ground state. In most cases, neither of the molecules is chemically altered in the collisional quenching process. The mechanisms for collisional quenching include electron transfer, spin-orbit coupling, and intersystem crossing to the excited triplet state.

A second type of quenching mechanism, termed static or complex quenching, arises from non-fluorescent complexes formed between the quencher and fluorophore that serve to limit absorption by reducing the population of active, excitable molecules. This effect occurs when the fluorescent species form a reversible complex with the quencher molecule in the ground state, and does not rely on diffusion or molecular collisions. In static quenching, fluorescence emission is reduced without altering the excited state lifetime. A fluorophore in the excited state can also be quenched by a dipolar resonance energy transfer mechanism when in close proximity with an acceptor molecule to which the excited state energy can be transferred non-radiatively. In some cases, quenching can occur through non-molecular mechanisms, such as attenuation of incident light by an absorbing species, including the fluorophore themselves.

Scattered excitation light can also interfere with the fluorescent signal in the detection arm in the form of quenching. This scattered light is mostly generated by the Rayleigh scattering of the excitation light and its effect becomes more significant at low concentrations of the fluorophore when the fluorescent light intensity becomes comparable with the intensity of scattered light

Photo-bleaching occurs when a fluorophore permanently looses the ability to fluoresce due to photon-induced chemical damage and covalent modification.

Upon transition from an excited singlet state to the excited triplet state, fluorophores may interact with another molecule to produce irreversible covalent modifications. The triplet state is relatively long-lived with respect to the singlet state, thus allowing excited molecules a much longer time frame to undergo chemical reactions with components in the environment. The average number of excitation and emission cycles that occur for a particular fluorophore before photo-bleaching is dependent upon the molecular structure and the local environment. Some fluorophores bleach quickly after emitting only a few photons, while others that are more robust can undergo thousands or millions of cycles before bleaching (Lakowicz, 1999).

Photo-bleaching is reduced by limiting the exposure time of fluorophores to illumination or by lowering the excitation energy. These techniques can also reduce the measurable fluorescence signal. Limiting exposure of the fluorophores to intense illumination has been found to be the best protection against photo-bleaching (Lakowicz, 1999).

Quantitative fluorescence dynamic measurements enable investigators to distinguish between fluorophores that have similar spectral characteristics but different decay constants and can also yield clues to the local environment. In addition, dynamic measurements are less sensitive to photo-bleaching artifacts than are intensity measurements (Lakowicz, 1999).

Fluorescence from fluorophores is studied either by varying the excitation wavelength while detecting the emissions at a fixed wavelength, producing excitation spectra, or by a fixed excitation wavelength and the fluorescence being

69

detected at different wavelengths, resulting in fluorescence emission spectra. Excitation spectra can be helpful in indicating the most appropriate wavelength (Lakowicz, 1999), in laser-induced fluorescence studies.

Laser-Induced Fluorescence (LIF) is the fluorescence emission from atoms or molecules that have been excited to higher energy levels by absorption of laser radiation. In the laser-induced fluorescence technique, a laser is tuned to the allowed dipole transition from a lower to an upper state of the fluorophore under consideration, and the fluorescence light that is emitted during the subsequent decay is observed. Laser-induced fluorescence methods can make use of pulsed or continuous lasers for steady state and dynamic processes.

Lasers with wavelength ranging from UV to visible have been used in both laboratory and field fluorosensors or fluorometers (Svanberg, 2004). With the advent of the diode lasers, these fluorosensors have become compact for easy handing especially in areas such as environmental protection, medical or agricultural technologies (Lang et al., 1995; Barócsi et al., 2000; Gustafsson et al., 2000; Anderson et al., 2004). Fluorosensors using diode lasers have now become relatively inexpensive compared to the conventional ones, which use excitation sources like Nd:YAG lasers and nitrogen lasers.

Important instrument considerations in fluorescence measurement are the type of application and site, e.g. research, monitoring or control in laboratory or field measurements, method of sensing-remote or contact- and versatility including, e.g., portability and measurement options availability of programmable on-board calculation (Barocsi et al., 2000). Fluorescence measurements can either

be performed by point measurements or in an imaging geometry. Point measurements involve the collection of spectroscopic information in a small fluorophore area, frequently using an optical fibre probe to guide the excitation to the sample and to collect the fluorescence emission.

Chlorophyll Fluorescence

Light energy absorbed by carotenoids and chlorophylls, the photosynthetic pigments of green leaves, is primarily used for photochemical quantum conversion in photosynthesis, whereas only small proportions are re-emitted as chlorophyll fluorescence light or heat depending on the intensity of the illuminated light (Krause & Weis, 1984; Govindjee et al., 1986). The ultrastructure of the leaves, the pigment composition and the function of the chloroplasts, which contains the chlorophylls and carotenoids, can efficiently be adapted either to high light or to low light conditions (Lichtenthaler, 1981).

The light-absorbing pigments that act as antenna collect photon energy and funnel it efficiently to reaction centres. The excitation energy antenna molecules are transferred to the reaction in picoseconds. This time period is significantly shorter than the excited-state lifetime (nanoseconds range) thus allowing almost all the absorbed photon energy to reach the reaction centre where it is used to perform appropriate photochemistry.

There has been a demonstration that at least one of the steps in photosynthesis is under genetic control (Levine, 1968). This genetic control of photosynthesis can be envisaged as proceeding along two pathways. First, the

control can be direct. For example, there may be genetic control over the synthesis of enzymes specifically involved in photosynthetic reactions. This control may be independent of a second pathway in which genetic changes in chloroplast structure alter the site of photosynthesis as to affect numerous photosynthetic reactions.

A leaf may not be able to carry out certain light-requiring reactions of photosynthesis if it possesses genetic blocks that lay along the first pathway. In the case of the second pathway, the leaf pigments may be altered or the leaf may be pigment-deficient, and therefore are mutants which act indirectly on photosynthesis. Genetic alteration at a locus may control the process of photosynthesis. A mutation at this locus may result in either a genetic uncoupling of photosynthetic phosphorylation or a disruption of electron transfer below the level of the release of molecular oxygen. There is also the possibility of a genetic block affecting acceptors of phosphate from adenosine triphosphate.

In nature the condition for chlorophyll fluorescence from leaves and plants is found at sun light exposure. However, because chlorophyll absorption bands possess a wide spectral range, different artificial light sources such as lasers light, light emitting diodes (LEDs) and lamps, covering the 300 – 650 nm range (Barocsi et al., 2000; Gustafsson et al., 2000;Anderson et al., 2004; Ek et al., 2008) have been used as sources of excitation for chlorophyll fluorescence. The wavelength of the excitation especially if it is long influences the shape of the chlorophyll fluorescence emission.

Important features of an instrument for chlorophyll fluorescence depend on the type of application and measurement conditions. A compact and portable

analytical instrumentation deployable in the laboratory and in the field is very attractive. Size of the light source and other components of the instrument obviously become very important.

When the emitted chlorophyll fluorescence intensity or the chlorophyll fluorescence yield is measured as a function of the wavelength, the chlorophyll fluorescence signal is referred to as the chlorophyll fluorescence spectrum. When chlorophyll fluorescence light is monitored as a function of time the study is termed chlorophyll fluorescence induction kinetics (Kausky effect) (Govindjee, 1995). Factors, such as temperature, carbon dioxide concentration, water radiant energy flux rate, and their interactions that affect the rate of photosynthesis, influence chlorophyll fluorescence spectra and induction kinetics.

Light, which is significantly essential for photosynthesis, can cause severe physiological stress when provided in excess. If a very high intensity light is delivered to the fluorophore, it renders the fluorophore unable to fluoresce, a phenomenon termed photobleaching. In the process of photobleaching free oxygen radicals are produced which cause visible tissue damage. However, chlorophyll fluorescence lifetimes are independent, to a larger extent, of the photobleaching of the fluorophore. On the other hand, this stress occurs when other factors, such as excess or limited water, very low or extreme temperatures, reduce rates of photosynthesis. In this situation the leaf is unable to utilize the absorbed light energy, a phenomenon termed photoinhibition.

However, the process of photosynthesis is also self regulatory, because carotenoids act as quenchers and dispose off the absorbed excess photon energy

73

analytical instrumentation deployable in the laboratory and in the field is very attractive. Size of the light source and other components of the instrument obviously become very important.

When the emitted chlorophyll fluorescence intensity or the chlorophyll fluorescence yield is measured as a function of the wavelength, the chlorophyll fluorescence signal is referred to as the chlorophyll fluorescence spectrum. When chlorophyll fluorescence light is monitored as a function of time the study is termed chlorophyll fluorescence induction kinetics (Kausky effect) (Govindjee, 1995). Factors, such as temperature, carbon dioxide concentration, water radiant energy flux rate, and their interactions that affect the rate of photosynthesis, influence chlorophyll fluorescence spectra and induction kinetics.

Light, which is significantly essential for photosynthesis, can cause severe physiological stress when provided in excess. If a very high intensity light is delivered to the fluorophore, it renders the fluorophore unable to fluoresce, a phenomenon termed photobleaching. In the process of photobleaching free oxygen radicals are produced which cause visible tissue damage. However, chlorophyll fluorescence lifetimes are independent, to a larger extent, of the photobleaching of the fluorophore. On the other hand, this stress occurs when other factors, such as excess or limited water, very low or extreme temperatures, reduce rates of photosynthesis. In this situation the leaf is unable to utilize the absorbed light energy, a phenomenon termed photoinhibition.

However, the process of photosynthesis is also self regulatory, because carotenoids act as quenchers and dispose off the absorbed excess photon energy

73

before photo oxidation damage can occur as a result of strong absorption (excess photon harvesting) during periods of high irradiance such as midday (Govindjee and Coleman, 1990).

Laser-induced Chlorophyll Fluorescence Spectra

Chlorophyll fluorescence emission from leaves excited by laser radiation is commonly termed laser-induced chlorophyll fluorescence (LICF). Laser-induced fluorescence methods make use of pulsed or continuous wave (CW) lasers for steady and dynamic processes. The laser-induced chlorophyll fluorescence emission spectrum of leaves is characterized by red band, 630 -700 nm and far-red band, 700 – 800 nm as shown in Figure 7.
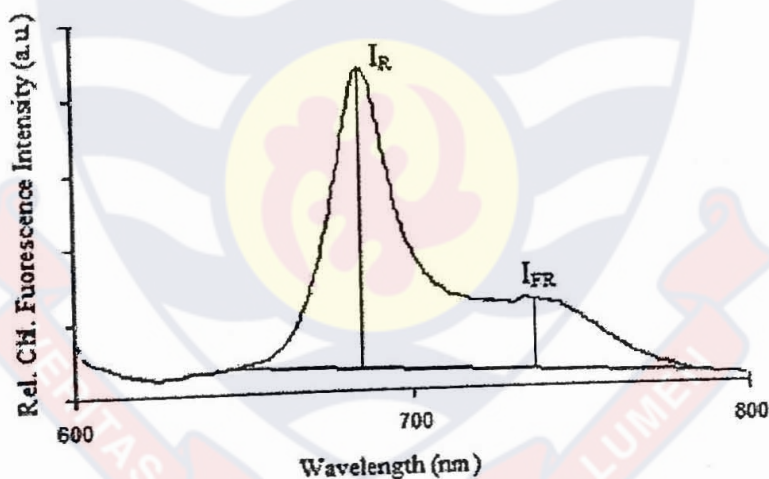
Figure 7. Chlorophyll fluorescence emission spectrum of a leaf excited with 396 nm laser light (Anderson et al., 2004).

Under ultraviolet (UV) laser light excitation, intact leaves emit red fluorescence (RF), a far-red   fluorescence (FRF) from chlorophyll a, and blue-green

74

fluorescence (BG) from hydroxycinnamic acids and other pigments, which are little known, within the 630 -700 nm, 700 – 800 nm and 400 – 500 nm regions, respectively (Harris & Hartley, 1976; Chappelle et al., 1984; Chappelle et al., 1985; Chappelle & Williams, 1986; Lang & Lichtenthaler, 1990; Stober & Lichtenthaler, 1993; Stober et al., 1994; Buschmann & Lichtenthaler, 1998; Cerovic et al., 1999; Meyer et al., 2003).

The chlorophyll fluorescence emanates from mesophyll chloroplasts and depends not only on the chlorophyll contents, but also on the flavonoid contents the epidermis that screen UV-excitation of the mesophyll (Day et al., 1994; Bilger et al., 1997; Ounis et al., 2001) and they can influence the leaf fluorescence signature. The peak wavelength within these bands depends on the leaf type and other factors (Lichtenthaler, 1986, 1988; Lichtenthaler & Rinderle, 1988 a,b; Rinderle & Lichtenthaler, 1988). Due to this screening, the UV light cannot penetrate much into the leaf and therefore the chlorophyll fluorescence is only coming from the surface of the leaf and the intensity of chlorophyll fluorescence is fairly low when excited with UV light (Lichtenthaler et al., 2005).

In contrast, excitation from violet-blue or red regions, where the photosynthetic pigments exhibit their main absorption, has been found to produce stronger chlorophyll fluorescence emission. However, the violet-blue and red radiation penetrates the leaf mesophyll to different degree and depth due to the same screening effect but with lower dependence as compared to UV light. The violet-blue radiation is not only absorbed by chlorophylls but also by carotenoids, and therefore passes into the leaf mesophyll to a lower degree than the red

excitation radiation being absorbed only by the chlorophylls. For this reason the violet-blue and red radiation induced chlorophyll fluorescence emission spectra have different shapes (Lichtenthaler & Rinderle, 1988, 1988b; Rinderle & Lichtenthaler, 1988). This is because the red radiation induced red band chlorophyll fluorescence, also emitted in the deeper mesophyll part of the leaf, and is reabsorbed by the absorption bands of the intact chlorophyll a to a higher degree than the violet-blue radiation induced chlorophyll fluorescence, which primarily emanates from the upper leaf parts (Lichtenthaler & Rinderle, 1988; Buschmann & Lichtenthaler, 1998).

In leaf tissue with densely packed chloroplasts, re-absorption strongly lowers the red band relative to far-red emission. It has been shown that the chlorophyll fluorescence spectral shapes of leaves are closely connected to the inner organic constituents through interlinked absorption, re-absorption, scattering and emission process (Saito et al., 1998).

Furthermore, irradiance from excitation sources of shorter wavelengths for example UV sources, compared to that from the longer wavelengths, reaches the leaf mesophyll only at the upper outer mesophyll range next to the upper epidermis (Lichtenthaler et al., 2005). Hence, the chlorophyll fluorescence signature and the information obtained from it is principally representative for a small chloroplast layer of the upper outer leaf. Thus, the chlorophyll fluorescence yield strongly depends on the wavelength of the excitation radiation.

The red chlorophyll fluorescence peak decreases with increasing chlorophyll content due to preferential re-absorption of the emitted red

fluorescence by the intact leaf chlorophyll (Lichtenthaler, 1990; Krause & Weis, 1991). Simultaneously, the shoulder in the far-red region develops into a new fluorescence maximum, the position of which may lie between 730 and 740 nm depending on the chlorophyll content.

Due to the variability of the chlorophyll fluorescence spectral a good characterization is provided by the chlorophyll fluorescence intensity ratio (I_R/I_{FR}) between the red band peak intensity (I_R) and the far-red band peak intensity (I_{FR}) or the chlorophyll fluorescence area ratio of the bands (Figure 7). The measured relative intensity of the individual chlorophyll fluorescence parameters and area ratios differ from instrument to instrument due to the dependence of excitation radiation and the spectral sensitivity of the fluorescence sensor.

Monitoring of leaves and plants by using laser-induced chlorophyll fluorescence (LICF) spectra has been a successful technique for chlorophyll content indicator and for detection of stress in plants (Chappelle et al., 1984). The fluorescence ratios are affected by structural factors such as chlorophyll concentration (Lichtenthaler, 1990), UV stress, water stress and high irradiance (Agati et al., 1995; Subhash & Mohanan, 1995).

The intensity ratio, also represented as F690/F735, has been observed increased under stress conditions due to a decrease or lower accumulation rate of chlorophyll as well as by a decline in the photosynthetic function (Lichtenthaler 1986, 1987; Lichtenthaler & Rinderle, 1988a, b; Rinderle & Lichtenthaler, 1988; Stober & Lichtenthaler, 1993). These factors normally result in lower chlorophyll contents of the leaves which, as noted above, can be sensed in a non-destructive

77

way through the chlorophyll fluorescence and the ratio of the peak intensities (I_R/I_{FR}). A temporary loss of the chlorophyll and the regeneration of the pigment content when the stress factors are removed have also been monitored by the ratio I_R / I_{FR} (Lichtenthaler et al., 1990; Krause & Weis, 1991).

Short-term and long-term stress effects are not only seen in changes of the ratio I_R / I_{FR} but also in many other chlorophyll fluorescence parameters (Lichtenthaler, 1988; Lichtenthaler & Rinderle, 1988b). The ratio (I_R / I_{FR}) not only increases due to a lower chlorophyll content but also when photosynthesis declines due to a short-term stress which does not affect the chlorophyll content immediately (Lichtenthaler & Rinderle, 1988; Rinderle & Lichtenthaler, 1988). The values of the ratio are quite different when the fluorescence is excited with UV, violet-blue or red light, but the increase in ratio due to the stress is seen in all cases (Lichtenthaler & Rinderle, 1988b; Lichtenthaler, 1988). Thus, the detection of the ratio has become useful, in both ground-truth control and remote sensing applications for monitoring the state of health of terrestrial vegetation (Zimmermann & Günther, 1986; Rosema et al., 1998; Svanberg, 2004).

Laser-induced chlorophyll fluorescence ratios from chlorophyll fluorescence intensities as well as the areas under the chlorophyll fluorescence bands have also been used to monitor plant growth and to predict the crop yield as well as to screen crop varieties (Anderson et al., 2004). The use of the laser-induced chlorophyll fluorescence ratio in assessing the behaviour of certain plants that exhibit leaf heliotropism has also been reported. Leaf growth with or without

mineral deficiency can also be followed using chlorophyll fluorescence spectra and ratios.

Laser-induced Chlorophyll Fluorescence Induction Kinetics

When green leaves are dark-adapted for at least 20 minutes, the photosynthetic photosystems become impaired. Under this condition, when light is again induced on such leaves, it takes a few minutes for the leaf to achieve cooperation of its two photosystems, PSI and PSII (Govindjee, 1990). This time lapse is required to guarantee the photosynthetic net CO_2 assimilation. This light-triggered induction period of the photosynthetic apparatus to its functional state, which is caused by several changes, can be detected and measured via laser-induced chlorophyll fluorescence induction kinetics (Kautsky effect) (Kautsky & Hirsch, 1931; Lichtenthaler, 1992; Govindjee, 1995).

This laser-induced chlorophyll fluorescence induction kinetics is characterized by a fast rise of chlorophyll fluorescence from the initial level called ground fluorescence, F_0 to a maximum fluorescence level, F_m within some few seconds depending the sample. It has been established that only PSII is involved in the chlorophyll fluorescence rise, thereafter, PSI starts to work and drains off electrons from PSII. The cooperation of PSII and PSI as well as the photosynthetic electron transport goes into full operation when the net CO_2 assimilation and oxygen generation are triggered (Lichtenthaler, 1992; Lichtenthaler et al., 2005). This is seen as a gradual decline of the relative chlorophyll fluorescence intensity from F_m within $3 - 5$ minutes to a much lower steady state F_s as shown in Figure 8,
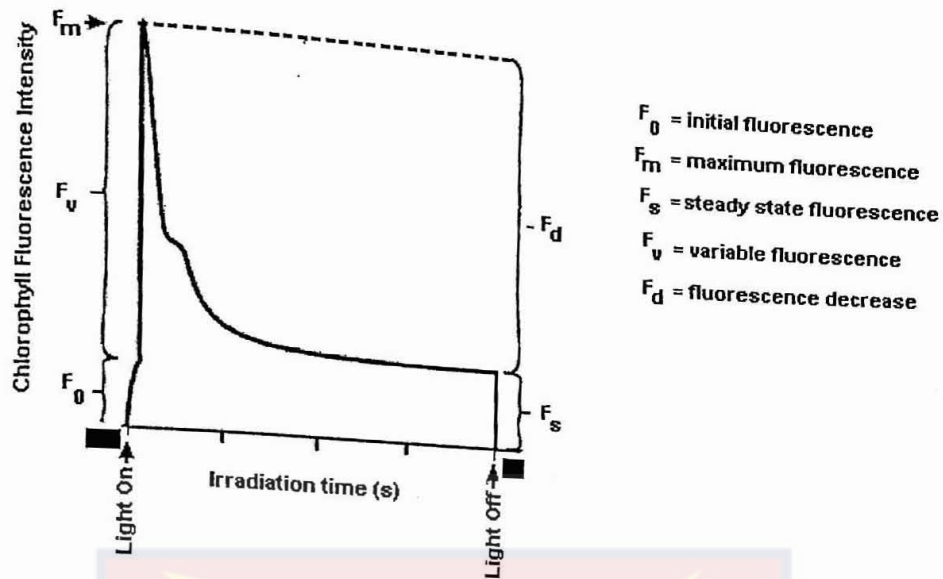
Figure 8. Laser-induced chlorophyll fluorescence induction kinetics (Kautsky effect) curve from a 20 minute pre-darkened green photosynthetically active leaf (After modification: [Lichtenthaler and Babani, 2004]).

known as slow induction kinetics. Thus, the chlorophyll fluorescence kinetics reflects various partial reactions in PSII occurring at different time scales.

Chlorophyll fluorescence induction kinetics curves can be determined with either conventional chlorophyll fluorometers or fluorosensors which use continuous radiation or pulse amplitude modulation (PAM) fluorometers (Barócsi et al., 2000; Lichtenthaler et al., 2005). The measuring principle of PAM fluorometers is quite different from those of the conventional chlorophyll fluorometers. PAM can be used to measure chlorophyll fluorescence induction kinetics curve with strong "white light" given as a saturating flash or continuous irradiation. The reason is that, as part of the essential requirement and standard condition of PAM measurements, the chlorophyll fluorescence induction kinetics in PAM fluorometer

is induced by non-saturating continuous red radiation (LED of 650 or 655 nm) called actinic light (Lichtenthaler et al., 2005).

The characteristic quantities of leaves have been derived from the rising (initial) or the slow decaying period of the curve or both of the chlorophyll fluorescence induction kinetics curves (Barocsi et al., 2000; Lichtenthaler et al., 2005). From the slow component of the chlorophyll fluorescence-induction kinetics, the chlorophyll fluorescence decrease, fd given as

$$fd_{(\lambda)} = F_m - F_s \qquad (36)$$

and the ratio of the fluorescence decrease, fd to the steady state fluorescence, fs, given as

$$Rfd_{(\lambda)} = \frac{fd}{F_s} = \frac{F_m}{F_s} - 1, \qquad (37)$$

have been used in many applications. Determination of the slow fluorescence induction kinetics and thus fd and Rfd values require only strong and continuous light, which must saturate the fluorescence emission and the process of photosynthesis (Haitz & Lichtenthaler, 1988; Lichtenthaler et al., 2005).

Research has shown that the greater the fd value, the higher the net photosynthetic rate of the leaf examined. This has been attributed to the fact that in fully or partially sun exposed leaves of green plants this chlorophyll fluorescence decrease fd value, is mainly caused by the photosynthetic quantum conversion process, however, also including some non-photochemical processes.

The *Rfd* values have been used as an inductor of photosynthetic activity of leaves (Lichtenthaler, 1984, 1986; Lichtenthaler et al., 1986; Nagel et al., 1987; Lichtenthaler & Rinderle, 1988). Research have shown that higher *Rfd* values reflect efficient photosynthetic activity, (Lichtenthaler 1984. 1986; Lichtenthaler et al., 1986; Lichtenthaler and Rinderle, 1988a). Thus, *Rfd* has been used as a quicker way of screening the vitality of stressed plants and plants that have been damaged (Lichtenthaler et al., 2005).

Measurements have shown that *Rfd* values determined in the red chlorophyll fluorescence band exhibit higher values than those determined in the far-red fluorescence band (Buschmann & Schrey, 1981; Haitz & Lichtenthaler, 1988; Lichtenthaler & Rinderle, 1988a). The reason is that the intensities of the chlorophyll fluorescence changes during the light-triggered induction kinetics are higher in the red than in the far-red band (Lichtenthaler et al., 2005). According to Pfündel (Pfündel,1998) and Franck and coworkers (Franck et al., 2002), the low *Rfd* values at the far-red band as compared to the red band are due to relatively high ground fluorescence of F_0. This is because at room temperature the far-red PSI chlorophyll fluorescence also contributes to this far-red band but rather little to the red band.

For example, measured *Rfd* values of sun exposed leaves are higher than shade leaves as well as leaves from green-houses, and they exhibit a highly significant linear correlation to net photosynthetic rate of the leaf, especially outdoor plants that are much less affected by photoinhibition (Lichtenthaler et al., 2005). For post-harvested leaves, *Rfd* values have been found to depend on the time

interval between plucking of the leaf and measurement and have been used as a measure for the efficiency of the photosynthetic activities (Schneckenburger & Bader, 1988).

From the Rfd values obtained from the two chlorophyll fluorescence bands (red and far-red), another parameter termed leaf adaptation index A_p, expressed as

$$A_p = 1 - \frac{1 + Rfd_{(FR)}}{1 + Rfd_{(R)}} = \frac{Rfd_{(R)} + Rfd_{(FR)}}{1 + Rfd_{(R)}}. \qquad (38)$$

where $Rfd_{(R)}$ and $Rfd_{(FR)}$ are the Rfd values for red and far-red band, respectively, can be calculated for intact and photosynthetically active green plant tissue. The A_p-values for example decline with senescence and are usually lower for damaged leaves (Lichtenthaler & Rinderle, 1988).

The fast rise of the chlorophyll fluorescence is from the initial level, the ground fluorescence F_0 to a maximum fluorescence level, F_m within $0.1 - 0.2$ s with saturating light. With non-saturating continuous radiation, such as LED at 650 or 655 nm, the maximum level is obtained within $0.3 - 0.8$ s.

The difference between F_m and F_0 has been termed variable fluorescence, F_v. Ratio, F_v/F_m is the most frequently applied chlorophyll fluorescence ratio because it is easy and fast to determine. A decline in F_v/F_m indicates a decline in quantum yield of PSII photochemistry and a disturbance in or damage to the photosynthetic apparatus, but the cause of the damage cannot be determined by this ratio. F_v/F_0 is another ratio much more sensitive to the photosynthetic apparatus of

a leaf. It contains the same information as F_v/F_m but exhibit higher values and a higher dynamic range.

Other parameters and ratio that have been used in analyzing chlorophyll fluorescence induction kinetics are the rise time $T_{1/2}$ and fall time T_p, expressed, respectively, as

$$T_{1/2} = 0.5(F_m - F_0),$$ (39)

$$T_p = (100\% - P)(F_m - F_0),$$ (40)

where P is F_m/F_0 and expressed in percentages.

Multivariate Data Analysis

Spectra containing data sets with many physical parameters have groups of these parameters varying together. One reason is that more than one parameter may be measuring the same driving principle governing the behaviour of the spectra. In many systems there are only a few such driving forces. Another reason is that important characteristics of the spectra may be completely or partially obscured during measurements, because individual measurements may be noisy and contain large variability. These problems can be simplified by replacing a group of variables with few representative new variables.

The task of extracting the driving principle governing the behaviour of the spectra from the many measured variables in general has been addressed by means of multivariate data analysis (MDA) techniques, which deals with optimum extraction of information from a set of measured data by application of relevant mathematics and statistical tools (Martens & Næs, 1991; Esbensen, 2002; Davies

84

and Fearn, 2005; Davies, 2005). This rather broad characterization reflects the fact that many techniques constituting MDA have evolved from a number of rather diverse fields, e.g. economics, psychology and chemistry. Hence, MDA lacks a distinctive definition.

Multivariate methods are robust to noise, and enable a filtering of the data such that the systematic information (the "effects") is highlighted. This is because the latent variables become stabilized by including many relevant variables, even if each of the measured variables is very noisy. Multivariate data analysis seeks to overcome the limitation of noisy variables registered, by using all variables at the same time.

Large data tables in general, and short and wide matrices in particular, require the use of multivariate projection methods, such as Principal Component Analysis (PCA), for analysis. Multivariate analysis by projection has the following advantages: it deals with the dimensionality problem, handles many variables and few observations, few variables and many observations, and almost square matrices of any size (Esbensen, 2002; Davies & Fearn, 2005; Davies. 2005). Further, it copes with multi-collinearity, missing data. robust to noise, separates regularities from noise, provides informative diagnostic and graphical tools (Esbensen, 2002; Davies & Fearn, 2005; Davies, 2005).

In multivariate data, the possibility of finding correlations by chance increases dramatically with increasing number of variables. In the comprehensive framework of MDA, extracting information from a multivariate data set may be approached in numerous ways, e.g. by applying principal component analysis or

discrimination and classification analysis (Esbensen, 2002; Davies & Fearn, 2005; Davies, 2005). Both of these approaches can be very effective, especially for classifying samples.

Calibration, as used in MDA, is in short to relate some more or less concealed characteristics of the system to a set of directly measurable parameters or in other words, to relate a set of implicit properties of a system to a set of explicit properties. These implicit and explicit properties are quantified by a set of so-called dependent and independent variables.

Principal Component Analysis

Principal component analysis (PCA), introduced in 1933 by H. Hotelling (Hotelling, 1933), is an exploratory statistical multivariate technique designed to identify unknown trends in a multidimensional data set, say X. PCA is an applied linear algebra technique that computes the most important basis to re-express a complex and noisy multidimensional data set. Application examples of PCA are numerous, from neuroscience to computer graphics (Esbensen, 2002; Davies & Fearn, 2005; Davies, 2005).

PCA is a non-parametric method of extracting relevant information from the multidimensional data set, X, by reducing the complex multidimensional data set to a lower dimension such that the principal hidden or latent factors are revealed. The reduced-dimensional space help build more effective data analyses for classification, pattern recognition clustering and so on.

PCA produces a new set of dimensions or axes against which the original multidimensional data set is represented, described or evaluated. This analysis approach enables one to discover and work with the principal latent components rather than the original data.

When two or more signals or dimensions are highly correlated or dependent, they are likely to represent highly related phenomena. Thus, the variances in the data are where the signals or dimensions can be best discriminated and key underlying phenomena observed. So, in PCA, correlated variables are combined and uncorrelated ones, particularly the observations that have high variance, are focused on. At the end of the analysis, smaller set of variables that explain most of the variance in the original data, in more compact and insightful form is sought for.

The new variables or dimensions in PCA are linear combinations of the original ones and uncorrelated with one another, that is, orthogonal in the original dimension space. They are captured as much of the original variance in the data set as possible and are called principal components, (PCs). The PCA as a projection method projects the experimental multidimensional data set onto new axes, the principal components (PCs), and gives better representation of the data set without losing much information.

Principal component analysis is considered as a form of rotation of the existing axes to new positions in the space defined by original variables. The new dimensions or axes are orthogonal and stand for the directions with maximum variability.

The multidimensional data set, X of n observations occurring in m dimensions or variables, which forms the naive basis reflecting the method used in measuring the data, is represented as

$$X = \begin{bmatrix} x_{1,1} & x_{1,2} & \cdots & x_{1,m} \\ x_{2,1} & x_{2,2} & \cdots & x_{2,m} \\ \vdots & \vdots & \ddots & \vdots \\ x_{n,1} & x_{n,2} & \cdots & x_{n,m} \end{bmatrix} = \begin{bmatrix} X_1 & X_2 & \cdots & X_m \end{bmatrix} \qquad (41)$$

Each column in the data table corresponds to one variable x_{lk} and one row x_{il} corresponds to the values observed at one point at a time. Thus, the data points are vectors in a multidimensional space and the principal component analysis of the data gives vectors of scores, with values that summarize all the variables entering the analysis. The projection, P of the vector x onto an axis (dimension) u is

$$P = ux = \begin{bmatrix} p_1 & p_2 & \cdots & p_m \end{bmatrix}, \qquad (42)$$

where p is the PC and u represents the direction of the PCs. The direction of greatest variability is that which the average square of the projection is greatest, such that the overall x is maximized.

Some of the PCs derived from the multivariate data can give an index which will provide the maximum discrimination between samples (Everitt & Dunn, 2001). In some applications, the PCs are an end in themselves and may be amenable to interpretation (Everitt & Dunn, 2001; Esbensen, 2002; Bengtsson et al., 2005).

More often PCs are obtained for the use as input to another analysis. One example is in principal component regression (PCR). PCs are useful when there are too many explanatory variables relative to the number of observations and are

highly correlated. Both situations lead to problems when applying regression techniques, and may be overcome by reducing the explanatory variables to a smaller number of principal components (Everitt & Dunn, 2001).

In order to compute for u, $\mathbf{X}$ is first mean-centered such that the new data set, Y, have zero mean, which is a prerequisite for PCA (Esbensen, 2002; Johnson & Wichern, 2002). In other words, Y is given as

$$Y = \begin{bmatrix} x_{11} - \bar{x}_1 & x_{12} - \bar{x}_1 & \cdots & x_{1m} - \bar{x}_1 \\ x_{11} - \bar{x}_2 & x_{11} - \bar{x}_2 & \cdots & x_{2m} - \bar{x}_2 \\ \vdots & \vdots & \cdots & \vdots \\ x_{n1} - \bar{x}_n & x_{n2} - \bar{x}_n & \cdots & x_{nm} - \bar{x}_m \end{bmatrix}$$

$$= \begin{bmatrix} y_{11} & y_{12} & \cdots & y_{1m} \\ y_{21} & y_{22} & \cdots & y_{2m} \\ \vdots & \vdots & \cdots & \vdots \\ y_{n1} & y_{n2} & \cdots & y_{nm} \end{bmatrix}, \quad (43)$$

with $\bar{x}_1$ $\bar{x}_2$ $\ldots$ $\bar{x}_m$ representing the sample means of the m variables in the multivariate data X. Y, thus, becomes a (n, m)-dimensional matrix like X. This approach centers the original axis system at the centroid of all data points.

In certain experimental results, the multidimensional data set need to be preprocessed in some way in order to improve the quality of the analysis (Reeves & Delwiche, 2003) before they are mean-centered. In its simplest form preprocessing can be a visual inspection of the data in order to exclude any outliers from the data before the analysis. If the data appears to be noisy, the data may also be smoothened by using for example Fourier transform filtering or spline interpolation. Baselines, especially in spectra, are often removed by differentiating the data once or twice so that the variations in the data are favoured over the

absolute levels. In some cases, interested part of the data is selected. For non-linear relationship data, preprocessing can take the form of linearization in order to obtain data with a simpler distribution and a more stable variance. However, these techniques sometimes greatly complicate the ability to provide interpretation or provide little to no improvement in the prediction (Kelley et al., 2004).

The covariance matrix, cov of Y, defined as

$$cov = \frac{1}{n-1} Y^T Y \qquad (44)$$

where Y^T is the transpose of Y and $1/(n-1)$ is a constant for normalization with n still denoting the number of observations in X, is computed. This covariance matrix provides important information on the spread of the variable values in X. The cov is a square symmetric matrix, m x m, with the m diagonal elements being the variances of X of particular measurement types. The off-diagonal terms of cov are the covariance between measurement types. The cov captures the correlations between all possible pairs of measurements and gives information on whether changes in any two variables move together. It contains the correlations (similarities) of the original axes based on how the data values project onto them. The correlation values reflect the noise and redundancy in the measurements. By assumption, large values of the variances correspond to the interesting trend or dynamics in the multidimensional data set and the vice versa. Large values in off-diagonal terms correspond to high redundancy.

In experiments where explicit variables are measured in different units with large numerical differences, the influence of each variable is normalized by

90

dividing the elements of Y by the standard deviation, σ_m to get a new matrix, Z (Esbensen, 2002; Johnson & Wichern, 2002). That is

$$Z = \begin{bmatrix} \dfrac{y_{11}}{\sigma_1} & \dfrac{y_{12}}{\sigma_1} & \cdots & \dfrac{y_{1m}}{\sigma_1} \\ \dfrac{y_{21}}{\sigma_2} & \dfrac{y_{22}}{\sigma_2} & \cdots & \dfrac{y_{2m}}{\sigma_2} \\ \vdots & \vdots & \cdots & \vdots \\ \dfrac{y_{n1}}{\sigma_m} & \dfrac{y_{n2}}{\sigma_m} & \cdots & \dfrac{y_{nm}}{\sigma_m} \end{bmatrix} = \begin{bmatrix} z_{11} & z_{12} & \cdots & z_{1m} \\ z_{21} & z_{22} & \cdots & z_{2m} \\ \vdots & \vdots & \cdots & \vdots \\ z_{n1} & z_{n2} & \cdots & z_{nm} \end{bmatrix} \tag{45}$$

This process enhances the influence of the variables with small variances and reduces the influence of the variables with high variance. The correlation matrix, $corr$, defined as

$$corr = Z^T Z \tag{46}$$

where Z^T is the transpose of Z, is then computed.

At this stage, we look for weights, w that maximize $u(cov)u^T$ or $u(corr)u^T$, subject to u being unit-length, that is, $u^T u = 1$. This is achieved when w is a principal eigenvector of the matrix cov or $corr$, such that

$$u(\text{cov})u^T = u\lambda u^T = \lambda \tag{47}$$

or

$$u(corr)u^T = u\lambda u^T = \lambda \tag{48}$$

where λ is a principal eigenvalue of the covariance matrix, cov or correlation matrix $corr$ and u^T is the transpose of u. In this case, there are two types of u, the left-hand u, LHU and right-hand u, RHU.

The elements of the LHU vectors are denoted PC loadings, also known as the variance, and the vectors themselves are called loading vectors, because it is the

91

transformation matrix between the original variables space and the space spanned by the orthogonal PC vectors. There are, in this case m coefficients for each PC making up the column vectors (loading vectors) in the matrix LHU. The RHU contains the new base data set onto which X was projected.

The loading vectors indicate how the variables are combined to form the PC scores. A plot of the PC loadings shows the variables that are responsible for the trends in the data set and how much each variable contributed to each PC. These indicate the variables that are important, and correspond to the directions in a PC score plot.

So, the new axes are the eigenvectors of the matrix of covariance or correlations of the original variables, which capture the similarities of the original variables based on how data samples project to them.

The first PC (PC1) retains the greatest amount of variation in the sample and corresponds to the line with maximal variance. The data points are projected with values along this new axis. The second PC, PC2 retains the second greatest amount of variation in the sample but orthogonal to PC1 and the data points are again arranged so that the variance is as large as possible. The procedure continues to PC3 and so on. Thus, the kth PC retains the kth greatest fraction of the variation in the sample but orthogonal to $(k-1)^{th}$ PC. The kth largest eigenvalue of the *cov* or *corr* is the variance in the sample along the kth PC. PCs once identified can be used for classification and discrimination or as parameters for modeling in other multivariate techniques.

The usefulness of this artificial variants (PCs) constructed from the observed variables is obtained by determining the proportions of the total variance for which it is accounted. The components of lesser significance can be eliminated without losing much information provided the eigenvalues are very small. If, for example, 95 % of the variation in a multivariate data set involving 20 variables can be accounted for in the PC 1 and PC 2, then almost all the variation could be expressed along a double continuum rather than in 20-dimensional space. This would provide a best summary of the data that might be useful in later analysis.

The new co-ordinate values, collected as columns along given PC, are called the PC scores. These columns are orthogonal and are PC score vectors. The PC scores are the co-ordinates of the data points in the PC space and a plot of these PC scores in the PC space results in a PC score plot.

The eigenvalue denotes the amounts of variability captured along that dimension and tell about the explanation grade and suggest the possible truncation or PCs to be retained. Factors often considered when determining the number of PCs to be retained include the amount of total sample variance explained, the relative sizes of the eigenvalue (variances of the sample components), and the subject-matter interpretations of the components.

A useful visual aid to determining an appropriate number of PCs has been a "scree plot", a graphical method of plotting the ordered v_k against k and deciding visually when the plot has flattened out, i.e., a bend in the scree plot. The number of PCs is taken to be the point at which the remaining eigenvalues are relatively small and all about the same size (Johnson & Wichern, 2002). Alternatively,

93

Kaiser's rule, which suggests that from all the m PCs only the ones whose variances are greater than unity or, equivalently, are the components that should be retained, explain at least $(1/m)100$ % of the total variance, can also be used. This criterion has a number of positive features that have contributed to its popularity but cannot be defended on a safe theoretical ground (Esbensen, 2002).

Outliers, duplicates or other strange measurements, if any, are identified and in some cases removed from the data set for better classification and so on. In other times, the outliers may be the most interesting trends in the data set. These outliers are identified in loading plots or PC score plots.

An idea about where the PCA fails is obtained by comparing a reconstructed and a raw data set. The mean of the squared residuals give the absolute mean residual for each observation that has been compressed.

Two Group Discrimination and Classification

For groups of observations, a subset of variables of the groups and associated functions of this subset and a set of associated variables can be located in order to maximum separation among these groups using discriminant analysis. Discriminant analysis is one of such exploratory multivariate methods of determining variables and reduced set of functions concerned with maximally separating set of observations obtained for the groups. This analysis method is employed on a one-time basis in order to investigate observed differences when causal relationships are not well understood. The following references (Everitt &

Dunn, 2001; Johnson & Wichern, 2002; Esbensen, 2002) are good sources for more comprehensive discussions on discrimination and classification.

The objectives of any discriminant analysis is to construct a set of discriminants that can be used to explain or characterize the group separation with a reduced set of variables, as well as to analyze the contributions of the original variables to the separation and evaluate the degree of separation. The immediate objective of discrimination analysis is to describe, either graphically or algebraically, the differential features of the observation from the several known collections. The numerical values of the discriminants are such that the collections of the data are separated as much as possible.

Maintaining maximum separation for the subset of the original variables in discriminant analysis requires a number of functions known as rank or dimensionality of the separation. Such functions when linear are referred to as linear discriminant functions (LDF) and can locate the exact contrast, up to a constant of proportionality that lead to significant separation. When comparing the significance of two means with a common covariance matrix, Σ of the population, a two group LDF can be develop to obtain a contrast in the sample mean vectors that can lead to maximum separation of the sample group means.

In order to locate a meaningful mean difference, a variable-at-a-time, independent of the other variables in order to assist in a model when the mean difference is found to be significantly different from zero, correlation between the discriminant function is calculated. Correlations of variables with the linear discriminant function have been used as a past-hoc data analysis tool.

For two group discriminant analysis, it is assumed that the two independent samples from two multivariate normal populations have common covariance matrix, Σ and unknown means μ_1 and μ_2. A linear combination of the variables from the two groups that provides for the maximum separation between the groups is the Fisher's two group linear discriminant function, L. given as

$$L = v'x = \sum_{j=1}^{p} v_j x_j ,\tag{49}$$

The discriminant scores that brings about a maximum separation between the two groups is a vector defined as

$$v = S^{-1}(\bar{x}_1 - \bar{x}_2)\tag{50}$$

where S is the common sample variance, an unbiased estimate of Σ and $\bar{x}_i$ is the sample mean for the observations in groups 1 and 2.

The discriminant scores are evaluated at the group mean vector $\bar{x}_i$, using the difference in the mean discriminant scores such that it is exactly equal to Mahalanobis' D^2 statistic defined as

$$D^2 = \left(\bar{x}_1 - \bar{x}_2\right)' S^{-1}\left(\bar{x}_1 - \bar{x}_2\right)\tag{51}$$

Hotelling's T^2 statistics, defined as

$$T^2 = \left(\frac{n_1 n_2}{n_1 + n_2}\right) D^2\tag{52}$$

is used to test for the difference in the mean vectors of the two groups. If T^2 is significant then the sample group centroids for the two classes are said to have good separation. However, the square of the univariate student t^2 statistic is equal to

96

T^2, thus a simple t test on the discriminant scores is equivalent to calculating T^2 for testing for the difference in the mean vectors for the two groups.

For discriminant scores, say y, representing the dependent variable and the dummy independent variables $x_1 = -1$ and $x_2 = 1$ for the two groups. A regression equation of the form

$$y = v_1 + v_2 x \tag{53}$$

where v_1 and v_2 are the constant coefficients, is fitted to the discriminant scores. A sample linear discrimination function, LDF, $L = \alpha' x$ as the estimate of the LDF, where $\alpha = \Sigma^{-1}(\mu_1 - \mu_2)$, will lead to significant separation between the two groups. The number of variables can be reduced and yet maintain significant discrimination, which can be approached using F statistic.

Classification analysis is another multivariate method technique that is closely connected with discriminant analysis. While discrimination analysis is often done to sharpen the separation between groups of observations and to understand the variables that carry the groups separation information, the classification analysis is often performed to predict a probable group membership from an observation. The objectives of these two methods tend to overlap because linear discrimination functions are often used to develop classification rules. The primary difference is that variables used to develop classification rules are usually applied to a group of known number of groups.

Classification analysis seeks to sort observations into classes with the emphasis on a rule that can be used to optimally assign new observations to the already labelled classes. So the concern of classification analysis is the

development of rules for allocating or assigning observations to one or more groups. This leads to well-defined rules that can be used to assign new observation. This analysis method usually requires more knowledge about the parametric structure of the groups.

So, creating rules for assigning observations to groups that minimize the total probability of misclassification of the average cost of misclassification are the objectives. A good and optimal classification procedure results in few misclassifications, that is, the probability of misclassification is small and accounts for the costs associated with misclassification taking prior probabilities of occurrence into account.

Supposing two groups are labeled α and β and have probability density functions (*pdfs*) $f_1(x)$ and $f_2(x)$ respectively, associating with them. Again, supposing p_1 and p_2 are their prior probabilities that x is a member of α and β respectively, where $p_1 + p_2 = 1$. And, let $c_1 = C(2|1)$ and $c_2 = C(1|2)$ represent the misclassification cost of assigning an observation from β and α and from α and β. Then, assuming the *pdfs* are known, the total probability of misclassification (*TPM*) is equal to p_1 times the probability of assigning an observation to β given that it is from α, $P(2|1)$, plus p2 times the probability of assigning an observation into α given that it is from β, $P(1|2)$. Hence,

$$TPM = p_1 P(2|1) + p_2 P(1|2) \tag{54}$$

The error rate that minimizes the TPM is the optimal error rate (OER). Considering cost, the average or expected cost of misclassification (*ECM*) is defined as

$$ECM = p_1 P(2|1)C(2|1) + p_2 P(1|2)C(1|2) \tag{55}$$

A reasonable and better classification rule is established when the *ECM* is made as small as possible. However, costs of misclassification are hardly known.

Using *LDF* and assumptions that $\Sigma_1 = \Sigma_2 = \Sigma$ and $p_1 = p_2$ and that $C(1|2) = C(1|2)$ Fisher developed a *LDF* known as Fisher's Linear discriminant (*FLD*) function (Fisher, 1936). This discriminant function is used to find the linear combination of features that best separate the two groups. The *FLD* function simply uses unstandardized discriminant coefficients and may be used as a classification rule for classifying an observation x into α or β. The *LDF* as a rule does not required normality because *pdf* is not assumed. The groups' covariance matrices are assumed to be equal, because a pooled estimate of the common covariance matrix is used.

The method transforms the multivariate observation x, by taking a linear combinations of x to create univariate observations, y's such that the y's derived from the groups α and β are separated as much as possible. A fixed linear combination of the x's takes the values of y's for the observations from group α and the values of y's for the observations from group β. The difference between the means of the univariate y's of the two groups, $\bar{y}_1$ and $\bar{y}_2$ expressed in standard deviation units is used to assess the separation of these two sets. That is,

$$R = \frac{|\bar{y}_1 - \bar{y}_2|}{S_y}, \qquad (56)$$

where .

$$S_y^2 = \frac{\sum_{J=1}^{n_1}(y_{1J} - \bar{y}_1)^2 + \sum_{J=1}^{n_2}(y_{2J} - \bar{y}_2)^2}{n_1 + n_2 - 2}, \qquad (57)$$

is the pooled estimate of the variance. The objective of this process is to select a linear combination of x to attain maximum separation of the sample means $\bar{y}_1$ and $\bar{y}_2$.

The ratio of the variance between the groups to the variance within the groups is the separation, R between the two group distributions as defined by Fisher. That is

$$R = \frac{\sigma_{between}^2}{\sigma_{within}^2} = \frac{\left[w'(\bar{x}_1 - \bar{x}_2)\right]^2}{w' S_{pooled} w} \tag{58}$$

where $w'\bar{x}_i$ is the weighted mean and $w' S_{pooled} w$ is the weighted variance for group $i = 1, 2$ as a result of the linear combinations of the variables of the groups. The w is the overall possible coefficient vectors. The R is in a sense represents the measure of the signal-to-noise ratio for the group labeling.

The linear combination

$$Y = w'x = (\bar{x}_1 - \bar{x}_2)' S_{pooled}^{-1} x \tag{59}$$

maximizes the ratio and thus the separation over all the possible coefficient vectors w. The maximum of this ratio, from equation (50), is

$$D^2 = (\bar{x}_1 - \bar{x}_2)' S_{pooled}^{-1} (\bar{x}_1 - \bar{x}_2) \tag{60}$$

In allocating a new observation x_0 to say α, if

$$Y_0 = (\bar{x}_1 - \bar{x}_2)' S_{pooled}^{-1} x_0 \geq M \tag{61}$$

where

$$M = \frac{1}{2}(\bar{x}_1 - \bar{x}_2)' S_{pooled}^{-1} (\bar{x}_1 + \bar{x}_2) \tag{62}$$

100

else x_0 is allocated to β if

$$Y_0 < M \tag{63}$$

The group mean and group covariance are estimated from the training sets. Although the estimates of the covariance may be considered optimal in some sense, this does not mean that the resulting discriminant obtained by substituting these values is optimal in any sense, even if the assumption of normally distributed classes is correct.

When the number of observations of each sample exceeds the number of samples, the covariance estimates do not have full rank, i.e. sorting of the covariance estimates into order and replacing each value by its relative position in the order will not be complete, and so cannot be inverted. One way of dealing with such situation is the use of pseudoinverse; a matrix inverse-like object that may be defined for a complex matrix, even if it is not necessarily square. Another way, regularized discriminant analysis, is to artificially increase the number of samples by adding white noise to the existing samples. These new samples do not actually have to be calculated, since their effect on the class covariances can be expressed mathematically as

$$\Sigma_{new} = \Sigma + n^2 I \tag{64}$$

where I is the identity matrix, and n is the amount of noise added, called the regularization parameter. The value of n is usually chosen to give the best results on a cross-validation set. The new value of the covariance matrix is always invertible, and can be used in place of the original sample covariance in the above formulae.

101

CHAPTER THREE

EXPERIMENTAL SET UP, MATERIALS AND METHODS

The experimental set up was in two parts corresponding to the two fields of investigation; fluorescence spectroscopy, in particular diode laser-induced fluorescence, and absorption spectroscopy in particular tunable diode laser spectroscopy. The equipment was used to understand different characteristics of leaves of nutmeg plants. The equipments and components used are described below.

Compact Continuous Violet Laser-induced Fluorosensor

Laser-induced chlorophyll fluorescence studies in this research were conducted with a compact continuous violet diode laser-induced fluorosensor (Gustafsson et al. 2000, Anderson et al. 2004). The fluorosensor consists of a continuous violet diode laser, optics, a probe, detector system and a data acquisition and control unit. The continuous violet diode laser (Nichia NLHV500), was powered by an LDD200-Ip series type laser diode driver (Wavelength Electronics) that had a maximum power dissipation of 2.5 watts. The diode laser could generate a maximum operating power of 5 mW at room temperature and lases at a wavelength of 396 nm. The laser diode driver was operated with a 9 V DC source. The amount of laser power for excitation could be adjustable from the diode laser

102

driver. The laser was in a tube fitted with a lens (Geltech C230TM-A) for collimating the laser output radiation and a narrow band interference filter (CVI F25-400-4-0.5) for the 'cleaning' of the output broadband spontaneous emission beam.

The output laser beam was guided to the sample by a 600 μm core diameter fused silica step index multimode optical fibre, of 0.22 numerical aperture, via a dichroic beam splitter and fibre-port lens assembly (PAF-SMA-6-NUV-Z). The output end of the fibre was supported by a fibre holder and kept in contact with the leaf surface. Laser-induced fluorescence was emitted spatially in all directions and a fraction of it was collected by the same fibre and guided back to an Ocean Optics miniature fibre optics spectrometer, USB2000, through a coloured glass cut-off filter (GG420; $\lambda > 400$ nm, T = 99%). The filter was placed in front of the detector unit, to eliminate any elastically back-scattered violet laser radiation from the sample.

The detector unit had been configured into a plug and play mode and had a 2048-element linear silicon CCD array detector (SonybILX511) and a grating system optimized for UV-IR detection. The USB2000 plugs into the USB port of any desktop or notebook PC, thus eliminating the need for any external A/D converters. Wavelength calibration, which was unique to the USB2000 spectrometer, had been programmed into its memory chip (EEPROM). OOIBase32 software (Ocean Optics Inc.) read these values from the output of the spectrometer. This software enables a computer to read the wavelength calibration coefficients and the spectrometer serial number installed on the memory chip for the computer

103

to communicate with the USB2000 spectrometer. The software is a 32-bit user-customizable and advance acquisition program which enables a real time display of its data. The spectrometer was driven by the computer via the USB connection. The operating temperature was in the range of 10^0 to $50\ ^0C$. Its signal to noise ratio for a single acquisition at full signal is 250:1.

The detector unit, the violet diode laser and the optics of the system were mounted in a dark housing which was made of a plastic (dimension 12 x 22 x 6 cm^3) with an aluminum cover. This further reduces the amount of stray light (ambient light) intrusion.

The 00IBase32 software allows users to evaluate the effectiveness of the experimental setup and data processing selections and make changes to the parameters instantly and thus read their effect and ultimately save data either manually or automatically. It allowed for the use of process functions such as signal averaging, boxcar pixel smoothing, electrical dark signal correction and stray light correction.

Fluorescence signals were acquired in the scope mode for both full spectra acquisition and/or discrete wavelengths for induction kinetics. The time could be normalized and the normalization function allowed for the designation of separate integration times for reference and sample scan. As part of the discrete wavelength acquisition function, up to six (6) single wavelengths and two (2) mathematical combinations of these wavelengths can be monitored and recorded.

The main programmed functions during the measurement were the following: starting measurements for the peak wavelengths; configuration of

wavelength channels and mathematical combinations; configuration of time channels for induction kinetics and saving data. This fluorosensor could be used to detect and measure fluorescence, both in the field and in the laboratory.

The use of this fluorosensor as a system to measure laser-induced chlorophyll fluorescence induction kinetics was demonstrated by Anderson et al. (Anderson et al. 2004; Anderson et al., 2008). An alternative version of this compact fiber-optics fluorosensor employing three light-emitting ultraviolet diodes as excitation sources has also been produced (Ek et al., 2008).

Measurements of Chlorophyll Fluorescence Spectra of Nutmeg

Completely developed male and female nutmeg leaves, second from the apex of a branch, were used in this research. In all, 20 leaves were used, 10 leaves for each sex. They were obtained from the Council for Scientific and Industrial Research (CSIR), Plant Genetic Resources Centre in Bunso, Eastern region of Ghana. The studies started in 2003. Figure 9 shows the experimental arrangement for the detection of the violet diode laser-induced chlorophyll fluorescence from in-vivo green nutmeg leaves.

In order to check the wave calibration of the spectrometer in the fluosensor, the spectrum of a helium-neon laser of known output wavelength was observed. The intensity level of the diode laser light was measured with a handheld power meter (NT54-018, Edmund Optics) and a background spectrum was recorded through the optical fibre by sending the light to clean aluminium plate without a sample at 396 nm.

105

Compact Fluorosensor

A — Spectrometer
B — Diode laser driver
C — Diode Laser
D — Interference filter
E — Beam splitter
F — 9V Battery
G — Cut-off filter
H — Fibre port
I — Fibre

Laptop computer
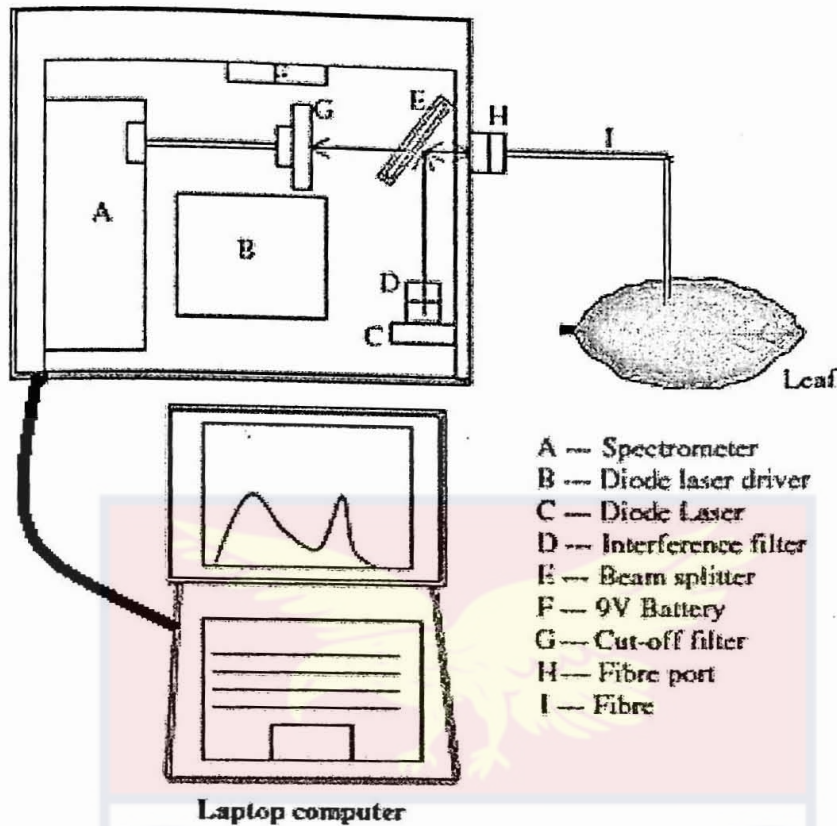
Figure 9. Experimental set-up for the detection of chlorophyll fluorescence from *in vivo* leaf using the violet diode laser fluorosensor.

The lower side of the leaf was placed on aluminium plate for background cover to avoid collection of ambient light coming through the back of the leaf. Violet diode laser light lasing at 396 nm and of 1.2 mW output power was sent to the nutmeg leaf under investigation. Male and female leaves of the nutmeg plants were studied. In each case, chlorophyll fluorescence intensity within 600–800 nm spectral range was recorded at steady-state conditions of the fluorescence. Excitation and detection of the fluorescence was performed via the upper surface of the leaves and at an ambient temperature of 29 ^{0}C.

106

Measurements of Chlorophyll Fluorescence Induction Kinetics of Nutmeg

The same set up as in Figure 9 was used for chlorophyll fluorescence induction kinetics (Kautsky effect). Two characteristic chlorophyll fluorescence peak wavelengths from the nutmeg leaves from the initial measurements were selected for the chlorophyll fluorescence induction kinetics study. An initial calibration test for chlorophyll fluorescence induction kinetics was also conducted on the samples for optimizing the time of exposure.

All the leaves from the male and the female nutmeg plants were then pre-darkened for 20 minutes and placed on a non-fluorescent aluminum plate for each measurement. These samples were then illuminated with the violet laser diode for 180 seconds. The laser light and the chlorophyll fluorescence lights emitted were guided via the same 1.0 m fibre cable onto the sample and then back to the spectrometer. Data were collected on an interfaced laptop computer. For each of the samples, the chlorophyll fluorescence induction kinetics at the two wavelength regions, red and far-red band, as well as their ratio, red band to far-red band, were recorded. The two characteristic chlorophyll fluorescence bands (red-F690 and far-red-F730) and their ratio were measured using two channels and a mathematical combination of these bands.

After these measurements the leaves were kept in different physiological conditions, that is, they were separately immersed into distilled water and stored in a normal ambient environment with an average temperature of 27 ^{0}C. Chlorophyll fluorescence induction kinetic measurements from the leaves of the male and the female plant sets were then taken after 24 hours. The leaves were put back into the

same distilled water and after another 24 hours, recordings of the chlorophyll fluorescence induction kinetics were again made. The procedure was continued until the 72nd hour.

Gas in a Scattering Medium Absorption Spectroscopy (GASMAS) Setup

The gas in a scattering media absorption spectroscopy (GASMAS) set-up consists of a diode laser (Sharp LT031MDO) as a light source with a lasing wavelength of 757.0 nm at 25^{0}C and an output power of approximately 7.0 mW. This is placed in a thermo-electrically cooled mount and controlled by a precision diode laser driver (Melles Griot 06DLD203A) with a temperature and a current controller. The injection current of the diode laser is periodically ramped, using a ramp generator (Tektronix RG501A), in order to scan the frequency across the absorption line of the gas, in this case free oxygen, and sinusoidally modulated, using a function generator (Philips PM5139). The signals are then mixed together using a power divider (Suhner, 50Ω 6dB, 1W DC-2000 MHz) and the signal connected to the diode laser driver. The thermo-electrically cooled mount with the diode laser are placed in a nitrogen-flushed chamber.

Two measurement geometries can be used in this setup, namely, trans-illumination and backscattering. Complete schematic set-up of GASMAS for trans-illumination measurements is shown in Figure 10a. The arrangement used for backscattering geometry is slightly more complicated as can be seen in Figure 10b.

108
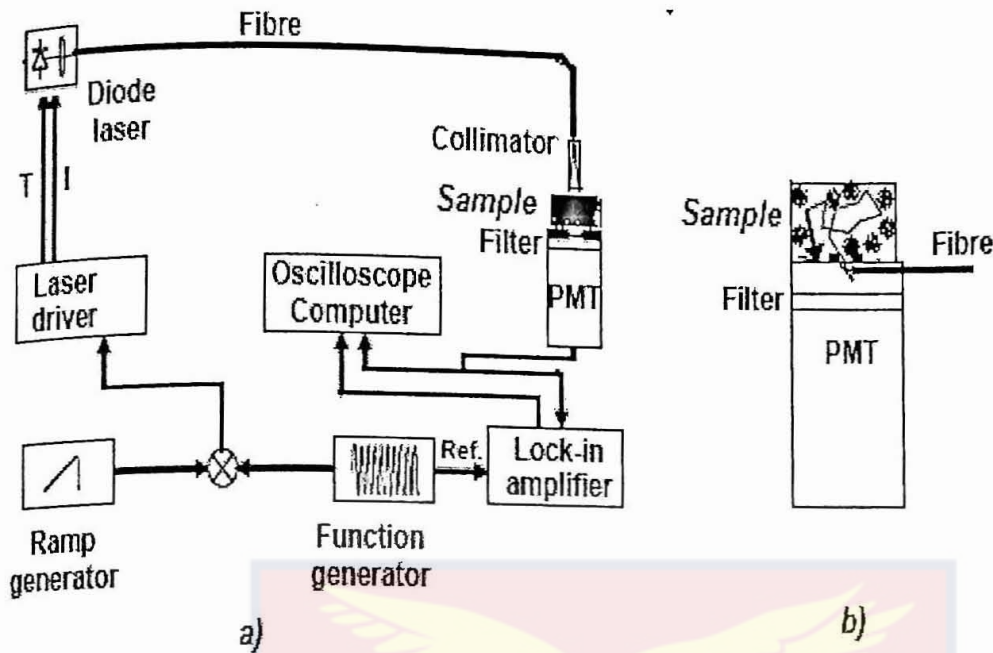
Figure 10. a) Complete schematic set-up of GASMAS for trans-illumination measurements b) modified GASMAS schematic setup for backscattering (single-sided) measurements.

A small right-angle prism providing total internal reflection is positioned in front of the fibre centrally located over the detector.

The modulated light from the diode laser is transported through an optical fibre to the sample and at the end of the fibre the light is sent through a collimating lens placed in a nitrogen-flushed adapter. The collimated light is sent through the sample under study and detected using a photomultiplier tube (PMT) (EMI 9558 QA) detector with a 50 mm diameter photo cathode. The PMT is used with a DC power supply (Hewlett-Packard, 6525A). The signal from the PMT is divided into two signals, one is sent directly to a digital oscilloscope (Tektronix TDS520B), and is called the direct absorption signal, and the other signal sent to the phase-sensitive second-harmonic detection using a lock-in amplifier (EG & G

Princeton Applied Research 5209). The output signal from the lock-in amplifier is then sent to the digital oscilloscope as the extracted second-harmonic component, called the $2v$ signal. The peak-to-peak value of the $2v$ signal (S_{WMS}), in the absorption regime, is normalized by dividing it by the interpolated light intensity at the peak of the direct absorption signal (S_{Dir}) to get the GASMAS signal, GMS.

At the sensitivity fall-off towards longer wavelengths of the PMT, a Schott RG695 coloured-glass long-pass filter is attached directly to the photo cathode of the PMT. This makes it possible to create a window of detection approximately around the desired wavelength of the gas (oxygen), suppressing much of the unwanted light. This is because the light power of interest is extremely low in contrast to the ambient room light. A circular aperture, placed on the PMT, is used to limit the detection area. The extracted second-harmonic component from the lock-in amplifier and the direct signal are accumulated for several scan in the digital oscilloscope. The signals are computer controlled through GPIB (National Instruments$^\copyright$, 2003) communication by a LABVIEW (National Instruments$^\copyright$ 2003) program.

The set up described can be modified at times depending on the type of sample and laser being used, as well as the objective of the research work. A photograph of a set-up (Plate 5), without the nitrogen-flushed optics, is now in place at Fibre Optics Centre in Cape Coast, Ghana.
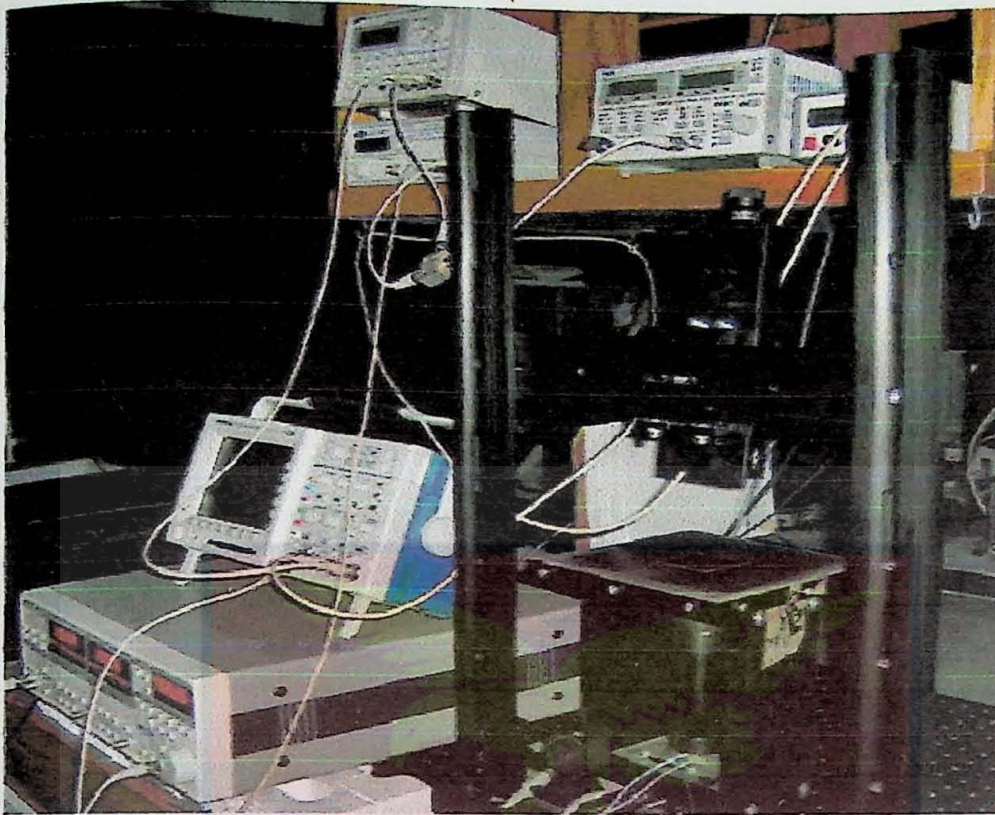
Plate 5. Complete set-up for gas in scattering media absorption spectroscopy (GASMAS) for trans-illumination measurements, without the nitrogen-flushed optics, at Fibre Optics Centre in Cape Coast, Ghana.

Oxygen Gas in Scattering Medium Absorption Measurements

Different sets of samples, wood, fruits and mushroom, were used in these studies. The wood samples were made up of Balsa (*Ochroma pyramidale*), Norway Spruce (*Picea abies*), European Larch (*Larix decidua*), Alder (*Alnusgltinosa*) Aspen (*Populus tremula*), Ash (*Fraxius excelsior*), Birch (*Betula sp*) and Scots Pine (*Pinus sylvestris*). The fruits were Granny Smith apple (*Malus domestica*), orange and avocados. They were bought in a local supermarket. The selection of the samples was made to test the effectiveness of the GASMAS technique.

An ideal second derivative ($2v$) wavelength modulation spectroscopy (WMS) signal was then obtained by recording an experimental curve with a good signal-to-noise ratio using polystyrene foam (Sjöholm et al., 2001; Somesfalean et al., 2002). This curve was used as the standard curve to fit all other measured curves in an automated mode.

The wood samples were placed directly on the photomultiplier tube cathode. The diode laser was temperature tuned to the molecular oxygen line at 761.003 nm, the R7R7 transition of the A-band. The laser injection current was swept at a repetition frequency of 4 Hz, allowing a linear scan over the absorption line. A 55 kHz sine wave modulation was superimposed on the current ramp, and the signal from the PMT was divided into two parts, one is sent directly to the digital oscilloscope and the other signal is sent to the phase-sensitive second-harmonic detection using the lock-in amplifier. The output signal from the lock-in amplifier was then sent to the digital oscilloscope as the extracted $2v$ signal. Signal averaging of between 32 and 1024 scans depending on the level of the noise, was performed on the digital oscilloscope.

The optical densities of the samples varied by several orders of magnitude and so did the light levels reaching the detector. The PMT gain was adjusted by changing the supply voltage to achieve high amplification and linearity in the detected signal.

First, measurements of 6 mm thick slabs of the wood of the different species and different densities were performed. Different aspects relating to the light propagation and embedded gas in the wood were studied. By shining light

through the samples and adding known distances of ambient air, the gas content in the porous samples was expressed as an equivalent mean path length, that is, the path length in air rendering the same absorption as encountered by oxygen in the sample. Each sample was measured at three different points, and at each point three different averages consisting of 512 individual scans were acquired using a circular detection area with a diameter of 25 mm. Measurements were also performed on denser species of wood. namely; Pear, Norway Maple. Beech. Pedunculate Oak, Wych Elm, wild Cherry and Hornbeam.

The inherent anisotropy of the wood was also investigated using cubes of 15 mm side length using Norway spruce and Scots pine. The oxygen light absorption and the light transmission were measured for both kinds of wood through the cube by letting the laser beam entering them through three different principal directions, that is. radially through the annual rings, longitudinally along the annual rings along the stem, and tangentially along the annual ring layers, respectively. Each principal direction was measured from both sides, and for each side three different averages consisting of 512 individual scans were acquired using a circular detection area with a diameter of 6 mm.

Dynamic processes related to gas diffusion in wood were also investigated by measuring the light absorption of oxygen in samples of wood directly after keeping them in a pure nitrogen gas for some time and then being brought out into ambient air. Measurements were done on one sample for different storage times in pure nitrogen gas as well as on different samples at the same storage time. All the measurements were done in transillumination mode.

In the case of the fruits and mushroom, both transillumination and backscattering techniques were used. Additionally, sinusoidal modulation of about 9 kHz was superimposed on the diode laser injection current to achieve a wavelength modulation of the light allowing sensitive wavelength modulation spectroscopy (WMS). In the transmission geometry a circular aperture with a diameter of 6 mm was used to limit the detection area.

Launching the laser light into the scattering medium, in the case of the backscattering geometry is slightly more complicated, as shown in figure 14b. The backscattered light that had travelled through the medium was collected in an annular aperture with an inner and outer aperture diameter of 10 and 21 mm, respectively.

Measurements were made for both transillumination and backscattering geometries in ambient air after different treatments; pre-treated by immersion in nitrogen gas for 24 hours and pre-exposed to atmosphere with higher oxygen concentration than that in the ambient air for 12 hours.

Preliminary backscattering geometry measurements on avocados were measured to explore their maturity. The conventional approach of hardness measurement of the avocados was performed with a Stevens LFRA Texture Analyzer equipped with a circular probe with a diameter of 25 mm. Each avocado was compressed about 2 mm with a probe speed of 0.2 mm/s while the maximum force was measured. Gas exchange into an intact orange was also measured after nitrogen exposure.

CHAPTER FOUR

RESULTS, ANALYSIS AND DISCUSSIONS

This section deals with the results, analysis and discussion of the diode laser-induced fluorescence measurements on the leaves of the male and female nutmeg plants, as well as the gas in scattering medium absorption spectroscopy (GASMAS) measurements from the wood samples and the fruits.

Chlorophyll Fluorescence

Figure 11 shows some of the fluorescence intensity spectra recorded from the *in vivo* green leaves of the female and male nutmeg plants, which show characteristic chlorophyll fluorescence features.

It can be observed that the peak intensities of the red band are higher than that of the far-red band in all spectra. This is as a result of the chlorophyll fluorescence coming from only chlorophyll and accessory pigments from the mesophyll region near the surface. The emitted light from the red band was reabsorbed only from the few surface chlorophyll pigments yielding also some far-red band emission. This is because the violet light, which has a short wavelength, cannot penetrate much into the leaf due to absorption.

Considering the wavelength (396 nm) of the continuous violet diode laser, and the chlorophyll fluorescence emission peak wavelengths of the leaves from the

male and female nutmeg plants, the energy of the fluorescence emission was typically less than that of the excitation source. There were Stokes shifts in the fluorescence as discussed above. The cause of this Stokes shift might be the energy transfer within the pigments for photosynthesis or rapid decay of the excited electrons to the lowest vibrational level of the singlet state of the chlorophyll molecule or both.
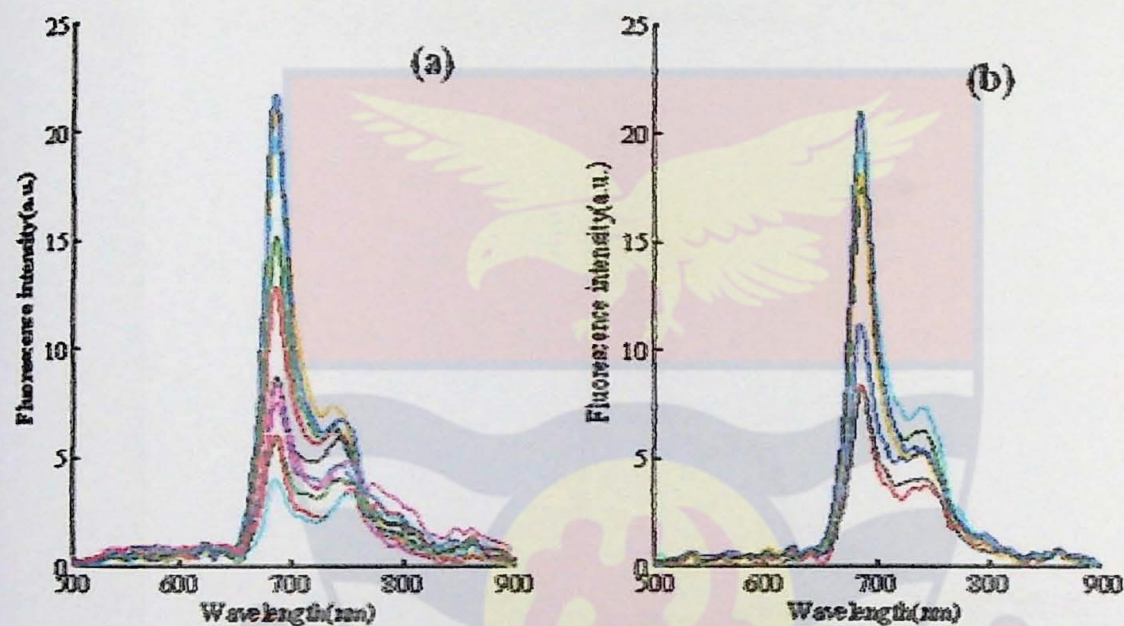
Figure 11. Fluorescence intensity spectra of *in vivo* leaves, second from the apex, from a) female and b) male nutmeg plants excited with continuous violet diode lasing at 396 nm wavelength.

As seen from Figure 11, almost the same chlorophyll fluorescence emission spectra, in terms of shape, were observed around peak wavelength of 685 nm in the red band and 740 nm in the far-red band but the fluorescence intensities varied. This means that the chlorophyll pigments from the leaves of the nutmeg plants, both male and female, have the same Stokes shift. These chlorophyll fluorescence

116

intensities give information about the reemitted light after photochemical quantum conversion in photosynthesis, which suggests that different parts of the leaves have different photochemical quantum conversion response.

On the average, the chlorophyll fluorescence intensity of the leaves from the male nutmeg plants was higher than that of the female, as shown in Figure 12. This suggests that, on the average few photons were being used by the male leaves for photosynthesis compared to that of the female leaves.

Figure 12. Average chlorophyll fluorescence intensity spectra of the *in vivo* leaves from the female and the male nutmeg plants excited with continuous violet diode lasing at 396 nm wavelength.

Using paired t-Test at 0.05 level on the chlorophyll fluorescence spectra from female and male leaves t = -19 and p = 0 were obtained, which shows that the two means are significantly different. Also, One-Way ANOVA at the 0.05 level gave F = 5 and p = 0, indicating that the means are significantly different.

117

However, there is obviously no large variation between chlorophyll fluorescence spectra for classification and therefore discrimination power between the leaves of male and female plants seems to be absent. The ratio of the peak intensities of red to far-red bands did not also show much difference between the leaves from the male and the female nutmeg plants.

Figure 13 shows typical male and female chlorophyll induction kinetic curves recorded in the red band at 685 nm. While the maximum fluorescence intensities from the leaves of the male plants range between 40 and 550 arbitrary units (a.u.) those from the female plants range from 250 and 400 a.u.

The minimum values of the steady intensities range between 20 and 150 a.u. in the case of the leaves from the female plants. For the leaves from the male plants the steady state intensities range between 80 and 110 a.u. It can also be observed that it takes a longer time for the leaves from the female plants to get to the steady state compare to the leaves from the male plants. This can be seen from the average induction curves as shown in Figure 14.

The different shapes of the slow chlorophyll fluorescence induction curves observed in these experiments may reflect different functional state of the system of CO_2 fixation in the individual leaves. In fact, the decreased in fluorescence intensity may have resulted from stimulation of Calvin cycle activity by enzyme
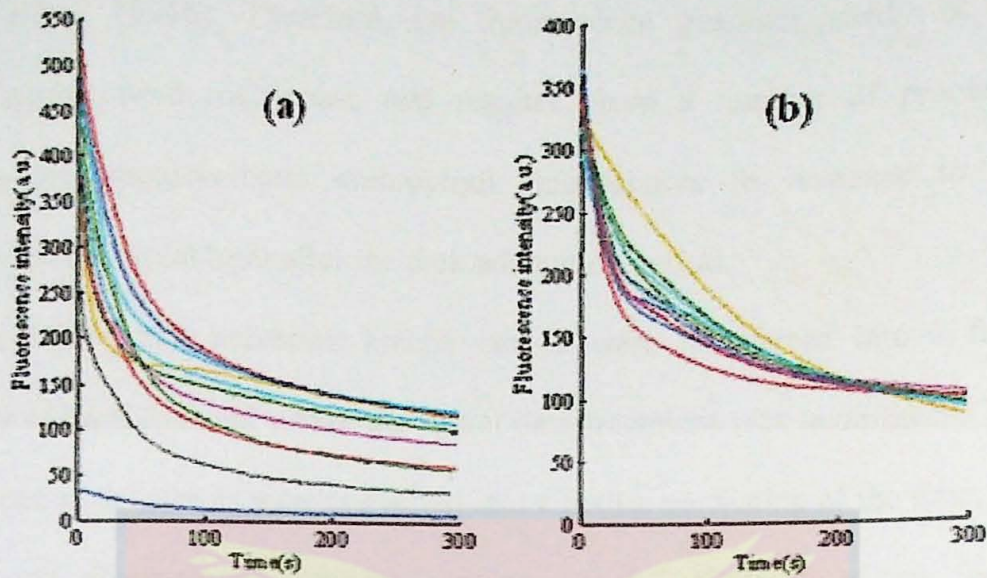
Figure 13. Typical chlorophyll fluorescence induction kinetics of *in vivo* leaves second from the apex, from a) female and b) male nutmeg plants excited with continuous violet diode lasing at 396 nm wavelength and detected at 685 nm in the red band.
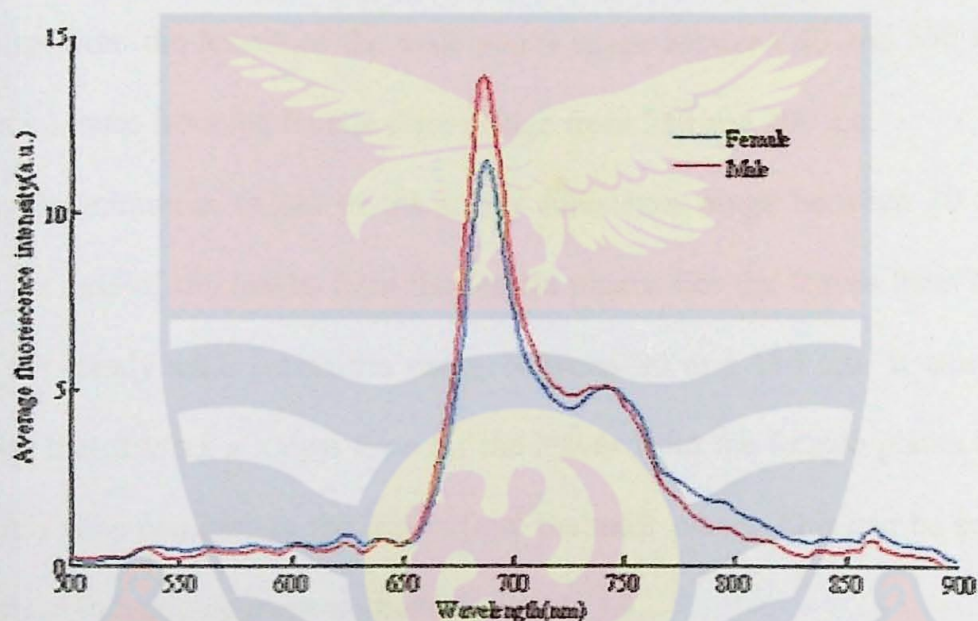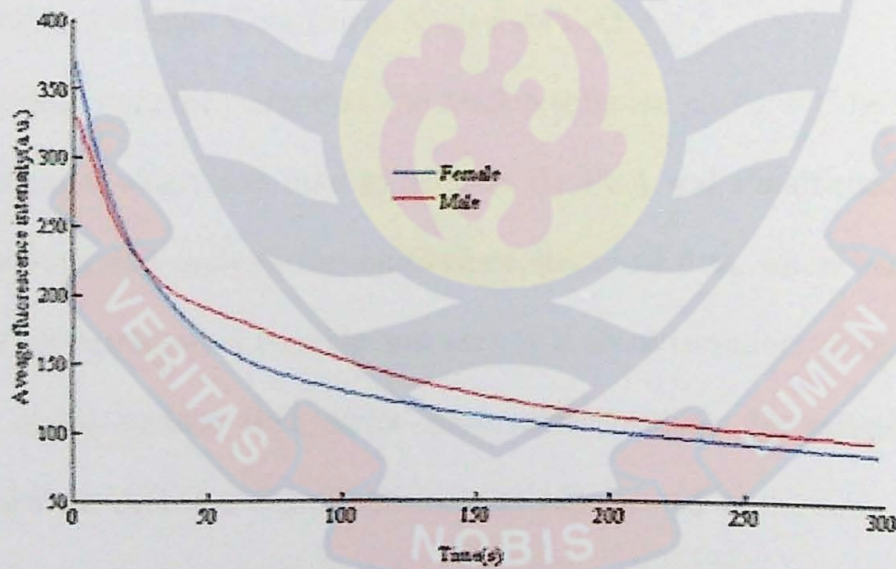

Figure 14. Average chlorophyll fluorescence induction curves of *in vivo* leaves, from female and male nutmeg plants excited with continuous violet diode lasing at 396 nm wavelength and detected at 685 nm in the red band.

119

activation (Dau, 1994b). Therefore, the fluorescence quantum yield of the induction curves were multiphase and resulted from a number of processes proceeding the photosynthetic chlorophyll fluorophores in response to the illumination of the violet light after the dark adaptation period.

The chlorophyll induction kinetic curves were transferred into a form readable by Microsoft Excel where the initial data treatment was undertaken. The data contained in the curves were converted into a matrix consisting of the time, the variables, and fluorescence intensity values as the observations in Excel spreadsheets. The data were grouped as 685 band, 740 band, and their ratio. In all, there were 306 variables and 44 observations, so the data was made up $44 \times 306 = 13464$ data points. Randomly, 11×306 data points of chlorophyll fluorescence induction kinetic curves each from the female and the male plants were prepared as training data for Principal Component Analysis (PCA).

The data were then exported into Matlab software platform (MATLAB 7.0, Mathworks Inc.), which was used to perform the PCA and classification. Matlab uses column-oriented analysis for multivariate statistical data, where each column in the data set represents a variable and each row an observation. In this case the intensities at the various time series were represented as the variables in the columns, and the different measurements were represented as the rows, such that the (i,j)th element is the ith intensity of the jth time.

Using the principal component analysis (PCA) tool of the Matlab software the same set of fluorescence data was used in order to achieve the main purpose of our studies to address the screening for early detection of the plant sex by violet

120

laser-induced chlorophyll fluorescence induction kinetic. PCA was first performed on the raw fluorescence data of 22 x 306 data points for 685 nm and 740 nm bands, and the ratios, to establish whether the differences could be utilized to classify the individual bands and the ratio for the individual plant sex. Orthogonal principal component (PC) scores, loading, latent and t-square values were generated for each band as well as for their ratio.

The fluorescence PC scores were the fluorescence data formed by transforming the original data into the space of the principal components. This output was the same as the input data. The loadings represented the PC coefficients. The loadings were the linear combinations of the original fluorescence data variables that generated the new variables in the PC scores. The latent contains the eigenvalues of the covariance matrix of fluorescence data. The latent was a vector containing the variance explained by the corresponding PC. Each column of PC scores had a sample variance equal to the corresponding element of variances. The t-square had the Hotelling's T^2 statistics for the data and it is a measure of the multivariate distance of each observation from the centre of the data set.

The eigenvalues of the principal components (PCs) contributing to the total variance of chlorophyll fluorescence induction kinetics curves of the 685 nm band, 740 nm band and the ratio were plotted as illustrated as a scree plot for the first 20 PCs in Figure 15. It can be observed that the eigenvalues drop off rapidly with increasing PC numbers and the first few PCs retained the maximum variance of the fluorescence data. The percent of the variability explained by each PC was

calculated in order to know the contribution of each PC and to select the important PCs for classification and discrimination.
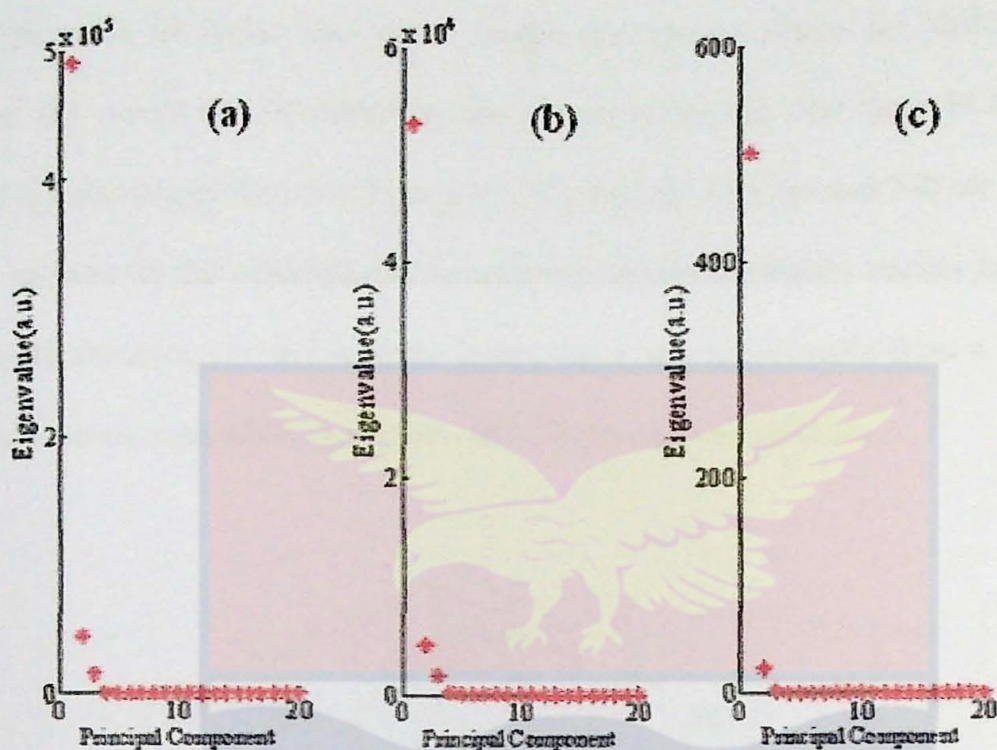
Figure 15. The scree plot showing the eigenvalues of the first 20 principal components (PCs) out of the 306 PCs contributed to the total variance of the chlorophyll fluorescence induction kinetics curves for (a) 685 nm band, (b) 740 nm band and (c) the ratio.

Using the Kaiser Criterion, which retains eigenvalues greater than 1 in the scree plot, only 3 PCs were retained in the 685 nm and 740 nm bands as well as for their ratio. In the case of the 685 nm and 740 nm bands the 3 PCs contribute 99.67 % and 99.47%, respectively, to the total variance of their chlorophyll fluorescence induction kinetics curves, while the 3 PCs of the ratio contribute 99.45%. However, the score plots showed no clear distinction between the two sexes after considering

122

possible outliers and replicates using mean squared residuals. This can be seen in Figures 16, 17 and 18.

In order to locate the region within the curves where the differences between the curves can be observed, the variances for the first three PCs were plotted against time as shown in Figure 19. PC1 for both 685 nm and 740 nm bands of the variance in the chlorophyll fluorescence induction kinetics curves indicate that the fluorescence intensities of the leaves decrease exponentially from a higher value to a steady state while their ratio (685/740) increases with time.
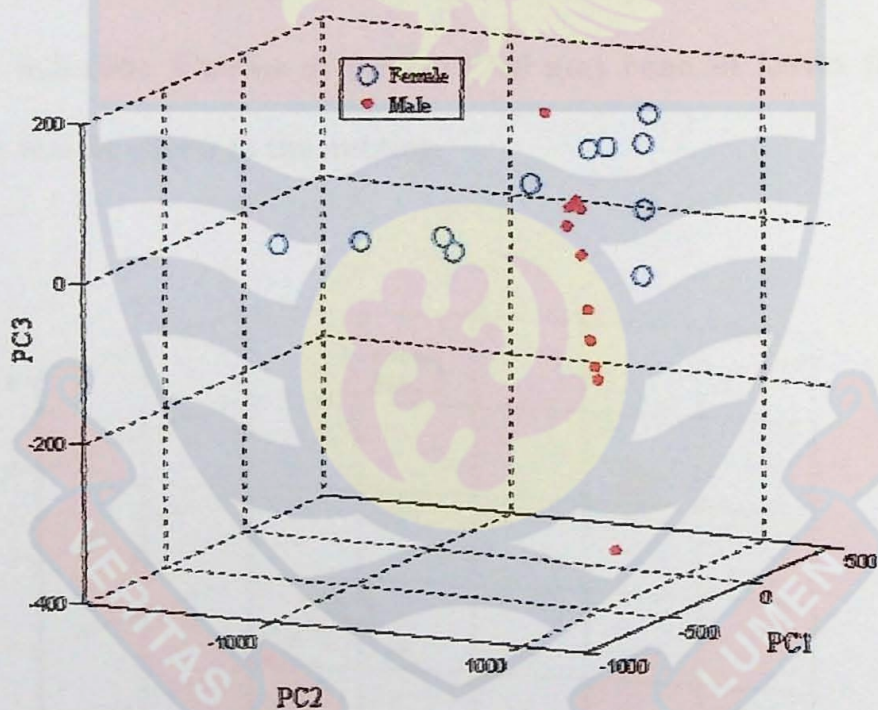

Figure 16. The scatter plots of the three principal components of the fluorescence induction kinetics at red (685 nm) band of leaves from the male and the female plants of nutmeg.
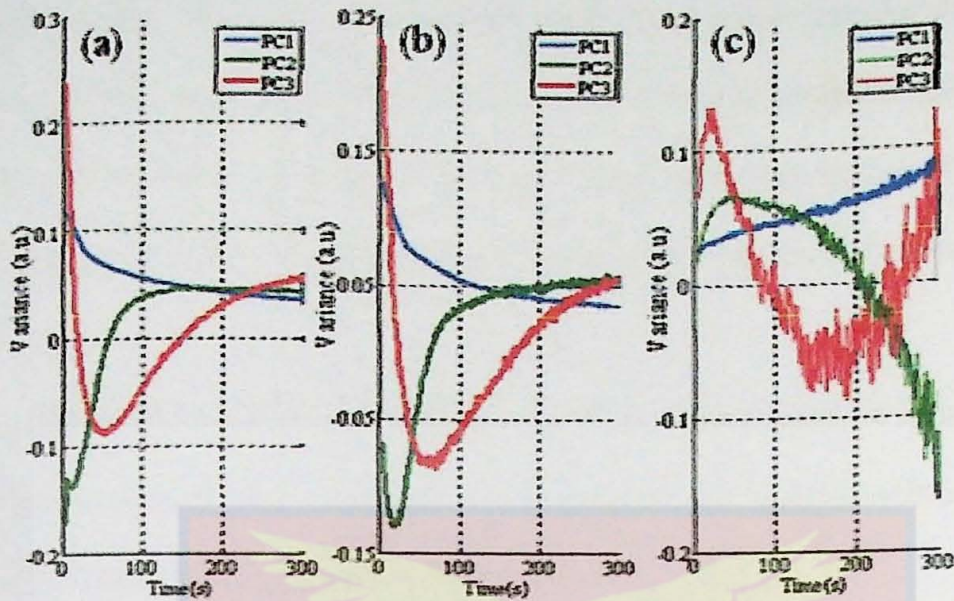
Figure 19. The slow chlorophyll fluorescence induction kinetic curves of the three principal components in their new basis after principal components analysis. The new basis curves represent that of (a) the 685 nm band , (b) the *740 nm band and (c) the 685/740 ratio.*

The PC2 for both 685 nm and 740 nm bands shows that some of the leaves have an exponential growth in their fluorescence contributions up to 150 s before coming to a steady state. PC1 and PC2 intersect at 150 s and remain almost the same to the end.

In the case of the ratio, PC2 increased within the first 50 s and started decreasing, but intersected PC1 around 150 s. PC3 indicates in both 685 nm and 740 nm bands that some fluorescence intensities of the leaves decrease to a point and start increasing before it comes to a steady state. Thus, the leaves show common fluorescence intensity properties at 150 s and beyond, and their differences can be found within the first 150 s. These suggested that fluorescence

125

intensities curves below 150 s contain information that can be used for discriminant analysis. The 3D score plot of PC1, PC2 and PC3 for the chlorophyll intensities for the first 100 s, shown in Figures 20, 21 and 22, indicates that the use of the region of the spectrum below 150 s facilitates improved discrimination between the two sexes.

Based on the result obtained from the PCA, a discrimination linear function was created using the three PCs from the red and far-red band as well as the ratio. For the red band the discrimination function is

$$Y_R = 0.4737 - 0.0002X_{1R} + 0.0028X_{2R} + 0.0004X_{3R}$$

where X_{1R}, X_{2R} and X_{3R} represent PC1, PC2 and PC3, respectively, of the chlorophyll fluorescence induction curves in the red band.

Figure 20. Scatter plots of red (685 nm) band for the first 100 s of the chlorophyll fluorescence induction kinetic curves of leaves from male and the female plants of nutmeg.

126

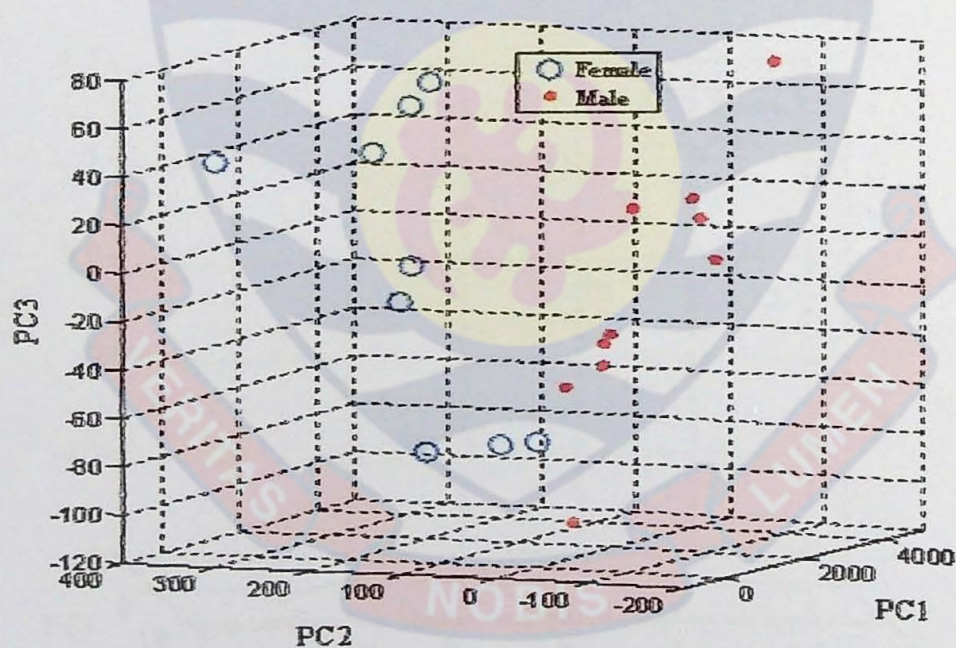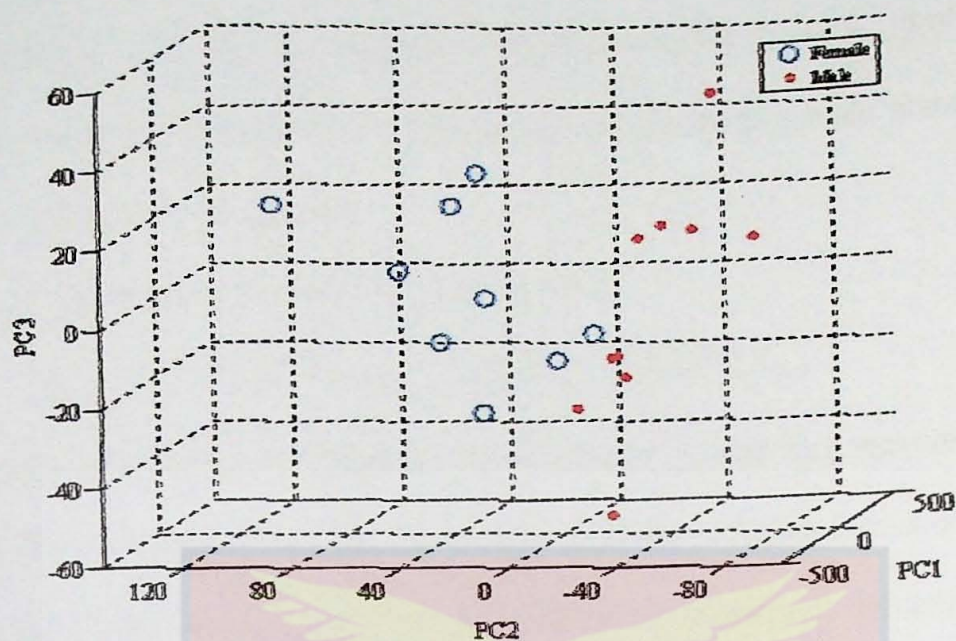Figure 21. Scatter plots of far-red (740 nm) band for first 100 s of the chlorophyll fluorescence induction kinetic curves of leaves from male and the female plants of nutmeg.
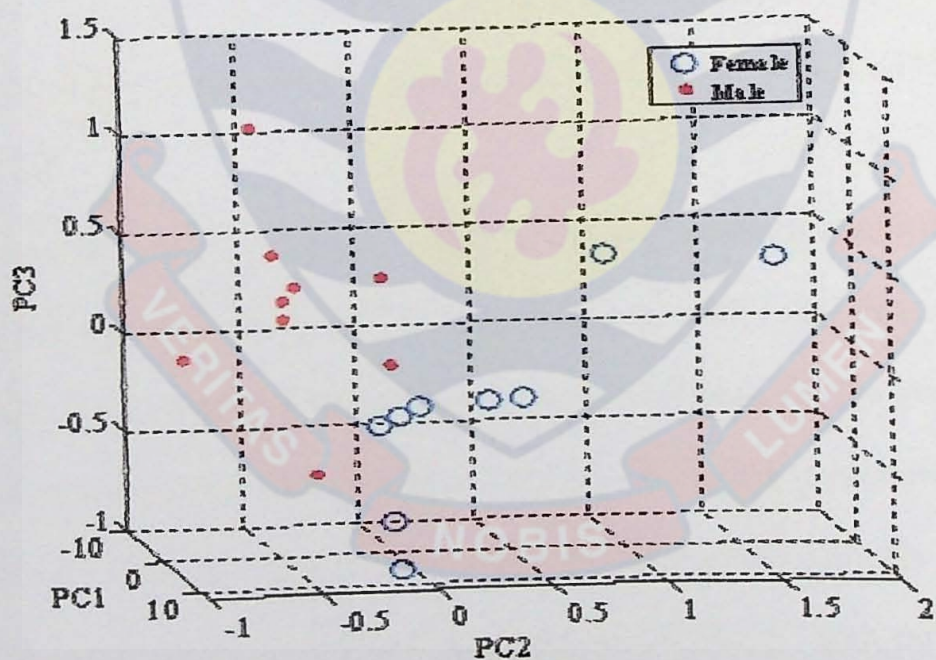

Figure 22. The scatter plots of red to far red ratio for the first 100 s of the chlorophyll fluorescence induction kinetic curves of leaves from male and the female plants of nutmeg.

The critical value, CV, for classification is 0.3561, such that $Y_R < CV$ implies that the slow chlorophyll fluorescence induction curve belongs to a male plant else it belongs to a female nutmeg plant.

The discriminant function for far-red band is

$$Y_{FR} = 0.4737 + 0.0005X_{1FR} + 0.0096X_{2FR} + 0.0012X_{3FR} \qquad (65)$$

with critical value, $CV_{FR} = 0.3550$ and where X_{1FR}, X_{2FR} and X_{3FR} represent PC1, PC2 and PC3, respectively, of the slow chlorophyll fluorescence induction curves in the far-red band. When $Y_{FR} < CV_{FR}$ then the slow chlorophyll induction curve belongs to a male plant else it belongs to a female nutmeg plant.

For the slow chlorophyll fluorescence intensity ratio:

$$Y_{RAT} = 0.47 + 0.02X_{1RAT} + 0.55X_{2RAT} - 0.04X_{3RAT} \qquad (66)$$

where X_{1RAT}, X_{2RAT} and X_{3RAT} represent PC1, PC2 and PC3, respectively, of the slow chlorophyll fluorescence intensity ratio for the first 100 s, with a critical value, $CV_{RAT} = 0.55$.

The distribution of the chlorophyll fluorescence induction kinetic curves, from the red (685 nm) and far-red (740 nm) bands and their ratio, from the leaves of the male and the female nutmeg plants is shown in Figure 23. The graph shows the performance of the discrimination functions with three PCs as parameters.

Figure 24 shows the average chlorophyll fluorescence ratio for the intact male and female leaves of the nutmeg plants within 100 s. Each ratio was an average of 44 measurements of the male and the female nutmeg leaves. The chlorophyll fluorescence ratio of the female is higher than that of the male though

128
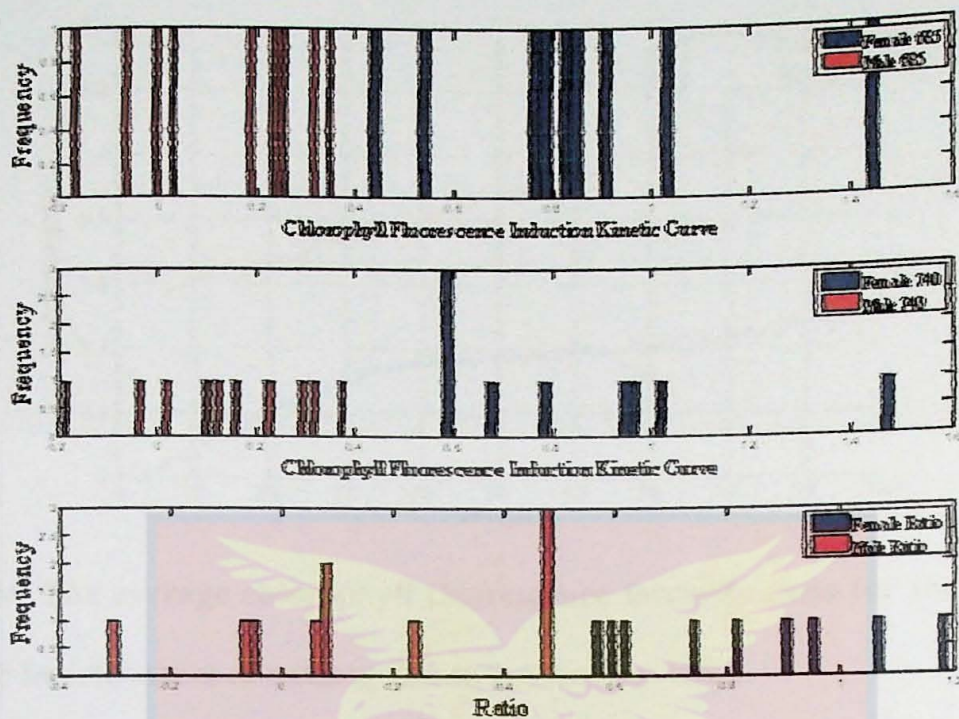
Figure 23. Distribution of the chlorophyll fluorescence induction kinetic curves from red (685 nm) and far-red (740 nm) bands and their ratio from the leaves of the male and the female nutmeg plants showing the performance of the discrimination function with three PCs

the chlorophyll fluorescence intensities at 685 nm and 740 nm of the female are less than that of the male.

Three-dimensional plots of the chlorophyll fluorescence ratios for the first 100 s for the male and the female leaves of the nutmeg plants for the four measuring days are shown in Figure 25. They show that the female plants are higher in ratio than the male plants.

In both *in vivo* leaves and the leaves kept in water the chlorophyll fluorescence ratio of peak red band to peak far-red band is higher for the leaves from the female plants when excited with violet diode laser.

129

Figure 24. The average chlorophyll fluorescence intensity ratio for the intact male and female leaves of nutmeg plants for the first 100 s.

Figure 25. The chlorophyll fluorescence ratios within 100 s of the nutmeg leaves for the (a) first, second and third day, (b) first, third and fourth day (c) first, second and fourth day and (d) second, third and fourth day measurement of the male and female nutmeg plants.

130

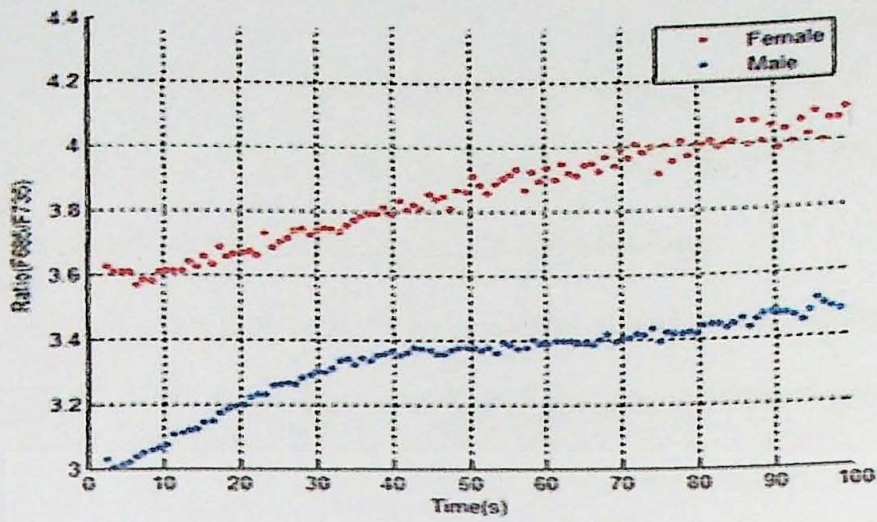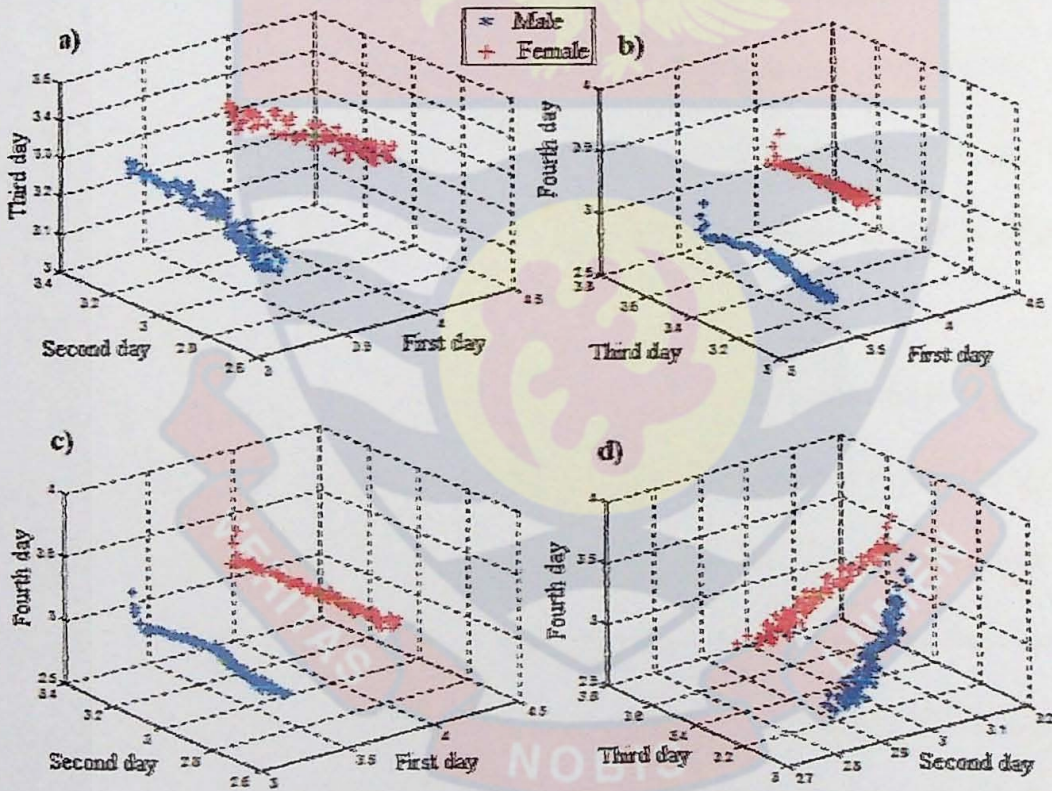These chlorophyll fluorescence ratios reflect the chlorophyll content of the leaves (Lichtenthaler, 1987a; Lictanthaler & Buschmann, 1987; Guyot & Major, 1988; Lichtenthaler et al., 1990) from the male and the female plants.

Chlorophyll fluorescence depends to a great extent on the pigment content and the re-absorption of leaves (Buschmann & Lictanthaler, 1988; Guyot & Major, 1988; Dahn et al., 1992). This is due to the fact that, in green leaves about 90 % of the emitted chlorophyll fluorescence at the red band is re-absorbed by the chlorophyll pigments of the leaf (Gitelson et al., 1999). The effect of re-absorption is high when the leaves possess relatively high chlorophyll pigment content, thus resulting in a lower chlorophyll fluorescence ratio (Dahn et al., 1992; Agati, 1993; 1995; Gunther et al., 1994; Gitelson et al., 1999). These explanations suggest that the leaves from the male plants had higher chlorophyll pigments concentration than that from the female plants.

Chlorophyll fluorescence decrease ratios (Rfd), calculated from the average values of the slow chlorophyll fluorescence induction kinetics curves for both the male and the female plants, are shown Figures 26 and 27. The graphs show Rfd-values of the in vivo leaves of the male and female nutmeg plants as well as when the leaves were subjected to 72 hours in water, for the red band (685 nm) and the far-red-band (740 nm), respectively. For both red and far-red bands, the Rfd-values of the female intact leaves were greater than those of the male fresh leaves. The same patterns were observed when the leaves were kept in water for 24 hours, however, with decreased Rfd-values in both male and female plants.

Figure 26. The chlorophyll fluorescence decrease ratio, from the male and female nutmeg plants, derived from the chlorophyll fluorescence induction kinetics curves at red band of the intact leaves (first day) and leaves kept in water (second to fourth day).
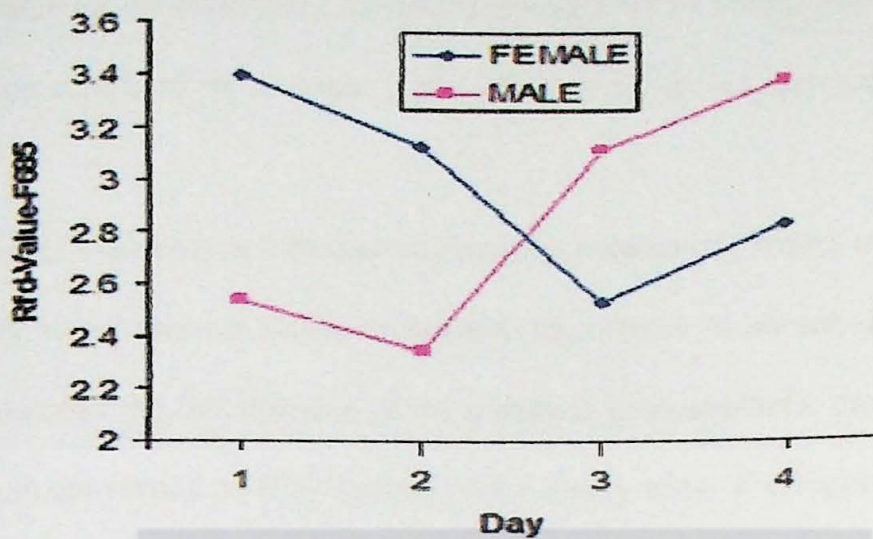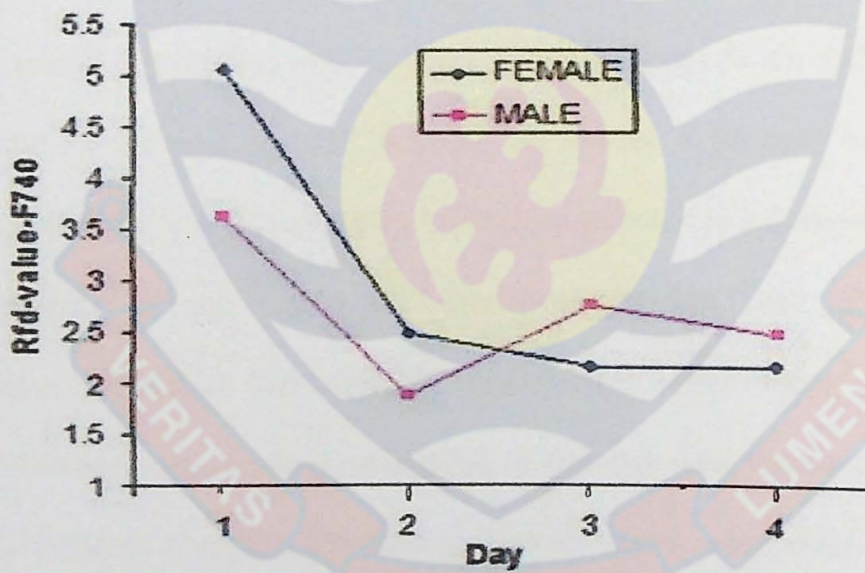

Figure 27. The chlorophyll fluorescence decrease ratio, from the male and female nutmeg plants, derived from the chlorophyll fluorescence induction kinetics curves at far-red band of the intact leaves (first day) and leaves kept in water (second to fourth day).

The *Rfd*-value for the male plant started increasing after 24 hours, while that of the female plant continued its decrease to the 48th hour before an increase in the 72nd hour.

The *Rfd*-values give information about the number of photons emitted at the onset of the slow induction kinetics relative to the number of photons at the steady state. It indicates the functionality of the complete photosynthetic processes from the quantum conversion to CO_2 fixation under steady state. The higher *Rfd*-values of the leaves from the female plants within 24 hours reflect higher capacity of the leaves for photosynthetic quantum conversion and CO_2 fixation. The general decrease in the *Rfd*-values indicates that the leaves loss much more photons in the form of fluorescence emission reflecting a progressive damage of the photosynthetic apparatus as well as the stress on the leaves by the water. For now, no or only partial explanation may be given to the increases in the *Rfd*-values from the 48th hour for the male and 72nd hour for the female. A partially explanation to that effect is that the leaves may have closed their stomata as a defence mechanism to the presence of the water and therefore reducing their photosynthetic functionalities, until they were able to withstand the water stress. A test, using statistical ANOVA, was made on the ratios of the male and female plants for the differences between the predetermined positions, which were used as variables. The result of the p-value was less than 0.0001 for both male and female nutmeg leaves, indicating very significant differences among the variables. A t-test using a significant level of 5 % on the average data between the sexes indicate that the mean for the male and the female leaves were different. The p-value was less than

0.0001 indicating a very significant difference between the male and the female plants.

Using 25 sample data as the training data, Fisher's discriminant linear function with equal cost and equal priors for the ratios of the male and the female plants, and for maximum separation of the two sexes, gave an allocation rule

$$Y_0 = 87X_1 + 57X_2 - 107X_3 - 93X_4 + 25X_5 + 98X_6 \qquad (67)$$

where X_1, X_2, ... ,X_6 represent the ratios of the six predetermined positions used as variables, with a critical value, $CV = 295$. So that, if $Y_0 \geq CV$, then the ratio belongs to the female plant else it is a male plant. The maximum separation in the sample was 173. Evaluating the above Fisher's discriminant linear function with 5 sample data showed 95 % success of the discrimination function for intact leaves from the male and the female plants of the nutmeg.

Using the Fisher discrimination linear function with equal cost and equal priors for the ratios of 25 sample data of the water stressed leaves of the male and the female plants, and for maximum separation of the two sexes also gave an allocation rule

$$Y_s = 300r_1 + 316r_2 + 260r_3 \qquad (68)$$

with a critical value $CV_s = 2870$, where r_1, r_2 and r_3 representing the average ratios of the 24th, 48th and 72nd hour, respectively, in water. Thus, if $Y_s \geq CV_s$, then the ratio belongs to the female plant, else it is a male plant. The maximum separation in the sample was 166. Evaluation of the function with the evaluation data of 5 water-stressed sample data showed 97 % success of the discrimination function using the ratio of the stressed leaves of the male and the female plants of the nutmeg.

134

Fisher discriminant function classifies the sample data in a satisfactory level. It was observed that misclassification was 5 % in the case of intact leaves and 3 % in the case of the water-stressed leaves. Thus, the difference in male and female leaves of nutmeg plants is enhanced when the leaves are kept in water.

Gas in Scattering Medium Absorption Spectroscopy (GASMAS)

An experimental wavelength modulation spectroscopy signal of a 10-m column of oxygen in free air and the corresponding pure absorption imprint are shown in Figure 28. The slight asymmetry of the WMS signal is due to the variation of the modulation depth during the laser scan. It is convenient to perform experiments, of gas in scattering medium absorption spectroscopy (GASMAS) using oxygen, since it is a common gas with a suitable absorption wavelength, around 760 nm.
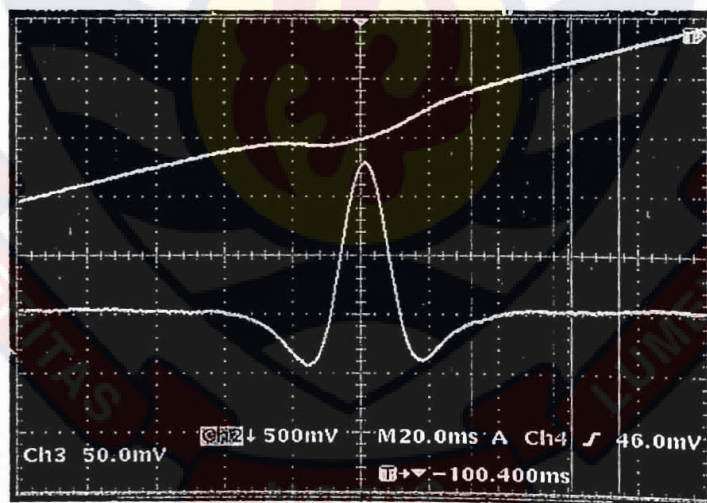

Figure 28. Experimental wavelength modulation spectroscopy signal of a 10-m column of oxygen in free air and corresponding pure absorption imprint.

Molecular oxygen normally diffuses into porous materials from the surrounding atmosphere. Wavelength-modulation spectroscopy (WMS) employing the lock-in technique was used to pick up the second-harmonic component of the signal. The component of the signal oscillating at the modulation frequency is similar to the first derivative of the direct signal, and, correspondingly, the component oscillating at twice the modulation frequency is similar to the second derivative, etc.

Since the direct signal is sloping, due to the simultaneous change in both wavelength and intensity as a function of injection current, the 1f signal is subject to a disadvantageous offset. This gives an advantage in using higher-order components. However, the amplitude normally decreases by increasing the harmonic order. These are the reasons why the component of the signal oscillating at twice the modulation frequency was selected as the output from the lock-in amplifier.

In the measurements, the diode laser and the lens that coupled the laser light into the fibre were placed in an enclosure flushed with nitrogen to eliminate oxygen from the ambient air. Also, the sample was placed directly on the photomultiplier tube (PMT) in order to obtain a high photon collecting efficiency and a high dynamic range. For high gains of the PMT it was necessary to work under dark conditions, not to saturate the detector with background light. With relatively high transmitted light intensities it was possible to spatially limit the detection areas by using the mask with a circular aperture. The maximum wavelength drift was less than 500 MHz/h. Thus, with a pressure-broadened oxygen linewidth of about 3.5

136

GHz at ambient pressure, the drift of the laser wavelength was negligible even during substantial averaging.

In the absorption regime explored, the peak-to-peak value of the signal (S_{WMS}) is linearly proportional to the gas-related differential absorption and to the light intensity reaching the detector. Hence the WMS signal was always normalized by dividing it by the interpolated light intensity at the peak absorption wavelength (S_{Dir}). The optical densities of the samples varied by several orders of magnitude and so did the light levels reaching the detector.

The information extraction was enhanced by first performing a least squares curve fit of an ideal WMS curve to the noisy recorded WMS curve. The ideal WMS curve was obtained by using an experimental curve recorded with a good signal-to-noise ratio. Therefore, instead of directly using the peak-to-peak value of the noisy curve, the corresponding fitting factor constitutes a measure of the gas absorption.

The standard addition method for which fixed lengths of light path through the air were added to the geometric length of the sample enabling the equivalent mean path length (L_{eq}) of the light through the samples to be estimated. Figure 29 shows a graph of how these equivalents mean path lengths were estimated.

On the wood samples, anisotropy related to the fibre structure was studied. This kind of measurement was of fundamental interest in the understanding of light transport in inhomogeneous porous materials. The results of the orientation of the annual rings relative to the direction of the impinging light, that is, the inherent
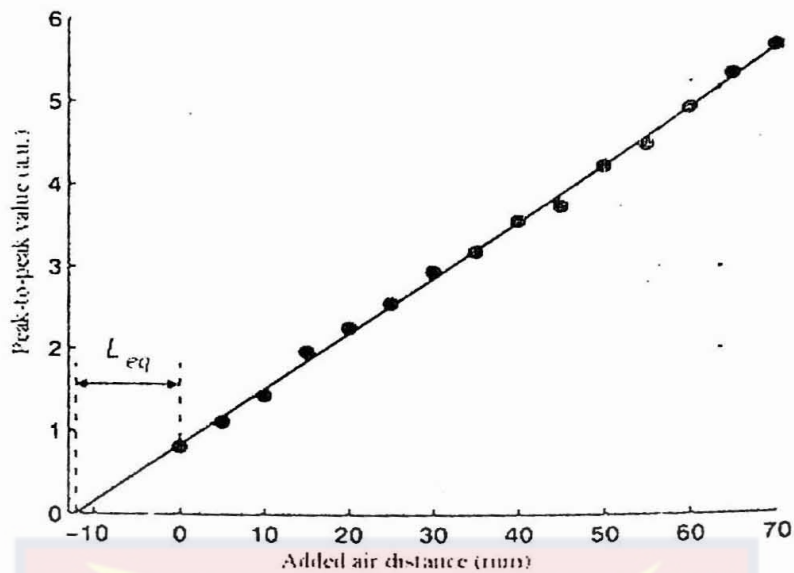
Figure 29. Graph of standard addition method for estimating equivalent mean path length, (L_{eq}) of the light source through the fruit and wood samples [After modification (Alnis et al., 2003)].

anisotropy influencing the light transport on the Norway spruce wood are presented in Figure 30. The error bars indicate the 95% confidence interval and it can be seen that the spread in the data increases for increasing gas absorption, which is related to longer path-lengths and a decreasing amount of light transmitted.

. The measurements on a cube of Scots Pine (*Pinus sylvestris*) ($\rho = 668$ g/dm^3), rendered the same relative difference between the three orientations but with equivalent mean path lengths approximately half the corresponding values for the less dense cube. The lowest gas absorption, and the highest light transmission, was found for the case in which the light was guided along the fibres, that is, when the light path in the wood was shortest.

138
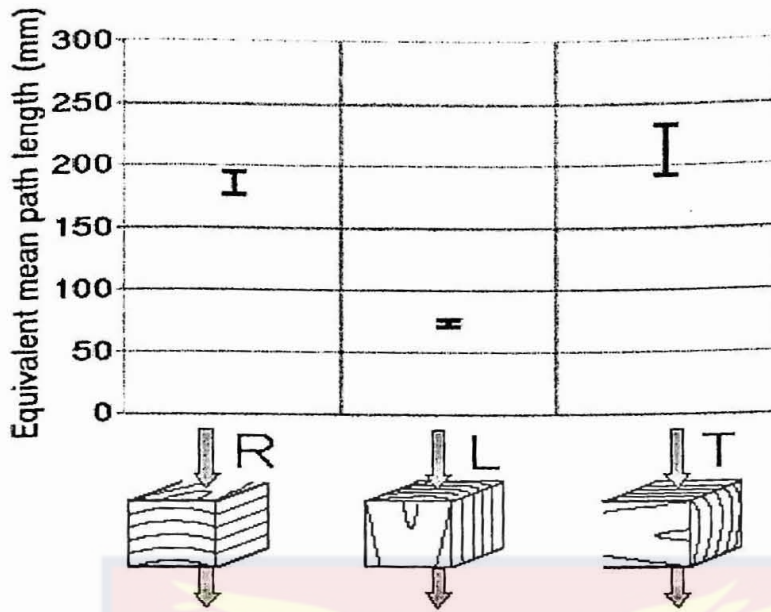
Figure 30. Oxygen absorption measurements through a cube (side 15 mm) of Norway spruce wood radially (R), longitudinally (L) and tangentially (T) along the annual ring layers (From Alnis et al., 2003).

The equivalent mean path lengths of oxygen in eight different types of wood as plotted against the density of the material (ten different densities) are shown in Figure 31. The annual rings in the measured samples had an inclination of approximately 45^0 to the primary impinging laser beam. Data are given for Balsa (*Ochroma pyramidale, curves 1–3*), Norway Spruce (*Picea abies, curve 4*), European Larch (*Larix decidua, curve 5*), Alder (*Alnus glutinosa, curve 6*), Aspen (*Populus tremula, curve 7*), Ash (*Fraxinus excelsior, curve 8*), Birch (*Betula sp., curve 9*), and Scots Pine (*Pinus sylvestris, curve 10*). The error bars indicated correspond to ± 2 standard deviations. The density of wood is an average of the whole sample, and that there could be local variations within the sample.
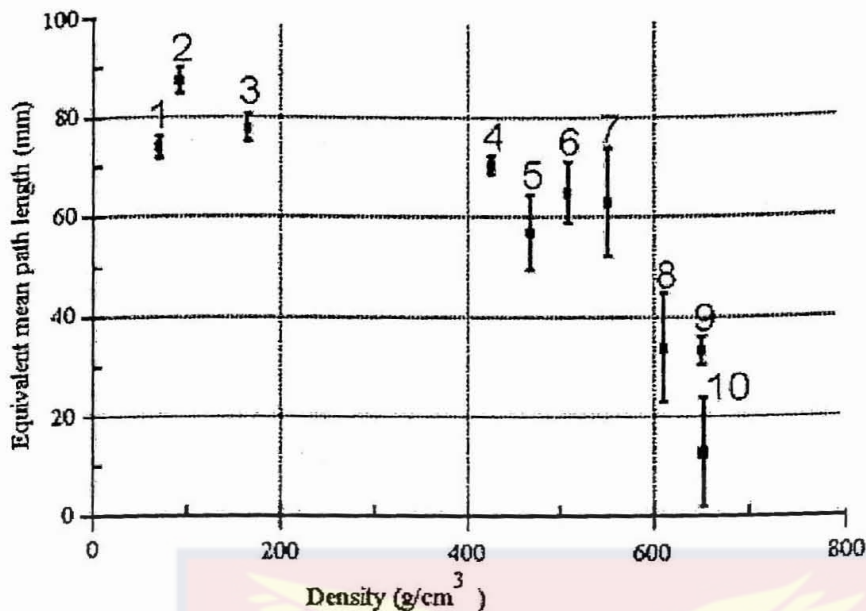
Figure 31. Equivalent mean path length of oxygen for eight different types of wood plotted versus the density of the material [From (Alnis et al., 2003)].

It can clearly be seen that with increasing wood density the oxygen absorption decreased. Measurements were also performed on denser species, Pear, Norway Maple, Beech, Pedunculate Oak, Wych Elm, Wild Cherry and Hornbeam, but the emerging light intensities were too low and consequently the gas absorption signals were too noisy with the present detection system. The most optically dense sample that still gave a measurable gas absorption signal was that of Ash. The lowest gas absorption, and the highest light transmission, was found for the case in which the light was guided along the fibres, that is, when the light path in the wood was shortest.

The dynamic processes related to gas diffusion in the wood are illustrated shown in Figure 32. The curves presented on each data point were obtained by

140
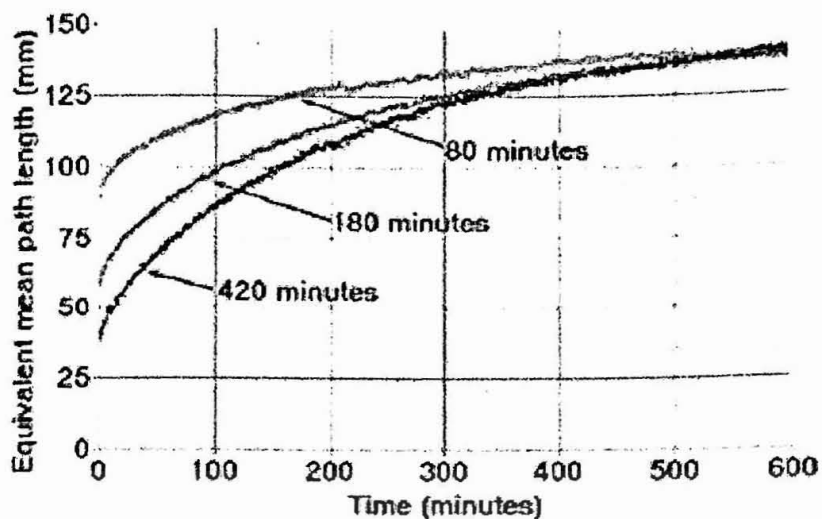
Figure 32. Diffusion of oxygen into the same 10-mm thick sample of Balsa wood that had been stored in pure nitrogen for 80, 180 and 420 minutes [From: (Alnis et al., 2003)].

averaging 64 individual scans on the oscilloscope, an integration time of 16 s. The curves show decay close to an exponential curve. The period of previous oxygen-free storage affected the amount of gas exchanged in the sample; the signal started from a lower level for longer periods in the oxygen-free environment. However, the time constant of re-invasion seemed not to be affected by the length of the pre-treatment, and was found to be approximately three hours.

The diffusion of oxygen into 10-mm-thick slabs of Norway spruce ($\rho = 431$ g/dm^3), Balsa ($\rho = 150$ g/dm^3), and Balsa ($\rho = 71$ g/dm^3) are presented in Figure 33. The graph reveals that the time scale of gas re-invasion was different in different samples of wood. Somewhat unexpectedly, the gas penetration was found to be fastest in the densest material. It was observed that both long and short time constants sometimes govern the gas transport. It seems that gas spreads quickly

141
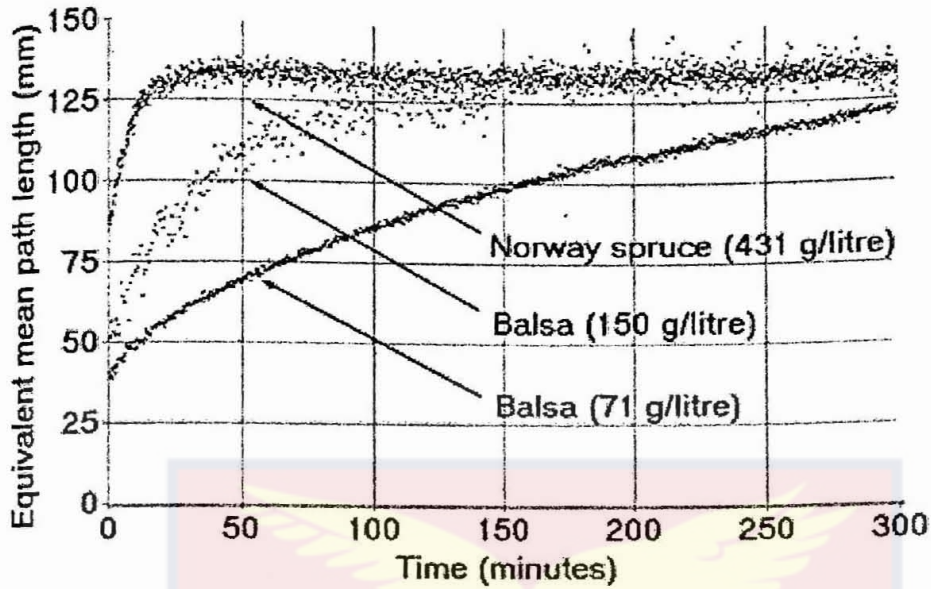
Figure 33. Diffusion of oxygen into 10-mm-thick samples of Norway Spruce (ρ = 431 g/dm^3), Balsa (ρ = 150 g/dm^3), and Balsa (ρ = 71 g/dm^3) [From (Alnis et al., 2003)].

through coarser structures, while penetration through the cell walls of the balsa wood was slow. The equivalent mean path length as a function of time for the Granny Smith apple under different treatments and different measurement geometries is shown in Figure 34.

They all show simple exponential curves with different time constants. For the 24 hours nitrogen exposed apple, the transillumination measurement (a) gave a time constant of 97 minutes and in the case of the backscattering measurement, the time constant was 77 minutes. This difference in time constant is due to the differences in the probe volumes of the measurement geometries.

142
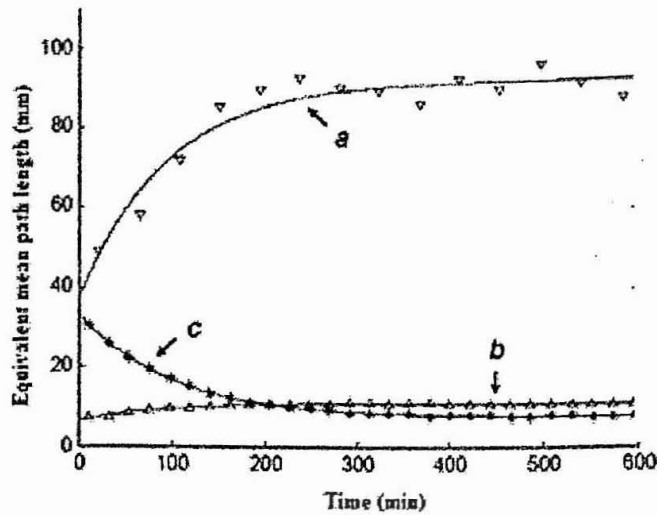
Figure 34. Gas exchange in ambient air on a Granny Smith apple after different treatments, (a) transillumination geometry measurement after apple immersion in nitrogen gas for 24 hours (b) backscattering geometry measurement after apple immersion in nitrogen gas for 24 hours and (c) backscattering geometry measurement after pre-exposing the apple to a higher concentration of oxygen gas [From (Persson et al., 2005)].

The time constant for the backscattering measurement geometry of the high concentrated oxygen gas exposure was 77 minute and the gas content equilibrium curve was slightly lower. This might be due to the extreme levels of oxygen the apple has been exposed to, which might have speeded up the fermentation process of the apple, thus producing more liquid water to reduce the gas content.

The result of the consumption of oxygen by mushroom and apple using backscattering geometry is shown in Figure 35. The samples were kept in a sealed environment and oxygen is consumed leading to lower signal. The change in the oxygen signal is faster for the mushroom than for the apple, which is as a result of

143
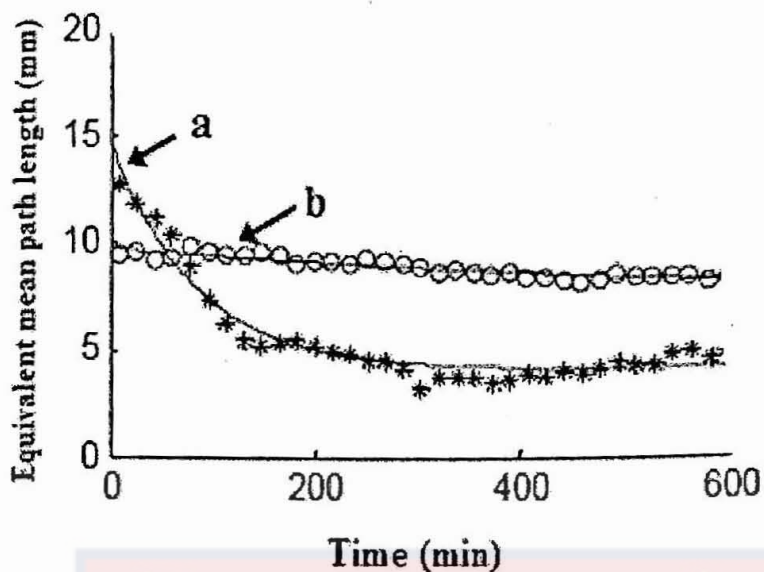
Figure 35. Gas exchange in ambient air in backscattering geometry on a (a) mushroom and (b) Granny Smith apple while sealed in plastic bags [From (Persson et al., 2005)].

the faster respiration rate of the mushroom compared to that of the apple (Gross et al., 2004).

The oxygen diffusion curve for an intact orange after nitrogen exposure is as shown in Figure 36. The time constant was estimated to be approximately 150 minutes. No change in the GMS value with time could be observed for the equally treated pealed orange, which could be due to the lower signals obtained compared to the background noise. However, the results indicated that there is the possibility to study oxygen dynamics in the peal of the orange.

The averages together with error bars corresponding to one standard deviation of the GMS values from three avocados with different maturity levels are shown as a bar graph in Figure 37. The average values were from four measurements.

144
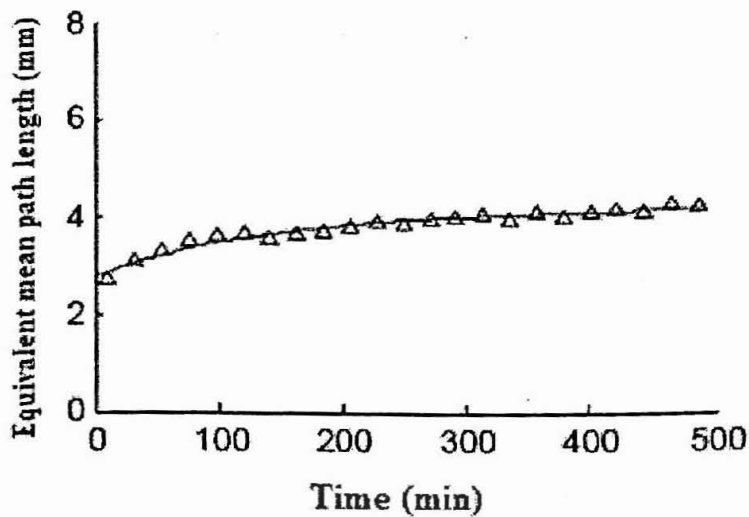
Figure 36. Gas exchange in backscatter geometry for an orange; data intact orange pre-treated by immersion in nitrogen gas for 24 hours. An exponential function is fitted to the data [From (Persson et al., 2005)].
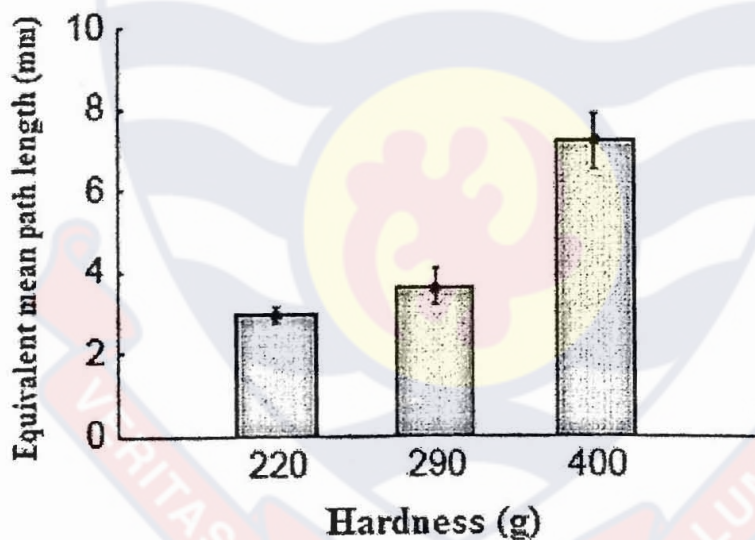
Figure 37. Equivalent mean path length measured for three avocados with different maturity, in backscatter geometry [From (Persson et al., 2005)].

With increasing maturity it was observed that the GMS values decreases which may be due to both lower gas contents and less scattering.

145

CHAPTER FIVE

CONCLUSIONS AND RECOMMENDATIONS

Conclusions

In this work, two diode lasers lasing within the visible and near infrared region at 396 nm and 760 nm respectively were used as spectroscopic sources to study biological materials. Chlorophyll fluorescence emission and gas in scattering medium absorption spectroscopy (GASMAS) were the spectroscopic techniques used. These lasers were generally having unique properties of compactness, wavelength tenability, relatively high output power and relatively narrow bandwidth.

Chlorophyll fluorescence slow induction kinetics for 100 s from the green leaves of male and female nutmeg plants in combination with multivariate analysis, specifically principal component analysis (PCA) and discrimination and classification functions, linear discrimination function for the male and female leaves was then generated. These functions made it possible to discriminate and classify the male and the female nutmeg plants. This is a potential technique for sex discrimination and classification for both in-vivo and in-vitro green leaves of dioecious plants.

The main difference between the slow chlorophyll fluorescence induction kinetics from the green leaves of the male and female nutmeg plants was found within the region where CO_2 fixation is initiated. This shows that slow chlorophyll

146

fluorescence induction kinetics measurement for a longer time tend to dilute the differences.

In the case of gas in scattering medium absorption spectroscopy (GASMAS), this research has established interesting facts on wood samples. The equivalent mean path length of light is short along the longitudinal annual ring layers of the wood and the longest when measured tangentially along the annual ring layer. Also, with increasing wood density the oxygen absorption decreases. The lowest oxygen gas absorption and the longest light transmission were found for the case in which the light was guided along the wood fibres.

In gas diffusion studies, for both wood samples and fruits, the GASMAS signals showed decay curves close to simple exponentials. Gas penetration was found to be fastest in the densest sample. The time constants of re-inversion of oxygen were the same for the same sample of different length of pre-treatments but different for different samples of woods and fruits. It has also been established that different probe volume of measurement geometries bring about different time constants.

The results from the measurements of the fruits show the potential of using the GASMAS technique as possible technique for diagnosis of gases in fruits for quality assessment.

This work has contributed to the study of plants and biological processes, by providing simple and fast technique for the discrimination of nutmeg plant sex and by using analysis of gases in porous biological materials from which two peer-reviewed papers has been published.

147

Recommendations

For increased monitoring and classification capability, multispectral techniques on data generated, using either light emitting diodes (LEDs) or diode lasers, can be used to get valuable information from the samples. Single source imaging or multispectral imaging in both spatial and temporal domains, such as using induction kinetic imaging, can also be used to advance this research.

For applications and advancements of gas in scattering medium absorption spectroscopy GASMAS, it is being recommended that additional gases with absorption compatible with the bulk material transmission are studied. Water vapour in scattering media is of special interest.. Time constants for fruits as a way of establish their shelf-life is also recommended. Gas diffusion and effusion studies using GASMAS in food also seem feasible, as recently demonstrated by Lewander et al. (Lewander et al., 2008).

The basic detection principle of GASMAS, that is wavelength modulation spectroscopy, can also be used to monitor environmentally important gases such as methane and NO_2.

REFERENCES

Agati, G., Fusi, F., Mazzinaghi, P. and Paola, L. M. (1993) A simple approach to the evaluation of the reabsorption of the chlorophyll fluorescence spectra in intact leaves. J. Photochem. Photobiol. B. Biol. **17**, 163–171.

Agati, G., Mazzinghi, P., Fusi, F., and Ambrosini, I. (1995) The $F685/F730$ chlorophyll fluorescence ratio as a tool in plant physio: response to physiological and environmental factors. J. Plant Physio. **145**, 228–238.

Agati, G., Mazzinghi, P., Lipucci, di Paola M., Fusi, F. and Cecchi, G. (1996) The F685/F730 chlorophyll fluorescence ratio as indicator of chilling stress in plants. Journal of Plant Physio. **148**, 384–390.

Alnis, J., Anderson, B., Sjöholm, M., Somesfalean, G. and Svanberg, S. (2003) Laser spectroscopy of free molecular oxygen dispersed in wood material. Appl. Phys. B **77**, 691-695.

Alnis, J., Gustafsson, U., Somesfalean, G., and Svanberg, S. (2000) Sum-frequency generation with a blue diode laser for mercury spectroscopy at 254 nm. Appl. Phys. Lett. **76**, 1234-1236.

Anderson, B., Buah-Bassuah, P. K. and Tetteh, J. P. (2004) Using violet laser-induced chlorophyll fluorescence emission spectra for crop yield assessment of cowpea (*Vignaunguiculata (L) Walp*) varieties. Meas. Sci. Technol. **15**, 1255–1265.

Andersson, M., Persson, L., Sjöholm, M. and Svanberg, S. (2006) Spectroscopic studies of wood-drying processes. Opt. Exp. **14**, 3641–3653.

Andrich, G., Zinnai, A., Silvestri, S., and Fiorentini, R. (1994) Automatic

149

control of aerobic and anaerobic respiration rates of fruit stored in refrigerated and controlled atmospheres. Auto. Cont. Food Biol. Proc. **36**, 281-287.

Armstrong, J. E. and Irvine, A. K. (1989) Flowering, sex ratios, pollen-ovule ratios, fruit set and reproductive effort or a dioecious tree myristica insipida (myristicaceae), in two different rain forest communities. Amer. J. Bot. **76**, 74-85.

Avetisov, V. G. and Kauranen, P. (1996) Two-tone frequency-modulation spectroscopy for quantitative measurements of gaseous species: theoretical, numerical and experimental investigations. Appl. Opt. **35**, 4705-4723.

Avetisov, V. G. and Kauranen, P. (1997) High-resolution absorption measurements by use of two-tone frequency modulation spectroscopy with diode lasers. Appl. Opt. **36**, 4043–4054.

Baker, N. R. and Rosenqvist, E. (2004) Application of chlorophyll fluorescence can improve crop production Strategies: an examination of future possibilities. J. Exp. Bot., **55**, 1607-1621.

Banwell, C. and McCash, E. (1994) *Fundamentals of Molecular Spectroscopy*, 4th ed., McGraw-Hill Publishing Company, London.

Barmore, C. R. (1987) Packing technology for fresh and minimally processed fruits and vegetables. J. Food Qual. **10**, 207–217.

Barócsi, A., Kocsányi, L., Várkonyi, S., Richter, P., Csintalan, Z. and Szente,

150

K. (2000) Two wavelength, multipurpose. truly portable chlorophyll fluorometer and its application in field monitoring of phytoremediation. Meas. Sci. Technol. **11**, 717-729.

Beaudry. R. M. (1999) Effect of O_2 and CO_2 partial pressure on selected phenomena affecting fruit and vegetable quality. Post-harvest Biol. Technol. **15**, 294-303.

Bengtsson, M., Wallström, S., Sjöholm, S., Grönlund, R., Anderson, B., Larsson A., Karlsson, S., Kroll. S. and Svanberg, S. (2005) Fungus covered insulator materials studied with laser-induced fluorescence and principal component analysis. Appl. Spec. **59**, 1037-1041.

Berg , C. J.. Harper, M. A., Atkinson, S. M., Bell, E. A., Brown, H. L., Hage, M. L., Mitra, A. G., Moise. K. J. Jr. and Callaghan, W. M. (2005). Preventability of pregnancy- related deaths: results of a state wide review. Obst. and Gyneco. **106**. 1228-1233.

Biffi. R., Restiva. F. M., Tassi F., Carboni A., Marziani G. P., Spada, A. and Falvigna (1995) A restriction fragment length polymorphism probe for early diagnosis of gender in *Asparagus officinalis*. L. Hort., Sci. **30**, 1463-1464.

Bilger. W., Veit, M., Schreiber, L and Schreiber, U. (1997) Measurement of leaf epidermal transmission of UV radiation by chlorophyll fluorescence. Physio. Planta. **101**, 754-763.

Bjorklund. G. C. (1980) Frequency modulation spectroscopy: a new method for measuring weak absorptions and dispersion. Opt. Lett. **5**, 15-17.

Bjorklund. G. C., Levenson, M. D., Lenth, W. and Ortiz, C. (1983) Frequency

modulation (FM) spectroscopy: theory of lineshapes and signal-to-noise ratios. Appl. Phys. B **32**, 145-152.

Bomse. D. S. (1991) Dual-modulation laser line-locking scheme. Appl. Opt. **21**, 2922-2924.

Bomse. D. S.. Stanton. A. C. and Silver, J. A. (1992) Frequency modulation and wavelength modulation spectroscopes: comparison of experimental methods using a lead-salt diode laser. Appl. Opt. **31**, 718-731.

Buschmann, C. and Lictenthaler. H. K. (1998) Principles and characteristics of multi-colour fluorescence imaging of plants. J. of Plant Physio. **152**, 297–314.

Buschmann, C. and Schrey. H. (1981) Fluorescence induction kinetics of green and etiolated leaves recording the complete in-vivo emission spectra. Photosynth Res. **1**, 233 – 241.

Buschmann, C., and Lichtenthaler. H. K. (1988) Reflectance and chlorophyll fluorescence signatures of leaves. In *Applications of Chlorophyll Fluorescence*, H. K. Lichtenthaler (Ed.). Kluwer Academic, Dordrecht. 325- 332.

Cameron A. C.. Talasila P. C., and Joles D. W. (1995) Predicting film permeability needs for modified-atmosphere packaging of lightly processed fruits and vegetables. Hort. Sci. **30**, 25-34.

Cassidy. D. T. and Reid. J. (1982). Atmospheric pressure monitoring of trace gases using tunable diode lasers. Appl. Opt. **21**, 1185 – 1190.

Cerovic. Z.. Samson, G.. Morales, F.. Tremblay. N., and Moya, I. (1999)

Ultraviolet-induced fluorescence for plant monitoring: Present state and prospects. Agronomie: Agr. Environ. **19**, 543–578.

Chappelle, E. W. and Williams, D. L. (1986) Laser-induced fluorescence (LIF) from plant. Proc. IGARSS' symp., Zürich, 1591 – 1598.

Chappelle, E. W., Wood, F. M. Jr, McMurtrey, J. E. III and Newcomb, W. (1985) Laser-induced fluorescence of green plants: I. A technique for the remote detection of plant stress and species differentiation. Appl. Opt. **23** 134–138.

Chappelle, E., McMurtrey, J., Wood, F. and Newcomb, W. (1984) Laser-induced fluorescence of green plants: 2. LIF caused by nutrient deficiencies in corn. Appl. Opt. **23**, 139–142.

Cooney, K. M., Gossage, K. W., McShane, M. J., Motamedi, M. and Cote, G. (1998) Development of an optical system for the detection of oral cancer using near-infrared spectroscopy. Proc. IEEE Eng. Med. Biol. **20**, 906-909.

Cooper, D. E. and Gallagher, T. F. (1985) Double frequency modulation spectroscopy: high modulation frequency with low-bandwidth detectors. Appl. Opt. **24**, 1327 – 1334.

Cooper, D. E. and Warren, R. E. (1987) Two-tone optical heterodyne spectroscopy with diode laser: theory of line shapes and experimental results. J. Opt. Soc. Am. B **4**, 470-80.

Cooper, D. E. and Watjen, J. P. (1986) Two-tone optical heterodyne spectroscopy with a diode laser tunable lead-salt diode laser. Opt. Lett. **11**, 606-608.

153

D'Amato, F. and De Rosa, M. (2002) Tunable diode lasers and two-tone frequency modulation spectroscopy applied to atmospheric gas analysis. Opt. and Lasers in Eng. **37**, 533-551.

Dadzie, B. D., Banks, N. H., Cleland, D. J. and Hewett, E. W. (1996) Changes in respiration and ethylene production of apple in response to internal and external oxygen partial pressure. Postharvest Biol. Technol. **9**, 297-309.

Dahn, H. G., Gunther, K. P. and Lodecker, W. (1992) Characterization of drought stress of maize and wheat by means of spectral resolved laser-induced fluorescence. EARSeL Adv. Remote Sens. **1**, 12–19.

Dam, J. S., Anderson, P. E., Dalgaard, T. and Fabricius. P. E. (1998) Determination of tissue optical properties from diffuse reflectance profiles by multivariate calibration. Appl. Opt. **37**, 772-778.

Dau. H. (1994). Molecular mechanisms and quantitative models of variable photosystem II fluorescence. Photochem. and Photobio. **60**: 1 – 23.

Davies, A. M. C. (2005) Back to basis: applications of principal component analysis, Spect. Euro. **17**, 30-31.

Davies, A. M. C. and Fearn, T. (2005) Back to basis: the principles of principal component analysis. Spect. Euro. **16**, 20-23.

Day, T. A., Howells, B. W., Rice, W. J. (1994) Ultraviolet absorption and epidermal-transmittance spectra in foliage. Physiologia Plantarum **92**, 207–218.

Demtroder W. (2003) *Laser spectroscopy - Basic concepts and instrumentation.* 3nd ed. Springer-Verlag, Berlin.

154

Everitt, B. S. and Dunn, G. (2001) *Applied Multivariate Data Analysis*. 2nd ed. Oxford University Press, London.

Ek, S., Anderson, B and Svanberg, S. (2008) Compact fiber-optic fluorosensor employing light-emitting ultraviolet diodes as excitation sources. spectrochimica Acta Part B **63**, 349–353.

Eriksson, L., Johansson, E., Kettaneh-Wold, N., Trygg, J., Wikstrom, C. and Wold, S. (2006) *Multi- and Megavariate Data Analysis: Basic principles and Applications*. 2nd ed. Umetrics AB, Sweden.

Esbensen, K. H. (2002) *Multivariate Data Analysis – In Practice*. Camo Process AS, Oslo, Norway.

Everitt, B. S. and Dunn, G. (2001). *Applied Multivariate Data Analysis*, 2nd ed. Edward Arnold, London.

Faist, J., Capasso, F., Sivco, D. L., Sirtori, C., Hutchinson, A. L. and Cho, A. Y. (1994) Quant. Casca. Laser. Sci. **264**, 553-556.

Fidler, J. C. and North, C. J. (1967) The effect of conditions of storage on the respiration of apples. I. the effect of temperature and concentrations of carbon dioxide and oxygen on the production of carbon dioxide and uptake of oxygen. J. Hort Sci. **42**, 189-206.

Fisher, R. A. (1936) The use of multiple measurements in taxonomic problems. Ann. of Euge. **7**, 179–184.

Flach, M. (1966) Nutmeg cultivation and its sex problems. Eng. sum. meded. Landh Hogesh. **66**, 1.

Franck, F., Juneau, P. and Popovic, R. (2002) Resolution of the photosystem I

and photosystem II contributions to chlorophyll fluorescence of intact leaves at room temperature. Biochimica and Biophysica Acta **1556**, 239-246.

Gable, R. S. (2006) The toxicity of recreational drugs. Amer. Scien. **94**, 206-208.

Gansert, D., Burgdorf, M. and Lösch, R. (2001) A novel approach to the in situ measurements of oxygen concentrations in the sapwood of woody plants. Plant Cell Env. **24**. 1055-1064.

Gillies, S. L., Cliff, M. A., Toivonen, P. M. E. and King, M. C. (1997) Effect of atmosphere on broccoli sensory attributes in commercial MAP and microperforated packages. J. Food Qual. **20**. 105 - 115.

Gitelson, A. A., Buschmann, C and Lichtenthaler, H. K. (1999) The chlorophyll fluorescence ratio F735/F700 as an accurate measure of the chlorophyll content in plants. Remote Sens. Environ. **69**, 296 – 302.

Govindjee (1982) *Photosynthesis* 2. Academic Press, N.Y.

Govindjee (1990) Photosystem II heterogeneity: the acceptor side. Photosynth. Res. **25**, 151 - 160.

Govindjee and Coleman. W. J. (1990) How plants make oxygen. Scien. Amer. **262**. 50 - 58.

Govindjee, Amesz, J. and Fork, D.C. (1986) *Light Emission by Plants and Bacteria*. Academic Press, Orlando.

Govindjee (1995) Sixty-three years since Kautsky: chlorophyll a fluorescence. Austra. Journ. of Plant Physio. **22**, 711–711.

Griffin. R. M., E. P. Webster, W. Zhang, C. T. Leon. and C. R. Mudge. (2004) Management of perennial grasses in Louisiana rice. Proc. South. Weed Sci. Soc. **57**, 302.

Gross. K.C.. Wang. C.Y. and Saltveit. M. (2004) The Commercial Storage of Fruits, Vegetables, and Florist and Nursery Stocks. Agric. Handbook **66**.

Gunther. K. P.. Dahn, H. G. and Lodecker, W. (1994) Remote sensing vegetation status by laser-induced fluorescence. Remote Sens. Environ. **47**, 10-17.

Gustafsson. U., Somesfalean, G., Alnis, J. and Svanberg, S. (2000) Frequency-modulation spectroscopy with blue diode lasers. Appl. Opt. **39**, 3774-3780.

Guyot. G. and Major, D. (1988) Coupled fluorescence and reflectance measurements to improve crop productivity evaluation. In *Applications of Chlorophyll Fluorescence*. H. K. Lichtenthaler (Ed.). Kluwer Academic, Dordrecht. 319 324.

Haitz. M. and lichtenthaler, H. K. (1988) The measurement of Rfd-values as plant vitality indices with the portable field fluorometer and the PAM-fluorometer. In: *Application of Chlorophyll Fluorescence*, H. K. Lichtenthaler, (Ed.), Kluwer Academic publishers. Dordrecht, 249-254.

Harris. P. J. and Hartley, R. D. (1976) Detection of bound ferulic acid in the cell walls of the Gramineae by ultraviolet fluorescence microscopy. Natu. **259**, 508 510.

Harvey. K. C. and Myatt. C. J. (1991) External-diode laser using a grazing-incidence diffraction grating. Optics Letters **16**, 910 -912.

157

Hecht. E. (2008) *Optics*. 4th ed. Addison Wesley.

Hertog. M. L. A. T. M., Peppelenbos, H. W., Evelo R. G. and Tijskens, L. M. M. (1998) A dynamic and generic model of gas exchange of respiring produce: the effect of oxygen, carbon dioxide and temperature. Posthharvest Biol. Technol. **14**, 335-49.

Hoadley. R. B. (1980) *Understanding Wood: a Craftsman's Guide to Wood Technology*. Taunton Press Inc. USA.

Hoadley, R. B. (1990) *Identifying Wood: Accurate Results with Simple Tools*. Taunton Press Inc, USA.

Hormaza. J. I., Dollo, L. and Polito, V. S. (1994) Identification of a RAPD marker linked to sex determination in *pistacia vera* using bulked segregant analysis. Theor. Appl. Genet. **89**, 9-13.

Hotelling. H. (1933) Analysis of a Complex of Statistical Variables Into Principal Components. Journal of Educational Psychology. **24**, 417-441 and 498-520.

Iguchi. T. (1986) Modulation waveforms for second-harmonic detection with tunable diode laser. J. Opt. Soc. Am. B **3**, 419-423.

Jacobsen. G., Olesen. H. and Birkedahl (1982) Current/frequency-modulation characteristics for directly optical frequency-modulation injection laser at 830 nm and 1.3 μm. Electron. Lett. **18**, 874-876.

Janik. G. R., Carlisle. C. B. and Gallagher, T. F. (1986) Two-tone frequency-modulation spectroscopy. J. Opt. Soc. Am. B **3**, 1070-1074.

Johnson. R. A. and Wichern. D. W. (2002) *Applied Multivariate Statistical*

Analysis, 5th ed. Prentice Hall. Upper Saddle River. NJ.

Karel. V. and Jurin. M. (1963) Studies on control of respiration of McIntosh apples by packaging methods. Food Technol. **17**, 782-786.

Kautsky. H. and Hirsch, A. (1931) Neue Versuche zur Kohlenstoffassimilation. Naturwissenschaften **19**, 969.

Kelley, S. S., Rials, T. G., Snell, R., Groom. L. R. and Sluiter. A. (2004) Use of near infrared spectroscopy to measure the chemical and mechanical properties of solid wood. Wood Sci. Technol. **38**. 257 276.

Kluczynski. P. and Axner. A. (1999) Theoretical description based on Fourier analysis of wavelength-modulation spectrometry in terms of analytical and background signals. Appl. Opt. **38**, 5803–5815.

Konopacka, D. and Plochatski, W. J. (2004) Effect of storage conditions on the relationship between apple firmness and texture acceptability. Posthharvest Biol. Technol. **32**, 205-11.

Krause. G. H. and Weis. E. (1984) Chlorophyll fluorescence as a tool in plant physiology II: Interpretation of fluorescence signal. Photosynth. Res. **5** 139- 157.

Krause. G. H. and Weis, E. (1991) Chlorophyll fluorescence and photosynthesis: The basics. Annu. Rev. Plant Physiol. Plant Mol. Biol. **42**, 313-349.

Lakowicz. J. R. (1999) *Principles of Fluorescence Spectroscopy*, 2nd ed. Kluwer, Academic /Plenum publishers, New York.

Lang. M. and Lichtenthaler, H. K. (1990) Changes in the blue-green and red

fluorescence emission spectra of beech leaves during the autumnal chlorophyll breakdown. J. Plant Phys. **38**, 550 – 553.

Lang, M., Lichtenthaler, H. K., Sowinska, M., Summ, P., Heisel, F., Miehe, J. A. and Tomasini, F. (1995) Application of laser-induced fluorescence imaging in the detection of plant stress Proc.2nd Int. Symp. Exhibition on Environmental Contamination in Central and Eastern Europe (Budapest, 1994). P. I. Richter and R. C. Herndon (Ed.), Rockville, USA: Government Institutes. 88 –90.

Laqua, K., Melhuish, W. H. and Zander, M. (1988) Molecular absorption spectroscopy, ultraviolet and visible (UV/VIS). Pure and Appl. Chem. **60**. 1449-1460.

Lenth, W. (1984) High frequency heterodyne spectroscopy with current modulation diode laser. IEEE, J. Quantum Electron. QE **20**, 1045-1050.

Lenth, W., Gerthz, M. and Young, A. T. (1985) High frequency modulation spectroscopy with tunable GaAs and lead salt diode laser. J. Opt. Soc. Am. A **2**, 99.

Levine, R. P. (1968) Genetic dissection of photosynthesis. Sci. **162**, 3855, 768 – 771.

Lewander, M., Guan, Z.G., Persson, L., Olsson, A. and Svanberg, S. (2008) Food monitoring based on diode laser gas spectroscopy. Appl. Phys. B **93**, 619- 625.

Lichtenthaler, H. K. (1988) *Application of Chlorophyll Fluorescence*. Dordrecht: Kluwer.

160

Lichtenthaler. H. K. (1981) Adaptation of leaves and chloroplasts to high quanta fluence rates. In: *Photosynthesis VI.* G. Akoyunoglou. Balaban. (ed.). International science. Philadelphia. 273 - 287.

Lichtenthaler. H. K. (1984) Influence of environmental factors on composition and function of the photosynthetic apparatus. In: *Advances in Photosynthesis Research* IV, C. Sybesma (Ed.). Martinus Nijhoff/Dr. W. Junk publisher. The Hague. 241 – 244.

Lichtenthaler. H. K. (1986) Laser-induced chlorophyll fluorescence of living plants. In: *Proceed. Internat. Geoscience and Remote Sensing symposium.* IGRASS Zürich. III. Noordwijk, ESA Publications Division. 1571 – 1679.

Lichtenthaler. H. K. (1987) Chlorophylls and carotenoids: Pigments of photosynthetic biomembranes. Methods in Enzymology 148. 350–382.

Lichtenthaler. H. K. (1987) Chlorophyll fluorescence signatures of leaves during the autumnal chlorophyll breakdown. J. Plant Physio. 131, 101–110.

Lichtenthaler. H. K. (1990) *Applications of Chlorophyll Fluorescence in Stress Physiology and Remote Sensing, Applications of Remote Sensing in Agriculture.* (M. Steven and J. A. Clark, Eds). Butterworths Scientific, London. 287-305.

Lichtenthaler. H. K. (1992) The Kautsky effect: 60 years of chlorophyll fluorescence induction kinetics. Photosynthetica 27, 45 - 55.

Lichtenthaler. H. K. and Babani. F. (2004) Light adaptation and senescence of the photosynthetic apparatus. Changes in pigment composition. chlorophyll fluorescence parameters and photosynthetic activity. In: *Chlorophyll a*

Fluorescence: a Signature of Photosynthesis. G. C. Papageorgiou and Govindjee (Ed.) Dordrecht. The Netherlands: Springer. 713-736.

Lichtenthaler. H. K. and Rinder. U. (1988) Chlorophyll fluorescence spectra of Leaves as induced by blue light and red laser light. In: Proc 4th Intern Sympos Spectr Signat of Objects in Remote Sensing, Aussois 1988.

Lichtenthaler. H. K. and Rinderle, U. (1988) The role of chlorophyll fluorescence in the detection of stress conditions in plants. CRC Crit. Rev. Anal. Chem. **19**, 29-85.

Lichtenthaler. H. K. and Buschmann. C. (1987) Chlorophyll fluorescence spectra of green bean leaves. J. Plant Physiol. **129**. 137-147.

Lichtenthaler. H. K.. Hak, R. and Rinderle. U. (1990) The chlorophyll fluorescence ratio F690/F730 in leaves of different chlorophyll content. Photosynth. Res. **25**. 295 – 298.

Lichtenthaler. H. K.. Langsdorf, G., Lenk. S. and Buschmann. C. (2005) Chlorophyll fluorescence imaging of photosynthetic activity with the flash-lamp fluorescence imaging system. Photosynthetica **43**, 3, 355-369.

Lichtenthaler. H. K.. Buschmann. C., Rinderle, U. and Schmuck, G. (1986) Application of chlorophyll fluorescence in ecophysiology. Radiation and Environmental Biophysics **25**, 4. 297-308.

Maiman. T. (1960) Stimulated optical radiation in ruby. Nature **187**, 493-494.

Mannapperuma. J. D.. and Singh, R. P. (1994) Modeling of gas exchange in

polymeric packages of fresh fruits and vegetables. In: *Process Optimization and Minimal Processing of Foods*, R. P. Singh (ed). Boca Raton, FL, USA: CRC Press, 437.

Martens, H. and Naes, T. (1991) *Multivariate Calibration*. John Wiley and Sons Ltd, Chichester.

Meyer, S., Cartelat, A., Moya I. and Cerovic, Z. G. (2003) UV-induced blue-green and far-red fluorescence along wheat leaves: a potential signature of leaf ageing. J. of Exp'l Bot. **54**, 383, 757 -- 769.

Mika, S., Ratsch, G., Weston, J., Scholkopf, B. and Muller, K. R. (1999) Fisher analysis with kernels. In: *Neural Networks for Signal Processing IX*, Y.H. Hu, J. Larsen and E. Wilson *et al.*, (Eds.). IEEE Press, New York, 41–48.

Miller, D.R., Devlin, D.R., and J.H. Borden (1994) The use of anti aggregation semio-chemicals in controlling pine engravers in stands of lodgepole pine. USDA For. Service Gen. Tech. Rep., PSW-150. Washington D.C.; 6.

Moses, E. I. and Tang, C. L. (1977) High sensitivity laser wavelength modulation spectroscopy. Opt. Lett. **1**, 115-117.

Mountney, G. J. and Gould, W. A. (1988) *Practical Food Microbiology and Technology*. 3rd edition. Van Nostrand Reinhold Co., New York, NY, 99-117.

Mulcahy, D. L., Weeden, N. F., Kesseli, R. and Carroll, S. (1992) DNA probe for Y-chromosome of silene latifolia, a dioecious angiosperm. Sex Plant Reprod. **5**. 86-88.

Nakamura, S., Pearton, S. and Fasol, G. (2000) *The Blue Laser Diode-the*

Complete Story, 2nd ed. Springer. Berlin.

Nayar. B. K., Rajendar, R. and Vathsala, P. (1977) A simple morphological technique to distinguish the sex of nutmeg seedlings. Curr. Sci. **46**, 156-157.

Nedbal. L., Soukupová. J., Kaftan, D., Whitmarsh, J. and Trtílek. M. (2000) Kinetic imaging of chlorophyll fluorescence using modulated light. Photosyn. Res. **66**, 3-12.

Negel. E. M., Buschmann. C. and Lichtenthaler. H. K. (1987) Photoacoustic spectra of needles as an indicator for the activity of the photosynthetic apparatus of healthy and damaged conifers. Physiol. Plantarum **70**, 427 – 437.

Nguyen. Q. V., Dibble. R.W. and Day. T. (1994) High-resolution oxygen absorption spectrum obtained with an external-cavity continuously tunable diode laser. Opt. Lett. **19**, 24, 2134-2136.

Nilsson. A. M. K., Heinrich. D., Olajos, J. and Andersson-Engels, S. (1997) Near infrared diffuse reflection and laser-induced fluorescence spectroscopy for myocardial tissue characterization. Spectrochim. Acta **53**, 1901-1912.

Nobel Laureates in Physics (1964) www.nobelprize.org/nobel_prizes/physics/laureates/1964/index.html. 20th June. 2008.

Olson. M. L., Grieble, D. L. and Griffiths, P. R. (1980) Second derivative tunable diode laser spectrometry for line profile determination Theory, Appl. Spect. **34**, 50-56.

Oomens, J., Zuckermann, H., Persijn, S., Parker, D. H., and Harren, F. J. M. (1996) Co-laser based photoacoustic trace-gas detection: applications in postharvest physiology. Appl. Phys. B **67**, 459-66.

Ounis, A., Cerovic, Z., Briantais, J., and Moya, I. (2001) Dual-excitation FLIDAR for the estimation of epidermal UV absorption in leaves and canopies. Remote Sens. of Env. **76**, 33–48.

Packiyasothy, E. V., Jansz, E. R. and Dharmadasa, H. M. (1991) Studies on some chemical components of nutmeg (*Myristica fragrans* Houtt) leaf directed at determination of sex of seedling. J. Natn. Sci. Coun. Sri Lanka **19**, 91-98.

Panshin, A.J. and De Zeeuw. C. (1980) *Textbook of Wood Technology*, 4th ed. McGraw-Hill, New York, NY.

Parasnis, A. S., Gupta, V. S., Tamhankar, S. A., Ranjekar, P. K., (2000) A highly reliable sex diagnostic PCR assay for mass screening of papaya seedlings. Mol. Breed. **6**, 337–344.

Persson, L., Anderson, B., Andersson, M., Sjöholm, M. and Svanberg S. (2005) Studies of gas exchange in fruits using laser spectroscopic techniques. FRUTIC 05, **12**, 543 -551.

Pfündel, E. (1998) Estimating the contribution of photosystem I to total leaf chlorophyll fluorescence. Photosyn. Res. **56**, 185 195.

Phadnis, N. A. and Choudhary, K. G. (1971) Sex determination in the seedling stage of nutmeg (*Myristica fragrans* Houtt.). Trop. Science **13**, 265-274.

Reeves, J. B., III. and Delwiche, S. R. (2003) SAS partial least squares

regression for analysis of spectroscopic data. J. Near Infrared Spectrosc. **11**, 415 – 431.

Reid. J. and Labrie. D. (1981) Second-harmonic detection with tunable diode lasers comparison of experiment and theory. Appl. Phys. B **26**, 203-210.

Reid. J.. Garside. B. K., Schewchun. J., El-Sherbiny and Ballik. E. A. (1978a) High sensitivity point monitoring of atmospheric gases employing tunable diode lasers. Appl. Opt. **17**, 1806-1810.

Reid. J.. Shewchum, J.. Garside, B. K. and Ballik. E. A. (1978b). High sensitivity pollution detection employing tunable diode lasers. Appl. Opt. **17**, 300 – 307.

Rinderle. U. and Lichtenthaler, H. K. (1988) The chlorophyll fluorescence ratio F690/F735 as a possible stress indicator. In: *Applications of Chlorophyll Fluorescence*, H. K. Lichtenthaler, (Ed.). Kluwer academin press, Dordrecht, The Netherlands. 176 – 183.

Ritter, K. J. and Wilkerson, T. D. (1987) High-resolution spectroscopy of the oxygen A band. J. Molec. Spectrosc. **121**, 1, 1-19.

Rosema. A.. Snel, J., Zahn, H.. Buurmeijer, W. and Van-Hove, L. (1998) The relation between laser-induced chlorophyll fluorescence and photosynthesis. Remote Sens. of Env. **65**, 143– 154.

Rothman, L. S., Rinsland, C. P.. Goldman, A.. Massie, S. T.. Edwards, D. P., Flaud, J. M., Perrin, A.. Camy-Peyret. C., Dana, V.. Mandin, J. Y., Schroeder, J.. McCann, A.. Gamache, R. R.. Wattson, R. B., Yoshino, K., Chance, K. V.. Jucks, K. W.. Brown, L. R.. Nemtchinov, V., and Varanasi,

P. (1998) The HITRAN molecular spectroscopic database and HAWKS (HITRAN atmospheric workstation): 1996 edition. J. Quant. Spect. Radiant. Trans. **60**, 665 – 710.

Rothman, L. S., Gamache, R. R., Tipping, R. H., Rinsland, C. P., Smith, M. A. H., Benner, D. C., Devi, V. M., Flaud, J. M., Camy-Peyret, C., Perrin, A., Goldman, A., Massie, S. T., Brown, L. R. and Toth, R. A. (1992) The HITRAN molecular database: editions of 1991 and 1992. J. Quant. Spect. Radiant. Trans **48**, 469-507.

Saito, Y., Kanoh, M., Hatake, K. I., Kawahara, T. D. and Nomura, A. (1998) Investigation of laser-induced fluorescence of several natural leaves of application to lidar vegetation monitoring. Appl. Opt. **37**, 431–437.

Saito, Y., Kanoh, M., Takeuchi, A., Kawahara, T. D., Nomura, A., Ishizawa, H., Matsuzawz, T. and Komatsu, K. (2000b) Application of laser-induced fluorescence to growth monitoring of agricultural products (lettuce), In: First International Conference of Geopatial Information in Agriculture and Forestry. Lake Buena Vista, Florida. 509 - 515.

Saito, Y., Saito, R., Kawahara, T. D., Nomura, A. and Takeda, S. (2000a). Development and performance characteristics of laser-induced fluorescence imaging lidar for forestry applications. Forest Ecol and Manag't **128**, 129-137.

Schawlow, A. and Townes, C. (1958) Infrared and optical masers. Phys. Rev. **112**, 1940-1949.

Schneckenburger, H. and Bader, J. (1988) Fiber-optic detection of chlorophyll

fluorescence. In: *Application of Chlorophyll Fluorescence*, H. K. Lichtenhaler. (Ed). Kluwer academin press. Dordrecht. The Netherlands. 255 258.

Shibu. M. P.. Ravishankar, K. V.. Anand, L.. Ganeshaiah. K. N. and Shaanker, U. (2000) Identification of sex-specific DNA markers in the dioecious tree, nutmeg (*Myristica fragrans* Houtt.). PGR Newsletter, FAO – IPGRI **121,** 59-61.

Shulgin, A. T.. Sargent. T. W. and Naranjo. C. (1967) Chemistry and psychopharmacology of nutmeg and of several related phenylisopropylamines. United States Public Health Serv. Pub. **1645,** 202–214.

Siegman. A. E. (1986) *Lasers.* University Science Books, Mill Valle.

Sigrist. M. W. (1994) Air monitoring by spectroscopic techniques, In: *Chemical Analysis* **127,** John Wiley and Sons, New York.

Silfvast. W. T. (2004) *Laser Fundamentals*, 2nd ed. Cambridge University Press. United Kingdom.

Silver. J. A. (1992) Frequency-modulation spectroscopy for trace species detection: theory and comparison among experimental methods. Appl. Opt. **31,** 707–717.

Silver. J. A. and Stanton. A. C. (1988). Two-tone optical heterodyne spectroscopy using buried double heterostructure lead-salt diode lasers. Appl. Opt. **27,** 4438-4444.

Silver. J. and Kane. D. (1999) Diode laser measurements of concentration and

temperature in microgravity combustion. Mea. Sci. and Tech. **10**, 845–852.

Simpson, W. and TenWolde, A. (1999) Physical properties and moisture relations of wood. Technical Report, Department of Agriculture, Forest Service. Forest Products Laboratory, Madison, U.S.

Simpson, R. J., Wood, T. R. and Hamlin, M. J. (1980) Simple self-correcting models for forecasting flows on small basins in real time. In *Hydrological Forecasting*, Proceedings of the Oxford Symposium. IAHS Publ., **129**, 433-443.

Sirtori, C., Page, H. and Becker, C. (2001) GaAs-based quantum cascade lasers: semiconductor light sources for mid-infrared applications. Phil. Trans.: Math. Phys. Eng. Sci. **359**, 1780, 505–522.

Sjöholm, M. (2001) Development of a laser spectroscopic technique for gas in scattering media. Lund Report on Atomic Physic. LRAP 271, Lund University.

Sjöholm, M., Somesfalean, G., Alnis, J., Andersson-Engels, S. and Svanberg, S. (2001) Analysis of gas dispersed in scattering media, Opt. Lett. **26**, 16 – 18.

Somesfalean, G., (2002) Concentration measurement of gas embedded in scattering media by employing absorption and time-resolved laser spectroscopy. Appl. Opt. **41**, 3539 – 3544.

Somesfalean, G. (2004) Environmental monitoring using diode-laser-based spectroscopic techniques PhD Thesis. Lund Reports on Atomic Physics LRAP-329, Lund University.

Snel, J. F. H. and van Kooten O. (1990) The use of chlorophyll fluorescence

169

and other non invasive spectroscopic techniques in plant stress physiology *Photosynth. Res.* **25** 146–332.

Song, J., Tian, M. S., and Dilley, D. R. (1997) Effect of 1-MCP on apple ripening and volatile production. Hort. Sci. **32**, 536.

Stober, F. and Lichtenhaler, H. K. (1993) Studies on the constancy of the blue and green fluorescence yield during the chlorophyll fluorescence induction kinetics (Kautsky effect). Radiat. Environ. Biophys. **32**, 357 – 365.

Stober, F., Lang, M. and Lichtenhaler, H. K. (1994) Studies on the blue, green and fluorescence signatures of green, etiolated and white leaves. Remote Sens. Env. **47**, 65-71.

Subhash, N. and Mohanan, C. N. (1995) Remote detection of nutrient stress in groundnut plants by deconvolution of laser-induced fluorescence Spectra. *Proc. Int. Geoscience and Remote Sensing Symp.*, Firenze **3**, 2323–2325.

Subhash, N., Wenzel, O. and Lichtenthaler, H. K. (1999) Changes in blue-green and chlorophyll fluorescence emission and fluorescence ratios during senescence of tobacco plants. Remote Sens. of Env. **69**, 215–223.

Supplee, J. M., Whittaker, E. A. and Lenth, W. (1994) Theoretical description of frequency modulation and wavelength modulation spectroscopy. Appl. Opt. **33**, 6294–6302.

Svanberg S. (1995) Fluorescence lidar monitoring of vegetation status. Phys. Scr. **58**, 7.

Svanberg, S. (2004) *Atomic and Molecular spectroscopy: Basic Aspects and Practical Applications*, 4th ed., Springer, Berlin.

Svelto, O. (1998) *Principle of Lasers*. 4th ed. Plenum Press. New York.

Takeuchi, A., Saito, Y., Kanoh, M., Kawahara, T. D., Nomura, A., Ishizawa, H., Matsuzawa, T. and Komatsu, K. (2002) Laser-induced fluorescence detection of plant and optimal harvest time of agricultural products (lettuce). Appl. Eng. In: Agric. **18**, 361 – 366.

Toivonen, P. M. A. and DeEll, Jnr. (2001) Chlorophyll fluorescence, fermentation product accumulation, and quality of stored broccoli in modified atmosphere packages and subsequent air storage. Postharvest Bio. and Tech. **23**, 61-69.

Valentini, R., Cecchi, G., Mazzinghi, P., Scarascia Mugnozza, G., Agati, G., Bazzani, M., De Angelis, P., Fusi, F., Mattcucci, G. and Raimondi, V. (1994) Remote sensing of chlorophyll a fluorescence on vegetation canopies: 2. Physiological significance of fluorescence signal in response to environmental stresses. Remote Sens. of Env. **47**, 39 – 35.

Varoquaux, P., Albagnac, G. and Gouble, B. (1995) Physiology of minimally processed fresh vegetables. Austral Postharvest Hortic. Conf., 437-443.

Weber, M. (1961) Ethnic groups, In: *Theories of Society*, Talcott Parsons, E. Shils, K. D. Naegle, and J. R. Pitts (Eds.), New York: Free Press, 303 - 309.

Whitmarsh, J. and Govindjee (1999) The photosynthetic process, In: *Concepts in Photobiology: Photosynthesis and Photomorphogenesis*. G. S. Singhal, G. Renger, S. K. Sopory, K. D. Irrgang and Govindjee, (eds). Narosa Publishers, New Delhi; and Kluwer Academic, Dordrecht. 11-51.

Wieman, C. E. and Hollberg, L. (1991) Using diode lasers for atomic physics.

171

Rev. Sci. Instrum. **62**, 1-20.

Winandy, J. E. (1994) Wood Properties. In: *Encyclopedia of Agricultural Science*, C. J. Arntzen, (ed). Academic Press. San Diego, CA. **4**, 549-561.

Wraight, C. (1982) Reaction centers, electron flow, and energy transduction. In: *Photosynthesis*. Govindjee, (ed). Academic Press. New York, NY. 17-61.

www.cn.wikipedia.org/wiki/Nutmeg. 15th September, 2006.

Yearsley, C. W., Banks, N. H. and Ganesh, S. (1997) Temperature effect on the internal lower oxygen limits of apple fruit. Postharvest Biol. Technol. **11**, 73-83.

Zachariah, J. A., Gopalan, A., Krishnamurthy, B. and Ravindran, P. N. (1986) Steroid degradation compound associated with sex expression in nutmeg (*Myristica fragrans* Houtt). Proc. Indian Natn. Sci. Acad. **52**, 685-688.

Zimmermann, R. and Günther, K. P. (1986) Laser-induced chlorophyll a fluorescence of terrestrial plants. In: *Proc Intern Geoscience and Remote Sensing Symposium, IGARSS*, Zürich. III, Noordwijk, ESA Publications Division, 1609 -- 1613.